UC Berkeley
UC Berkeley Electronic Theses and Dissertations

Title
Mechanisms of Circuit Plasticity in the Developing Retina

Permalink
https://escholarship.org/uc/item/6vw6w2r6

Author
Kirkby, Lowry

Publication Date
2014

Peer reviewed|Thesis/dissertation

Mechanisms of Circuit Plasticity in the Developing Retina

by

Lowry Anna Kirkby

A dissertation submitted in partial satisfaction of the
requirements for the degree of
Doctor of Philosophy

in

Biophysics

in the

Graduate Division

of the

University of California, Berkeley

Committee in charge:

Professor Marla Feller, Chair
Professor Daniel Feldman
Professor Ehud Isacoff
Professor Kristin Scott

Spring 2014

Mechanisms of Circuit Plasticity in the Developing Retina

Copyright 2014
by
Lowry Anna Kirkby

Abstract

Mechanisms of Circuit Plasticity in the Developing Retina

by

Lowry Anna Kirkby

Doctor of Philosophy in Biophysics

University of California, Berkeley

Professor Marla Feller, Chair

Across the developing nervous system, immature networks generate spontaneous activity that is highly correlated amongst neighboring cells, which is required for the correct establishment of adult neural circuits. Remarkably, correlated activity persists following disruption of the underlying circuits that mediate it, indicating that plasticity mechanisms exist to ensure correlated activity is maintained. Here, we examine this phenomenon in the developing mouse retina, where correlated activity is mediated by cholinergic transmission and propagates across the retina as a wave. The absence of cholinergic signaling leads to the generation of "recovered" waves that propagate through a distinct, gap junction mediated circuit. Our findings show that stimulation of melanopsin-expressing intrinsically photosensitive retinal ganglion cells (ipRGCs) facilitates recovery of correlated activity in the absence of cholinergic waves, which results in the emergence of a light-sensitive network. We tested whether pharmacological blockade of cholinergic waves altered retinal light-response properties. We observed an increase in the duration of light-evoked activity and number of light-responsive cells, which arose from signaling via gap junctions. These observations suggest that electrical coupling of ipRGCs increases in the absence of cholinergic input, allowing melanopsin-driven signals to propagate to other neurons. Furthermore, we show that light-sensitive waves are strongly modulated by dopamine signaling—a potent neuromodulator of gap junction coupling. We determine that this light-sensitive wave circuit is present but latent in wild type retina, where it is usually suppressed by a combination of cholinergic and dopaminergic signaling. Our observations indicate that dopamine signaling acts as a switch for network reconfiguration, where high dopamine silences the light-sensitive, gap junction coupled network under cholinergic waves and reduced dopamine activates it in the absence of cholinergic waves. We conclude that the wiring diagram of the developing retina includes several overconnected circuits, in which some circuits are closed and others activated depending on the internal state of the system.

To

My parents and my sister
Thank you for always supporting me

Contents

List of Figures

List of Tables

Acknowledgments

One of the most satisfying parts of reaching the end of graduate school is looking back over the years and realizing how far I've come in the process. I couldn't have reached where I am now on my own, and it's a pleasure to reflect on and thank all those who have helped me along the way.

I'd like to start with a warm thanks to my Ph.D advisor, Marla Feller. Marla, thank you for turning me into the scientist I am today. Thank you for your unwavering dedication and support, for always taking the time to perfect practice talks and manuscripts with me, for bringing fun and humor into the lab, and most of all, for always having more to teach me and for always being enthusiastic to do it. It has been a privilege to have you as my mentor.

Thank you to everyone else who I've had the pleasure of working with while in the Feller Lab. In particular, a special thanks to Justin Elstrott, for helping me with everything from dissecting retinas, to trouble shooting the multi-electrode array, to MATLAB programming, to career advice; to David Arroyo, for being my project team-mate and making it significantly more fun than it would have been on my own; to Georgeann Sack, for advising me and motivating me in all aspects of my life, both personal and professional. And a very warm thank you to the rest of the Feller Lab—Kevin Ford, Alana Firl, Michal Rivlin, Anna Vlasits, Rémi Bos, Juliana Rosa, Ryan Morrie, Melissa Panlasigui—it has been a lot of fun working with you and I will really miss having colleagues and friends like you. Thanks also to Paley Han for keeping lab business running smoothly and for all the genotyping.

I'd like to extend a thanks to everyone outside the Feller Lab who have helped me with various aspects of my project. To my committee members Dan Feldman, Udi Isacoff and Kristin Scott for your guidance and constructive comments throughout my thesis; to Caleb Smith for taking the time to teach me cell culture; to Hanmi Lee and Martina Blank for productive collaborations; to David Copenhagen for providing mice and to David Kleinfeld for providing CNiFER cells.

Thank you to my funding sources, Boehringer Ingelheim Fonds (BIF) and National Science Foundation (NSF). In particular, I'd like to give a warm thanks to Claudia Walther, Sandra Schedler, Anja Hoffmann and the rest of the BIF team. It's been a pleasure to be part of the BIF community and to have made good friends in the process. I benefited tremendously from the conferences and workshops you provided—thank you.

My time as a graduate student would have been much more difficult had it not been for all the support I received outside of the lab. Tenzing Joshi, thank you for being my rock. For grounding me when I was shaky, for motivating me when I was down, for

making me laugh when I needed a giggle. And importantly, thank you for all the fun we've had throughout graduate school—discovering new places, trying new things and developing new hobbies with you has been a blast. I'm excited to see where our lives take us next!

Thank you to all my friends who have supported me along the way. In particular, to Kelly Clancy for making my day to day life in lab frankly awesome, for being a constant source of inspiration, for introducing me to a whole world of creativity and fun I didn't even know existed; to Kelly Gardner and Maria Dadarlat for endless fun and laughs, for always being there when I needed a chat, for motivating and inspiring me in so many different ways; to Katie Harding, Laura Rosen and Ellen Demlow for being the best housemates I could have asked for, for being by my side through thick and thin. Thank you all for being such wonderful friends.

And most importantly, an enormous thanks to my family. To my sister, Eva, for continuously guiding me in the right direction, for encouraging me to challenge myself, for always giving me the right advice. Thank you to my parents, Rita and Jasper, for, well, everything. You have provided me with endless support, advice, belief in me; I can't begin to express how grateful I am for all of it. Thank you for setting an outstanding example; thank you for all you have done for me, for all you have given me and for all you continue to give me—none of it has gone unnoticed. Thank you, Eva, mum and dad, for always looking out for me. This thesis is dedicated to you.

Chapter I

Introduction and Thesis Objectives

Across the developing nervous system, immature networks generate spontaneous activity that is correlated amongst neighboring groups of cells and produces distinct spatial and temporal activity patterns (reviewed in Blankenship and Feller, 2010). During this period of patterned activity, sensory maps develop and initial coarse connections are refined, resulting in the correct establishment of adult neural circuits. Correlated patterns of spontaneous activity have been shown to be key to this refinement process, where they drive synaptic strengthening or elimination via activity-dependent mechanisms (refer to Chapter II for an overview of the role of correlated activity in the assembly of neural circuits; Kirkby et al., 2013). Studies of transgenic mice that show disrupted developmental refinement continue to elucidate the mechanisms and learning rules by which spontaneous activity patterns contribute to circuit refinement (refer to Chapter III).

One interesting feature of correlated spontaneous activity is that it is highly robust to perturbations in the network that generate it. This suggests that the neural circuits that mediate correlated activity are subject to regulatory mechanisms that maintain correlated activity in the face of perturbation. For example, motor neurons in the developing spinal cord undergo spontaneous network activity (SNA), which is generated by recurrently connected circuits involving GABAergic and glutamateric interneurons (Wilhelm and Wenner, 2008) and is thought to drive spontaneous limb movements of developing embryos (Blumberg et al., 2013; Crisp et al., 2011; Crisp et al., 2008). When SNA is reduced by blocking GABAergic transmission, embryonic limb movements are transiently reduced but recover to control levels within 12 hour blockade (Wilhelm and Wenner, 2008). The recovery of SNA is thought to arise from a combined increase in intrinsic excitability of motor neurons followed by an increase in GABAergic and glutamatergic synaptic strength (Chub and O'Donovan, 1998; Wilhelm and Wenner, 2008; Wilhelm et al., 2009). Similarly, the developing hippocampus undergoes spontaneous network events, termed giant depolarizing potentials (GDPs), which are mediated by excita-

tory GABAergic signaling. Transgenic mice that lack the chloride transporter NKCC1 (NKCC1 KO mice) cannot generate GABAergic GDPs. However, recovered GDP-like events are generated in NKCC1 KO mice via a glutamatergic network in place of a GABAergic one (Sipilä et al., 2009).

In the developing retina, several perturbations that disrupt endogenous retinal waves but exhibit recovered correlated activity patterns have been described (Syed et al., 2004; Stacy et al., 2005; Sun et al., 2008; Stafford et al., 2009; Hennig et al., 2011; Kirkby and Feller, 2013). For example, during the first postnatal week of mouse development, when retinal waves are mediated by activation of nicotinic acetylcholine receptors (nAChRs), prolonged GABAergic block results in an initial decrease in wave frequency, which returns to control levels within two days (Hennig et al., 2011).

A more striking compensation occurs following disruption of cholinergic signaling. This was first observed in a transgenic mice lacking choline acetyltransferase, the enzyme necessary for acetycholine production, which was found to exhibit recovered waves that propagate through a gap junction coupled network (Stacy et al., 2005). Similarly, mice lacking the $\beta2$ subunit of nAChRs ($\beta2$-nAChR KO mouse) exhibit gap junction waves in place of cholinergic ones. Furthermore, waves in $\beta2$-nAChR KO mice are modulated by external conditions, such as increased temperature (Stafford et al., 2009). Together, these observations suggest that gap junctions can compensate for the lack of cholinergic signaling, and that the network is subject to modulation by external factors. However, the cellular mechanisms that underly plasticity in retinal wave circuits and recovery of correlated activity following network perturbation remain an open question.

For my thesis research, I explored the neural circuit that mediates recovery of correlated activity in the absence of cholinergic retinal waves, under both genetic ($\beta2$-nAChR KO mice) and pharmacological blockade of cholinergic waves. I discovered that correlated activity patterns in $\beta2$-nAChR KO mice were highly sensitive to ambient light, in contrast to wild type (WT) patterns, which are largely light-insensitive (Renna et al., 2011). This discovery came as a surprise since the period of retinal waves corresponds to an age at which light is not thought to influence retinal firing patterns or retinal development.

This observation of a light-sensitive wave circuit led us to the hypothesis that intrinsically photosensitive retinal ganglion cells (ipRGCs) contribute to mechanisms of network plasticity in the developing retina. ipRGCs express the photopigment melanopsin and, unlike rod and cone photoreceptors, they are photosensitive early in development (Sekaran et al., 2005). ipRGCs are involved in diverse non-image-forming parts of vision, including entrainment of circadian rhythms and pupillary light reflex (Rollag et al.,

2003; Berson, 2003; Hattar et al., 2003), development of eye vasculature (Rao et al., 2013), and light avoidance behavior (Johnson et al., 2010). Furthermore, there is some evidence that ipRGCs undergo retrograde, intra-retinal signaling to dopaminergic amacrine cells (Zhang et al., 2008; Zhang et al., 2012a) and that they form gap junctions with GABAergic amacrine cells (Müller et al., 2010), making them a promising candidate for photic modulation of network activity during development.

The goal of my thesis was two-fold. First was to dissect apart the light-sensitive circuit, in order to identify the neurotransmitter signaling and cell connectivity that underly the recovery of correlated activity in retinal development. Second was to establish whether this light-sensitive circuit is present in WT retinas, and if so how it is usually suppressed during normal development. I used a combination of multi-electrode array recordings to quantify spatial-temporal patterns of spontaneous activity, pharmacology to block specific signaling pathways, and knockout mice to establish the contribution of certain components to the network. My research yields a mechanism by which dopamine signaling acts as a switch for network configuration, where high dopamine signaling silences the light-sensitive, gap junction coupled network under cholinergic waves and reduced dopamine activates it in the absence of cholinergic waves (refer to Chapters IV and V). We postulate that neuromodulation of gap junctions provides a means to rapidly change network properties without having to construct new circuits. These observations emphasize that neural circuits are not hard-wired, but rather are dynamic and malleable, and that alternate circuits and connections act to rescue functional output following network disruption.

Chapter II

Correlated Activity in the Assembly of Neural Circuits

This Chapter is a full reprint of Kirkby et al., *Neuron* (2013), in which I was the primary author. This review paper discusses the role of correlated spontaneous activity in the assembly of neural circuits, with an emphasis on the visual, auditory and motor systems. The work is included with permission from all authors.

Relevant publications:

Kirkby, L.A., Sack, G.S., Firl, A., and Feller, M.B. (2013). A role for correlated spontaneous activity in the assembly of neural circuits. *Neuron* **80**, 1129–1144.

Abstract

Before the onset of sensory transduction, developing neural circuits spontaneously generate correlated activity in distinct spatial and temporal patterns. During this period of patterned activity, sensory maps develop and initial coarse connections are refined, which are critical steps in the establishment of adult neural circuits. Over the last decade there has been substantial evidence that altering the pattern of spontaneous activity disrupts refinement, but the mechanistic understanding of this process remains incomplete. In this review, we discuss recent experimental and theoretical progress towards the process of activity-dependent refinement, focusing on circuits in the visual, auditory and motor systems. While many outstanding questions remain, the combination of several novel approaches have brought us closer to a comprehensive understanding of how complex neural circuits are established by patterned spontaneous activity during development.

Introduction

With almost one hundred billion neurons and one thousand as many synapses, the nervous system has a cumbersome task of ensuring that correct wiring is established during development. A major goal in developmental neurobiology is to elucidate the role that neural activity plays in this process. This review focuses on a particular period of development—after neuronal differentiation, migration, axon guidance and dendrite extension, and before the onset of sensory experience—in which activity is generated spontaneously within the network and correlated amongst neighboring cells. During this developmental period, neural circuits undergo significant sculpting and refining of their connections, resulting in the formation of sensory maps and the establishment of precise local circuits (Katz and Shatz, 1996). Correlated spontaneous activity has been observed in several species, throughout the developing nervous system, including the retina, cochlea, spinal cord, cerebellum, hippocampus and neocortex (Blankenship and Feller, 2010; Dehorter et al., 2012; Feldt et al., 2011; Moody and Bosma, 2005). This prevalence alone suggests that correlated spontaneous activity is an essential component of neural circuit maturation, and as such, understanding the role of and mechanisms underlying correlated spontaneous activity has been a dynamic area of research over the past few decades.

Two major questions that remain in the field are first, whether the endogenous patterns of activity are relevant for maturation of specific circuit features, and second, what the learning rules that guide refinement are. It has been postulated that patterned spontaneous activity drives circuit refinement via learning rules that are consistent with Hebbian principles of plasticity, which state that the repeated and persistent stimulation of

a postsynaptic cell by its presynaptic partner results in long term strengthening of the synapse (long term potentiation, LTP) (Hebb, 1949), while weak or ineffective stimulation results in long term weakening of the synapse (long term depression, LTD) (Katz and Shatz, 1996). Hence, the repeated stimulation provided by bursts of spontaneously active cells could provide the drive necessary for synaptic strengthening. Furthermore, the propagating nature and distinct spatial boundaries of spontaneous activity patterns would ensure that topographic maps are maintained across connected brain regions, as the connections between neighboring cells are strengthened while those from more distant ones are lost (Eglen et al., 2003).

In this review, we summarize recent progress made toward answering these questions. We focus on the development of three circuits: retinofugal projections in the visual system, which is the most extensively-studied system, cochlear projections to brainstem nuclei in the auditory system, and local motor networks in the spinal cord. In addition, we provide an overview of the theoretical frameworks that have contributed to our understanding of which spatial and temporal features of spontaneous activity are used for refinement of particular circuit features. By using optogenetic methods for precise control of firing patterns, elucidating the plasticity mechanisms that underlie map refinement, and creating models that allow for an interpretation of these results in the context of molecule-guided developmental processes, the field has made a significant step forward in the development of a comprehensive and mechanistic understanding of the role of spontaneous activity in circuit refinement.

Patterned spontaneous activity guides circuit maturation

Following the first observations of correlated spontaneous activity (Galli and Maffei, 1988; Landmesser and O'Donovan, 1984; Lippe, 1994; Meister et al., 1991), the question of whether specific activity patterns are relevant to the formation and refinement of nascent circuits emerged (Feller, 1999; O'Donovan, 1999). Since then, many lines of evidence point to patterned spontaneous activity playing a considerable role in the development of neural circuits. Spontaneous activity is conserved across species, throughout the nervous system, and is highly robust to perturbations, suggesting that developing networks have inherent redundancies to ensure that patterned activity is maintained (Blankenship and Feller, 2010). In addition, many studies have shown that altering patterns of activity results in deficits in network refinement, suggesting that the patterns themselves contain information that guides such development (for visual system review, see Huberman et al., 2008). Here, we highlight recent *in vivo* studies that have shown that patterned spontaneous activity in the live animal has similar spatial and temporal properties to what has been described *in vitro*. In addition, we describe recent approaches that combine optogenetics and synaptic physiology to probe the cellular and synaptic

basis of activity-dependent refinement driven by correlated spontaneous activity in the developing visual, auditory and motor systems.

Sensory map formation in the developing visual system

Retinal waves coordinate patterned activity across visual areas

The visual system has been an ideal model to study how correlated spontaneous activity influences the development of neural circuits (reviewed in Huberman et al., 2008; Wong, 1999). Before the onset of vision, the immature retina generates spontaneous, periodic bursts of action potentials that sweep across retinal ganglion cells (RGCs) as a wave. Retinal waves have been observed experimentally *in vitro* and *in vivo* using a variety of techniques, including calcium imaging of RGCs, multi-electrode array recordings, and paired patch clamp recordings (reviewed in Torborg and Feller, 2005). In rodents, retinal waves are mediated by acetylcholine over the first ten postnatal days of development, and by glutamate over the following three to four postnatal days. The endogenous patterns of cholinergic retinal waves are well-characterized and have been described extensively (for review, see Ford and Feller, 2012). Briefly, waves occur at a frequency of approximately once per minute. A single wave propagates laterally across large fractions of retina and firing patterns are highly correlated amongst groups of RGCs that are within approximately $300\,\mu$m of one another. Typically, an RGC bursts for a duration of around $3\,$s during a given wave, at a firing rate of around $10\,$Hz. It has commonly been assumed that waves occur independently in left and right eyes, however, recent data has shown that a subset of waves are bilaterally coordinated between eyes (Ackman et al., 2012). While the network underlying this coordinated activity remains unknown, observations of both descending retino-petal projections from higher brain areas (Gastinger et al., 2006) and retino-retinal projections between eyes (Ackman et al., 2012; Müller and Holländer, 1988) raises the possibility that it might be driven by common descending inputs or via inter-retinal connections.

RGCs project to the lateral geniculate nucleus (LGN) of the thalamus and the superior colliculus (SC), which in turn relay visual signals to the primary visual cortex (V1) (Fig. 2.1 A). A long-standing question has been whether retinal waves drive spontaneous activity in these downstream targets. Two approaches have been taken to answer this question. First, do the patterns of spontaneous activity in the LGN, SC, and V1 match what has been described in the retina? Second, does blocking inputs from the retina also block spontaneous activity of RGC targets in the brain?

Observing spontaneous activity in the visual system *in vivo* has been challenging because anesthetics such as isoflurane and urethane inhibit endogenous patterns of ac-

tivity even at sub-surgical doses, as had been demonstrated in cortex (Hanganu et al., 2006; Siegel et al., 2012). Several groups have recently studied endogenous patterns of spontaneous activity *in vivo* in unanethestized animals, including zebrafish (Zhang et al., 2010), mouse (Ackman et al., 2012), rat (Colonnese and Khazipov, 2010) and human (Colonnese et al., 2010). In unanesthetized rodents, the temporal and spatial patterns of spontaneous activity *in vivo* was found to be similar to what was previously observed *in vitro*, suggesting that *in vitro* studies are representative of what occurs in the live animal.

Remarkably, a recent *in vivo* study showed that retinal waves drive correlated patterns of activity throughout the visual system, resulting in concurrent waves propagating across downstream visual areas including the SC and V1 (Ackman et al., 2012). Spontaneous activity in the SC and V1 was found to be abolished (Colonnese and Khazipov, 2010) or greatly reduced (Ackman et al., 2012; Siegel et al., 2012) following enucleation or pharmacological block of retinal inputs. Similarly, correlated activity in the LGN was reduced following optic nerve transection (Weliky and Katz, 1999). These observations further support the conclusion that retinal waves coordinate patterned activity across developing visual brain areas. However, spontaneous activity in secondary visual cortex areas was found to be mostly uncorrelated with retinal waves, suggesting that activity in these areas is generated by a mechanism that is independent of retinal activity (Ackman et al., 2012).

Visual maps form in the SC and LGN over the period of retinal waves

Over the period of cholinergic retinal waves, RGC projections to their primary targets, the dorsal LGN (dLGN) and SC, undergo significant sculpting and refinement. Recent reconstructions of single axon arbors have provided a detailed description of refinement of mouse retinal projections (Dhande et al., 2011) that is similar to the classic work in cat (Sretavan and Shatz, 1986; Sretavan et al., 1988). This sculpting results in the formation of two sensory maps (refer to Figs. 2.2 A–B). One map reflects retinotopic location, where initially coarse axon terminals are refined to form precise terminals that map their location on the retina. Retinotopic map refinement occurs in both the SC and dLGN, and is particularly prominent in the SC. The second map reflects inputs from left and right eyes, which project to both sides of the brain in mammals. In the dLGN, contralateral axons initially project over the entire region while ipsilateral axons target a smaller patch that overlaps with the larger contralateral domain. During development, contralateral terminals are expelled from the ipsilateral patch and ipsilateral terminals refine and stabilize within the patch. Similar eye-specific segregation is observed in the anteromedial region of the SC. This region initially receives binocular input and, over the course of development, ipsilateral axons segregate into small patches of ipsilateral-only projecting neurons. These two sensory maps are referred to as retinotopy and eye-specific segrega-
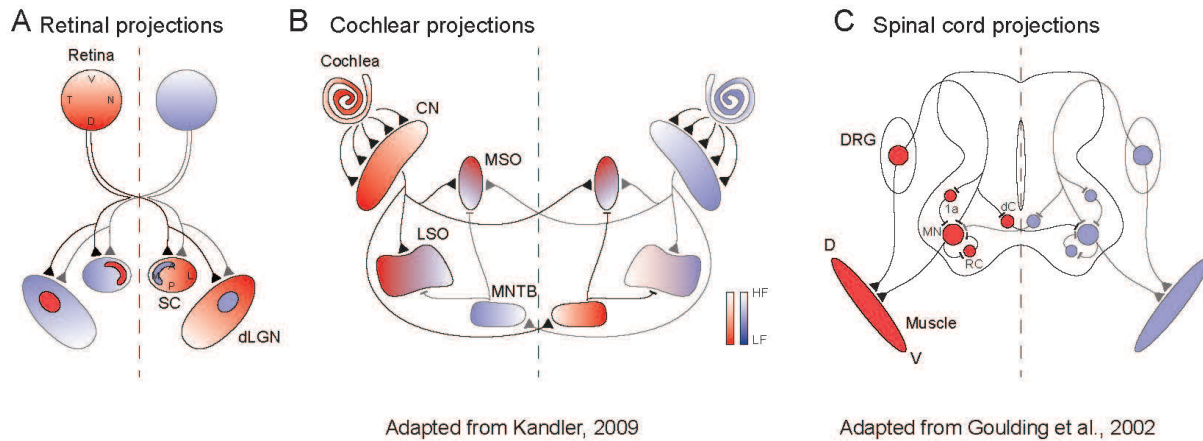
Figure 2.1: **Retinal, cochlear and spinal cord projections to their primary targets.** (A) Schematic representation of retinal ganglion cell (RGC) projections to their primary targets: the dorsal lateral geniculate nucleus (dLGN) of the thalamus and the superior colliculus (SC). Red areas in the dLGN and SC correspond to projections from the left (red) eye; blue areas correspond to projections from the right (blue) eye. Shading represents retinotopy. V: ventral, D: dorsal, T: temporal, N: nasal, A: anterior, P: posterior, M: medial, L: lateral. (B) Schematic representation of cochlear projections to primary brainstem targets: the cochlear nucleus (CN), the medial superior olive (MSO), the lateral superior olive (LSO) and the medial nucleus of the trapezoid body (MNTB). Red areas correspond to projections from the left (red) cochlea; blue areas correspond to projections from the right (blue) cochlea. Shading represents tonotopy. Both the LSO and MSO receive overlapping tonotopic maps originating from either cochlea. HF: high frequency, LF: low frequency. (Adapted from Kandler, 2009). (C) Schematic representation of some spinal cord cell types and their connections. MN: motoneuron, DRG: dorsal root ganglia, RC: Renshaw cell; 1a: 1a inhibitory interneuron, dC: commissural interneurons; D: dorsal, V: ventral. (Adapted from Goulding et al., 2002).

tion, respectively.

Experimentally, retinotopy is assayed using a focal DiI injection into a given location on the retina, which results in a labeled spot in the SC. The extent of retinotopic refinement is quantified by the size of the DiI-labeled target zone in the SC (for detailed methods, refer to (Chandrasekaran et al., 2005)). Eye-specific segregation is assayed using vitreal injection of cholera toxin fused to a fluorescent dye, which bulk labels most RGCs and their axon projections. By using two different fluorophores for either eye, typically one red and one green, the extent of segregation is quantified by measuring the fraction of the LGN that contains red-only or green-only fluorescence (segregated regions), compared to the fraction that contains an overlap of both red and green fluorescence (unsegregated region) (for more detail on quantification techniques, refer to

Huberman et al., 2003; Stellwagen and Shatz, 2002; Torborg et al., 2004b).

In addition to anatomical measures, physiological recordings of neurons in the SC and dLGN have been made to assess the formation of functional maps. Retinotopy has been assayed *in vivo* by measuring the receptive fields of SC neurons at the time of eye opening (Chandrasekaran et al., 2005). These measurements showed that the receptive fields are circular and compact, covering an area comparable to the size of retinocollicular projections as assayed using retinal DiI injections. In addition, the number of RGC inputs onto either collicular (Furman and Crair, 2012) or geniculate (Hooks and Chen, 2006) neurons has been quantified *in vitro* my comparing the saturated synaptic response of a neuron induced by high intensity simulation to the single-fiber response induced by minimal stimulation. Eye-specific segregation has been assayed *in vivo* by measuring single cell responses in the dLGN to visual stimulation at eye-opening (Grubb et al., 2003). These recordings showed that geniculate neurons were driven by monocular stimulation both within the contralateral region and the ipsilateral patch. Furthermore, *in vitro* recordings of dLGN neurons have shown that geniculate neurons initially receive binocular inputs, with one eye exerting a stronger synaptic drive onto a given neuron than the other eye, and that inputs from the weaker eye are eliminated as segregation proceeds (reviewed in Guido, 2008; Huberman, 2007). Together, these observations are consistent with anatomical changes occurring in the SC and dLGN over the same developmental period. Physiological measurements provide additional information over anatomical measurements, allowing researchers to put constraints on the underlying cellular and molecular mechanisms of map formation. For example, they allow researchers to test whether particular types of plasticity mechanisms, such as LTP or LTD, exist at target synapses (Butts et al., 2007; Ziburkus et al., 2009).

Manipulation	Retinal activity	Retinotopic refinement	Eye-specific segregation
Manipulations primarily affecting retinal activity			
Prenatal TTX application in cat (1)	Action potentials blocked	Unknown	No segregation
Postnatal introacular TTX injection in ferret (2)	Action potentials blocked	Unknown	Normal segregation
Binocular epibatadine (nAChR antagonist) injections in ferret and mouse (3-8)	Retinal waves blocked in both eyes	Reduced refinement	No segregation
Monocular epibatadine (nAChR antagonist) injections in ferret (1, 3)	Retinal waves blocked in one eye	Reduced refinement	Reduced segregation of inputs combined with increase in axonal territory of active eye
Binocular cpt-cAMP injections (2, 9)	Increase in wave frequency in both eyes	Unknown	Normal segregation
Monocular cpt-cAMP injection (3-9)	Increase in wave frequency in one eye	Unknown	Reduced segregation of inputs combined with increase in axonal territory of active eye
Binocular ChAT immunotoxin injection (kills 80–95% of SACs) (5, 10)	Retinal waves with reduced nearest neighbor correlations	Unknown	Normal
β2-nAChR KO mouse (lacks β2–subunit of nAChRs) (4, 11-13)	Gap junction mediated retinal waves with reduced nearest neighbor correlations; increased uncorrelated firing between waves	Reduced refinement	Reduced segregation
Rescue of β2–containing nAChRs in RGCs of β2-nAChR KO mouse (1, 14)	Small-range cholinergic retinal waves	Normal refinement	Reduced segregation
Cx36 KO and Cx45 KO mice (lack gap junction proteins Cx36 or Cx45) (2, 15, 16)	Retinal waves with increased inter-wave firing	Unknown	Normal segregation

No b-wave mouse (3-8, 17)	Retinal waves with abnormal retinal activity after P14	Unknown	Normal segregation at eye opening; segregation degrades after eye opening
Opn4 KO mouse (lacks photopigment melanopsin) (3, 18)	Retinal waves with increase in burst duration during waves	Unknown	Reduced segregation

Manipulations affecting either retinofugal synapses or the targeting of retinal projections			
AC1 KO mouse (lacks the calcium-dependent adenylate cyclase 1) (9, 19, 20)	Normal retinal waves	Reduced refinement	Reduced segregation
MAOA KO mouse (lacks monoamine oxidase A resulting in excess serotonin) (9, 21, 22)	Unknown	Reduced refinement	Reduced segregation
CREB KO mouse (reduced CREB expression) (5, 10, 23)	Unknown	Unknown	Reduced segregation
Monocular antisense BDNF injections (blocks BDNF mRNA in the retina) (4, 11, 12, 24)	Unknown	Unknown	Reduced axonal territory of treated eye
Binocular U0126 or PD98059 injections (reduces ERK activation) (25)	Unknown	Unknown	Reduced segregation
Altered ephrin expression/signaling (26-29)	Normal	Disrupted targeting but normal refinement	Reduced segregation
$\beta3$ KO mouse (lacks the $\beta3$ subunit of the L-type calcium channel) (30)	Unknown	Unknown	Reduced segregation
Knockout of molecules associated with MHC1 signaling (31-33)	Normal retinal waves	Unknown	Reduced segregation
NP1/2 KO mouse (lacks neuronal pentraxins NP1/2) (34, 35)	Normal retinal waves	Unknown	Reduced segregation

CD3zeta KO mouse (lacks the immune protein CD3zeta) (36)	Altered glutamatergic waves	Unknown	Reduced segregation
C1q KO mouse (lack complement proteins C1q) (37)	Normal retinal waves	Unknown	Reduced segregation
CR3 KO and C3 KO mice (lack microglia specific complement receptors) (38)	Normal retinal waves	Unknown	Reduced segregation
Ten-m3 KO and Ten-m2 KO mice (lack members of teneurin family of glycoproteins) (39, 40)	Normal retinal waves	Altered ipsilateral mapping	Reduced segregation
Intracranial infusion of FK506 (calcineurin blocking enzyme) in ferret (41)	Unknown	Unknown	Normal eye specific segregation; reduced ON/OFF segregation*
MeCP2 KO (lacks the transcriptional regulator MeCP2) (42)	Normal retinal waves	Unknown	Reduced segregation
DSCAM mutants (various mouse models of Down syndrome) (43)	Normal retinal waves	Unknown	Reduced segregation
Phr1 KO (lacks a protein that is a regulator of synapse formation and axon guidance) (44)	Normal retinal waves	Unknown	Reduced segregation

Table 2.1: **Manipulations affecting retinal activity, retinotopic refinement and eye-specific segregation.** Summary of manipulations affecting retinal activity, retinofugal synapses, and targeting of retinal projections on retinotopic map refinement of retinocollicular projections and eye-specific segregation of retinogeniculate projections. See end of Chapter II for references. *ON/OFF segregation is not discussed in this review.

Endogenous patterns of retinal waves instruct specific aspects of visual map formation

While the initial formation of retinotopic and eye-specific segregation maps is thought be largely laid out by molecular cues (Feldheim and O'Leary, 2010; Triplett and Feldheim, 2012), their subsequent refinement is considered to be activity-dependent (Cline, 2003; Goodman and Shatz, 1993; Huberman et al., 2008). In particular, the endogenous patterns of retinal waves have been implicated in the refinement of retinotopic and eye-specific maps. By conveying information about neighboring cells to higher brain regions,

the restricted propagating spatial structure of waves could provide an instructive cue for retinotopy, while the independent timing of inputs from left and right eyes could provide an instructive cue for eye-specific segregation via activity-dependent competition.

Classically, this hypothesis has been tested using pharmacological manipulations and transgenic mice that alter patterns of retinal activity (summarized in Table 2.1). The strongest and best-characterized phenotype has been a mouse model that lacks the $\beta2$ subunit of the nicotinic acetylcholine receptor ($\beta2$-nAChR KO), and as such lacks normal cholinergic waves (Bansal et al., 2000; McLaughlin et al., 2003; Rossi et al., 2001). $\beta2$-nAChR KO mice exhibit gap junction-mediated correlated firing patterns with spatiotemporal properties that are distinct from cholinergic waves (Kirkby et al., 2013; Stafford et al., 2009; Sun et al., 2008; Torborg et al., 2004a); gap junction waves in $\beta2$-nAChR KO mice are larger and faster than cholinergic waves, burst durations are shorter, firing rates during a burst are lower and waves occur less frequently. In addition, $\beta2$-nAChR KO mice exhibit high levels of uncorrelated firing in between waves (Stafford et al., 2009; Torborg et al., 2004a). $\beta2$-nAChR KO mice show striking defects in both retinotopy and eye-specific segregation (reviewed in Huberman et al., 2008) (Fig. 2.2 C). This led to the conclusion that normal patterns of retinal waves are required for normal map formation. However, the inability to distinguish between the effect of disrupting wave patterns with the effect of disrupting overall firing patterns led to different interpretations of how and whether patterned activity contributes to sensory map formation (reviewed in (Chalupa, 2009; Feller, 2009)).

More recently, researchers have used sophisticated transgenic and optogenetic tools to determine whether the precise pattern of spontaneous activity is important for map development. By generating a transgenic mouse in which expression of $\beta2$-containing nAChRs is restricted to the ganglion cell layer of the retina ($\beta2$(TG)), researchers developed a manipulation that independently affected refinement of retinotopic maps and eye-specific segregation (Xu et al., 2011), in contrast to the more extensive full-body $\beta2$-nAChR KO, which shows defects in both maps. $\beta2$(TG) mice exhibit "truncated" cholinergic waves, which propagate over shorter ranges compared to normal cholinergic waves, but otherwise show single-neuron RGC firing activity that is indistinguishable from WT mice. In $\beta2$(TG) mice, the retinotopy defects seen in $\beta2$-nAChR KO mice were rescued in both the SC and dLGN, indicating that correlated firing amongst small groups of neighboring cells can drive axon refinement (Fig. 2.2 D). However, the truncated wave pattern did not rescue eye-specific segregation defects seen in $\beta2$-nAChR KO mice in either the SC or the dLGN, suggesting that long-range wave propagation is necessary for normal segregation patterns.

Optogenetic techniques have provided a more systematic approach to test whether

the relative timing of inputs from left and right eyes provides an instructive cue for the formation of eye-specific segregation. By expressing and stimulating the light-gated cation channel channelrhodopsin-2 (ChR2) in approximately 20% of RGCs distributed uniformly across the retina, researchers were able to reliably manipulate the timing of retinal inputs to its primary targets in the brain (Zhang et al., 2012b). In WT mice, asynchronous stimulation of left and right eyes resulted in segregation patterns in the SC and dLGN that were similar to control conditions (Fig. 2.2 E). In addition, this stimulation protocol somewhat rescued eye-specific segregation defects seen in the SC of β2-nAChR KO mice, but did not alter segregation patterns in the dLGN, indicating that optogenetic stimulation was less effective in influencing eye-specific segregation in the dLGN compared to the SC (Fig. 2.2 F). In contrast, synchronous stimulation of both eyes in WT mice disrupted eye-specific segregation in both the SC and dLGN, for both WT and β2-nAChR KO mice (Figs. 2.2 G–H). The extent of segregation improved with increasing asynchrony of left and right eye stimulation. Furthermore, segregation was sensitive to bursting of RGCs with time scales on the order of 100 ms, rather than individual spikes, suggesting that burst-timing rather than spike-timing provides an instructive signal for segregation. This is expected, since the weak and diffuse connections of presynaptic cells during development (Chen and Regehr, 2000; Guido, 2008; Ziburkus et al., 2009) likely renders them impervious to plasticity on the fast time scales of individual spikes, which occur on the order of 10 ms (Butts and Kanold, 2010).

Surprisingly, the uniform stimulation protocol led to an improvement in retinotopy for some axons in WT mice, and a marked improvement in retinotopy for β2-nAChR KO mice, suggesting that the high frequency of bursting activity may be more important for retinotopic refinement than the specific spatial pattern of activity (Zhang et al., 2012b) (Figs. 2.2 E–H). However, since ChR2 was only expressed in a small subset of RGCs (approximately 20%), the authors proposed that sparse activation of RGCs during stimulation could produce inhomogeneous spatial patterns that drive retinotopy.

Together, these studies suggest that the endogenous burst-like and highly correlated pattern of retinal waves is indeed suited to refinement of these two visual sensory maps. With the further development of better optogenetic and transgenic techniques, researchers will be able to mimic and manipulate natural patterns of activity in ever more systematic ways, allowing us to unequivocally assess which spatial and temporal features of patterned retinal activity are used for refinement of which sensory map features.
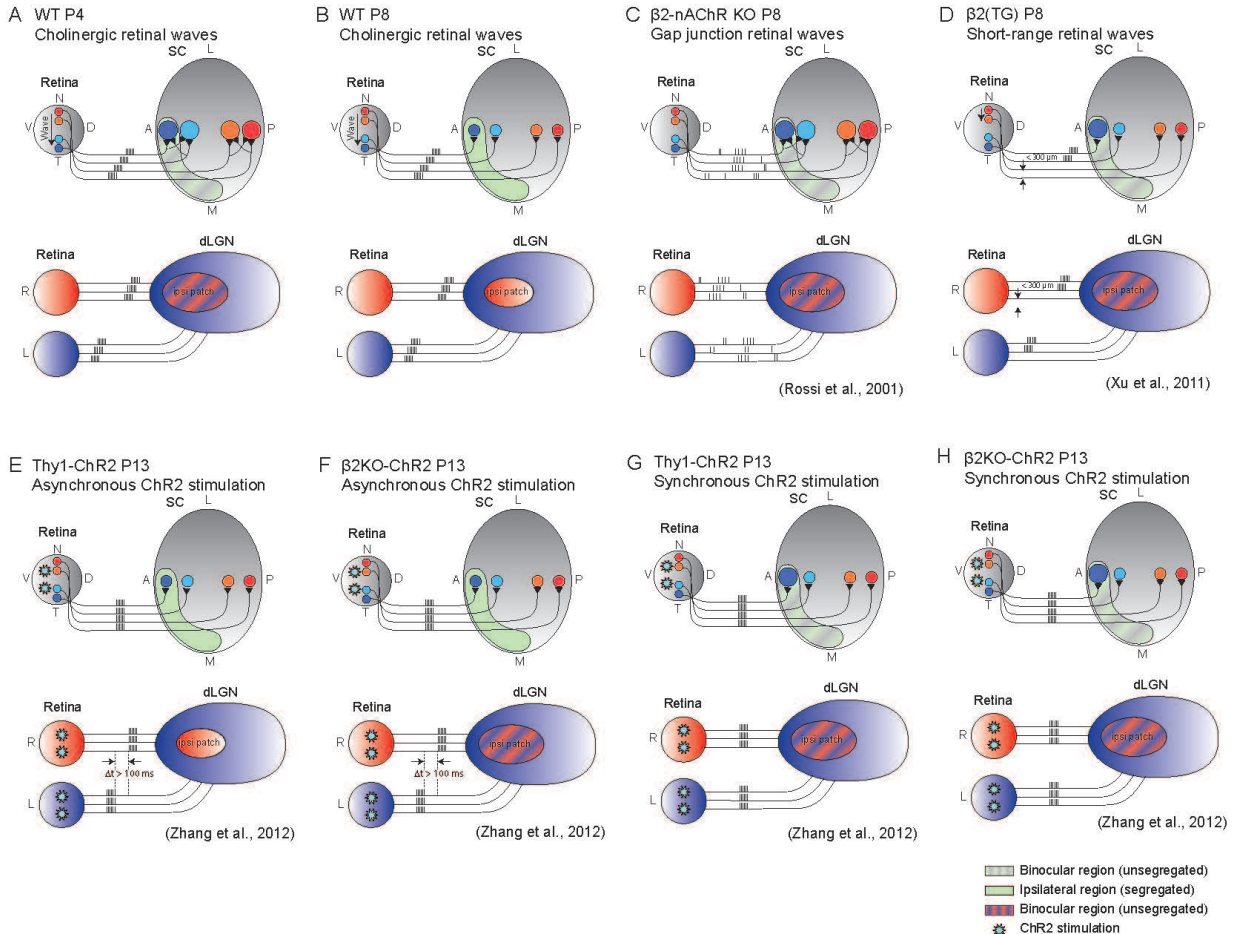
Figure 2.2: **Retinotopic map formation and eye-specific segregation under normal and disrupted spontaneous retinal activity patterns.** Schematic representations of retinotopic map formation in the SC and eye-specific segregation in the dLGN during normal development (A–B) and as a result of experiments that alter the spatial and temporal pattern of afferent RGC activity (C–H), as described in the text. Note that although the SC schematic is used to represent retinotopic mapping and the dLGN schematic to represent eye-specific segregation mapping, both maps refine in the two visual regions. Large and small circles depicted in the SC correspond to the termination zone size of RGC axons, shading corresponds to retinotopy, and striped regions correspond to unsegregated inputs from left and right eyes. SC: superior colliculus, dLGN: dorsal lateral geniculate nucleus, V: ventral, D: dorsal, T: temporal, N: nasal, A: anterior, P: posterior, M: medial, L: lateral, R: right eye, L: left eye, ChR2: channelrhodopsin-2.

Sensory map formation in the developing auditory system

Similar to visual system development, before the onset of hearing in the developing auditory system, the immature cochlea generates spontaneous activity that sweeps across inner hair cells (IHCs) and spiral ganglion neurons (SGNs) (for review, see (Kandler et al., 2009)). Rhythmic bursts of action potentials in IHCs and SGNS occur at a periodicity of approximately 3 per minute and are correlated amongst neighboring groups of cells. These events are triggered and synchronized by ATP release from supporting cells (Tritsch et al., 2007), although spike generation in IHCs may be intrinsic to the cell itself (Johnson et al., 2011). Furthermore, the frequency and pattern of IHC spiking activity varies along the length of the cochlea, where basal cells, which in the adult brain are tuned to high frequencies, show more sustained firing and higher mean firing rates compared to apical cells, which show bursting activity and lower mean firing rates (Johnson et al., 2011; Johnson et al., 2012).

SGN axons target the cochlear nucleus (CN) in the brain via the auditory nerve (Fig. 2.1 B). These projections are tonotopically mapped, resulting in a spatial separation of axon terminals from cochlear neurons that are tuned to high frequency sounds to those that are tuned to low frequency sounds. This tonotopy is further mapped onto three auditory nuclei downstream from the CN: the medial nucleus of the trapezoid body (MNTB), the lateral superior olive (LSO), and the medial superior olive (MSO). CN axons project to the contralateral MNTB, the ipsilateral LSO, and to both the ipsi- and contralateral MSO. Each MNTB in turn projects to its ipsilateral LSO and MSO. As such, both the LSO and MSO receive tonotopic input from both cochleae—excitatory input via the CN and inhibitory input via the MNTB. In these nuclei, the tonotopic maps from either cochlea are precisely aligned, such that single LSO or MSO neurons are excited and inhibited by the same frequency of sound (Kandler et al., 2009).

Because auditory circuits are tonotopically assembled early in development, it was originally thought that tonotopic map formation was hardwired by molecular cues (Gurung and Fritzsch, 2004; Kandler and Friauf, 1993; Rubel and Fritzsch, 2002). However, there is growing evidence that tonotopic precision in auditory nuclei increases during development (Kandler et al., 2009). In particular, the CN shows refinement of SGN axon terminals, and the LSO and MSO show significant synaptic reorganization, which results in the precise alignment of tonotopic maps from either cochlea. Whether correlated spontaneous activity in the immature cochlea drives this refinement and what the underlying cellular mechanisms are remain to be determined. One possibility is that tonotopy is relayed to auditory nuclei by the correlated activity of small groups of neighboring (tonotopically similar) cells, compared to the uncorrelated activity of non-neighboring (tonotopically distinct) cells. However, the observation of spatially inhomogeneous fir-

ing patterns between basal and apical hair cells raises the intriguing possibility that the temporal structure of IHC firing rates contains relevant instruction for guiding tonotopy and for establishing precise frequency tuning of downstream auditory neurons. Further support for this model comes from recent evidence that shows that synaptic release at IHC terminals is dependent on the pattern of action potential activity (Johnson et al., 2013).

With increased understanding of the cellular mechanisms underlying the generation of correlated spontaneous activity in IHCs, combined with directed transgenic and optogenetic manipulations, researchers will be able to alter IHC activity in controlled ways and test the effects of altered firing patterns on tonotopic refinement in auditory nuclei.

Circuit formation in the developing motor system

Before adult synaptic connectivity is established, neurons in the developing spinal cord exhibit periodic bursts of spontaneous activity that are correlated among neighboring cells and propagate down the length of spinal cord segments (O'Donovan, 1999) (Fig. 2.1 C). During early stages of development, this spontaneous network activity (SNA) is driven primarily by depolarizing GABA and glycine, while at later stages it is driven primarily by glutamate and acetylcholine (Momose-Sato and Sato, 2013). Mature connectivity is established once GABA signaling becomes inhibitory. SNA events occur at a frequency of approximately once per 1 to 3 minutes and occur synchronously between left and right sides of the spinal cord. SNA should not be confused with brainstem-driven correlated activity that occurs during later postnatal developmental stages, before central pattern generator circuits are functional (Nishimaru and Kudo, 2000). This evoked, correlated activity alternates between left and right sides of the spinal cord and is thought to contribute to the development of locomotion, which shows similar alternating activity patterns.

Correlated spontaneous depolarizations of motoneurons are thought to drive early spontaneous limb movements of developing embryos (Blumberg et al., 2013; Crisp et al., 2011; Crisp et al., 2008), a phenomenon that was first observed several decades ago (Hamburger and Balaban, 1963; Ripley and Provine, 1972). In addition, SNA has been implicated in several aspects of spinal cord circuit development, including axon pathfinding, changes in connectivity, cellular excitability, maturation of synaptic strength, and possibly functional circuit refinement (reviewed in Wenner, 2012). For example, the developing chick embryo shows reorganization of an inhibitory interneuron spinal cord circuit over the period of spontaneous activity, where GABAergic projections undergo functional refinement of initially coarse synaptic projections (Xu et al., 2007). However, unlike sensory systems, motor systems are not organized in spatial, sensory

maps. Thus, whether the precise patterns of spontaneous activity are necessary for the correct development of spinal circuits, in an analogous process to the refinement of sensory maps, remains an open question.

Recently, optogenetic tools have been used to address this question. One approach has been to use ChR2 to alter the firing properties of spinal cord motor neurons (Crisp et al., 2011; Kastanenka and Landmesser, 2010). For example, in wild type Drosophila, spontaneous motor neuron activity first drives disorganized muscular contractions at 17 hours post-fertilization (hpf). Contractions rapidly become coordinated, with the first peristaltic wave—a sequential activation of muscle segments from posterior to anterior— occurring approximately one hour later, at 18.25 hpf. ChR2 was expressed in all neurons and used to change the pattern of activity. Stimulating all neurons at 1 Hz from 17–18 hpf caused a delay of up to 90 minutes in the onset of mature peristaltic movement, indicating that the endogenous frequency of spontaneous neuronal activity is required for the normal maturation of coordinated motor function (Crisp et al., 2011).

In another example, the frequency of spontaneous network events was found to be required for normal motoneuron axon guidance in the developing chick (Kastanenka and Landmesser, 2010). Blocking or slowing the frequency of spontaneous events in the developing spinal cord using the GABA-A receptor antagonist picrotoxin results in marked motoneuron pathfinding errors axons in the limb (Hanson and Landmesser, 2004). However, normal pathfinding was rescued when endogenous patterns of neural activity were restored using ChR2 activation in the presence of picrotoxin (Kastanenka and Landmesser, 2010) (Fig. 2.3). These observations suggest that axon pathfinding in developing spinal circuits does not require GABA-A receptor activation in particular, but rather depends on specific patterns of activity.

An alternative optogenetic approach has been to use the light-gated inhibitory chloride pump Halorhodopsin (NpHR) to chronically inhibit neuronal activity, as has been recently done in zebrafish (Warp et al., 2012). Spontaneous network activity has been well characterized in the developing zebrafish spinal cord (Brustein et al., 2003). Briefly, activity of ipsilateral motoneurons becomes increasingly synchronous from 18–20 hpf. By 20 hpf, synchronous bursting alternates between the ipsilateral and contralateral spinal cord (Saint-Amant and Drapeau, 2001; Warp et al., 2012). Chronic inhibition of motoneuron activity from 18–19 hpf using NpHR stimulation resulted in a reduction of correlated activity among ipsilateral neurons, up to 22 hpf (Warp et al., 2012). Furthermore, neurons located at the midline of the spinal cord showed prolonged immature spontaneous transients, suggesting that correlated spontaneous activity is essential for integration of new cells into the motor circuit.

Together, these reports suggest that early patterned spontaneous activity in the spinal cord plays an instructive role in the formation of spinal cord circuits, and in particular, that axon pathfinding and neuron integration into developing circuits depend on endogenous patterns of activity in spinal cord neurons.
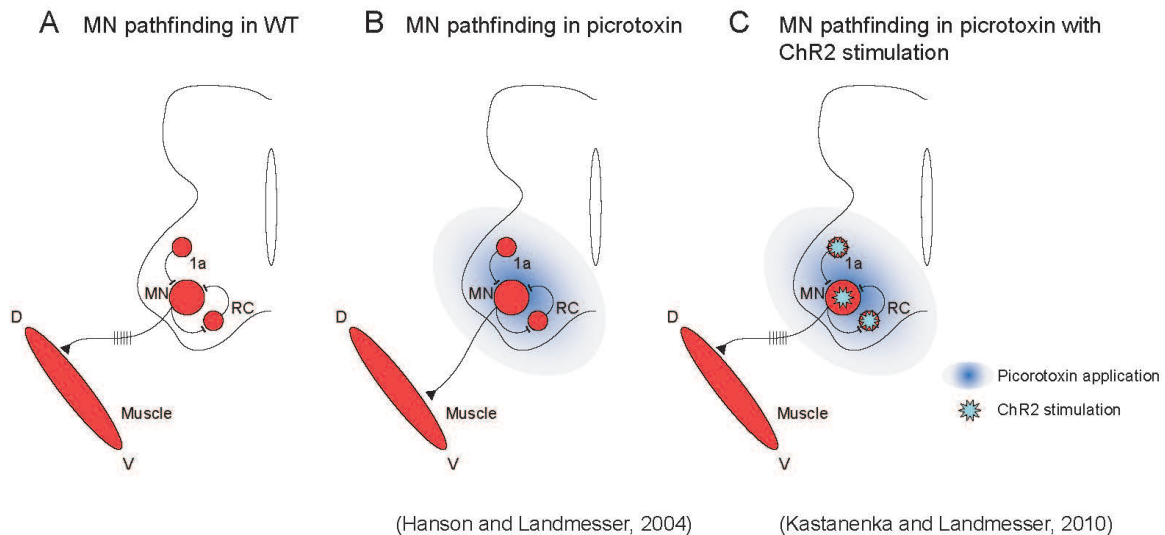
Figure 2.3: **Motoneuron pathfinding in the developing spinal cord under normal and disrupted activity patterns.** Schematic representation of motoneuron pathfinding in the developing spinal cord during normal development (A), in the presence of the GABA-A antagonist picrotoxin (B), and in the combination of picrotoxin and ChR2 stimulation (C). V: ventral, D: dorsal, MN: motoneuron, RC: Renshaw cell, 1a: 1a inhibitory interneuron; ChR2: channelrhodopsin-2.

Learning rules of activity-dependent circuit maturation

Although the refinement and maturation of sensory maps and motor circuits are considered to be activity-dependent, the learning rules that drive circuit refinement remain largely unknown. Based on studies in frogs and fish, the prevailing model of activity-dependent circuit refinement in the developing visual system is Hebbian-based, in which connections between pre- and postsynaptic cells that undergo coincident activation are strengthened and stabilized while those that do not are weakened and lost (Ruthazer and Cline, 2004). In these species, vision matures early and there is no evidence of correlated spontaneous activity (Demas et al., 2012). The same learning rules have been applied in mammals for how the repeated and persistent stimulation of a postsynaptic cell during periods of correlated spontaneous activity might drive similar refinement

processes (for reviews, see Butts, 2002; Huberman et al., 2008; Katz and Shatz, 1996). However, many studies that have addressed this question alter pre- and postsynaptic neural activity in conjunction with each other. Therefore, it remains unknown whether non-Hebbian mechanisms—which require activation of either a pre- or a postsynaptic cell but not coincident activation of both—contribute to circuit refinement during development. Below, we discuss recent progress made toward this question from studies in the developing visual system. In addition, we summarize recent insights gained from computer models into the learning rules that underlie circuit refinement.

Activity-dependent competition in the developing visual system

Eye-specific segregation in the dLGN combines Hebbian and non-Hebbian instruction

Eye-specific segregation in the dLGN has long been studied as an example of activity-dependent competition (for reviews, see Huberman et al., 2008; Katz and Shatz, 1996). In the classic model, the formation of eye-specific regions depends on a Hebbian-based learning rule, in which dominant inputs become stronger at the expense of weaker ones. In particular, ipsilateral inputs are thought to drive contralateral inputs out of the ipsilateral domain (reviewed in Torborg and Feller, 2005). Several studies that alter the relative activity of RGCs from either eye support this model. For example, blocking or increasing the frequency of waves in one eye results in the less active eye losing axonal territory to more active eye. In contrast, increasing activity equally in both eyes has no effect on segregation (reviewed in Huberman et al., 2008). Further support for this model comes from studies that show that segregation combines synaptic strengthening via LTP-like mechanisms and synaptic weakening via LTD-like mechanisms (Butts et al., 2007; Shah and Crair, 2008; Ziburkus et al., 2009). In addition, there is strong evidence that homeostatic mechanisms of plasticity exist during development to dynamically adjust and stabilize nascent synapses (Gonzalez-Islas and Wenner, 2006; Krahe and Guido, 2011, reviewed in Turrigiano and Nelson, 2004; Wenner, 2011). One interesting hypothesis is that some of the perturbations to retinal waves alter levels of activity in such a way to produce compensatory changes in synaptic strength, which may contribute to retinotopic or segregation defects.

Recently, single RGC axon reconstructions in the dLGN have revealed that eye-specific segregation involves the combination of two processes: the elaboration and refinement of appropriately-targeted axon arbors together with the elimination of inappropriately targeted ones (Dhande et al., 2011) (Fig. 2.4 A). Interestingly, these two processes appear to be distinct from one another. This was recently shown using a genetic approach to selectively reduce synaptic glutamate release from ipsilateral-projecting RGCs, while otherwise maintaining normal spontaneous retinal activity (Koch et al., 2011) (re-

fer to Fig. 2.4 B). This manipulation prevented coincident firing between ipsilateral RGC axons and their targets. Thus, a classic Hebbian model of competition would predict that these release-deficient axons should lose axonal territory to their more active counterparts. In agreement with this model, contralateral projections failed to be eliminated from the ipsilateral region. However, the ipsilateral axons refined and maintained their normal axon termination zones within the ipsilateral region. These findings therefore suggest that non-Hebbian mechanisms, requiring activation of just the presynaptic cell but not coincident activation of both pre- and postsynaptic cells, contribute to the synaptic stabilization of ipsilateral RGC axons in the dLGN. Although little is known about the mechanisms of non-Hebbian plasticity, calcium influx via voltage-dependent calcium channels or synaptic release of a factor such as a monoamine neurotransmitter could provide the molecular basis of this synaptic stabilization (Koch et al., 2011).

A similar finding was observed in another study, in which a subset of axons that normally project to the ipsilateral dLGN were genetically directed to project contralaterally (Rebsam et al., 2009) (refer to Fig. 2.4 C). This was achieved using a knockout mouse that lacks EphB1 (EphB1 KO), a molecular determinant for laterality, which is expressed in approximately 50% of ipsilateral-projecting RGCs. Eye-specific segregation was disrupted in the dLGN of EphB1 KO mice, showing significant overlap between ipsilateral and contralateral fibers compared to wild type, perhaps as a consequence of reduced ipsilateral fiber number or altered synaptogenesis (Rebsam et al., 2009). However, the remaining ipsilateral axons refined to form a small ipsilateral region. In addition, the misrouted axons, which targeted the correct topographic location but in the opposite dLGN, segregated from the other contralateral axons and refined to from an "ectopic patch". Both the ipsilateral and ectopic patches were eliminated upon pharmacological blockade of retinal waves, indicating that their refinement was activity-dependent. This finding is in contrast with a study lacking Ten-m2 (Ten-m2 KO), a member of the teneurin family of glycoproteins, which show a decrease number of ipsilateral projections but normal segregation of ipsi- and contralateral inputs (Young et al., 2013). It would be interesting to combine these genetic manipulations with reconstructions of single axon termination zones to observe whether the process of axon branch refinement occurs in a similar manner to wild type mice.

These studies are consistent with the model that the elimination of contralateral axons may follow learning rules based on Hebbian competition requiring activation of the postsynaptic cell, but that the refinement and stabilization of ipsilateral axons may depend predominantly on the activity of the presynaptic cell, thus perhaps pointing to a non-Hebbian learning rule. Recent studies have implicated activity-dependent activation of immune molecules (reviewed in Boulanger, 2009) as well as signals derived from microglia (Schafer et al., 2012) and astrocytes (reviewed in Clarke and Barres, 2013) as

perhaps being key to this process.

Learning rules for retinotopy in the SC differ for monocular and binocular inputs

Single axon reconstructions of RGC projections to the SC have shown that axon termi-
nals initially ramify coarsely over their approximate termination zone, with some sparse
collateral branches that overshoot the appropriate region. During development, these
coarse arbors refine to precise locations, combining an increase in arbor complexity to-
gether with an elimination of inappropriate collateral branches (Dhande et al., 2011).
This refinement has been shown to be dependent on the presence of distance-dependent
correlated firing between neighboring RGCs, with the requirement of nearby cells being
highly correlated in their firing and distant cells being uncorrelated. In this way, the
target cells in the SC may act as coincident detectors that measure the proximity of the
afferent RGCs to one another (reviewed in (Eglen et al., 2003)).

More recently, there is evidence that competition amongst same-eye inputs might
drive retinotopic refinement in the SC (Furman and Crair, 2012; Furman et al., 2013).
Whether this competition follows traditional Hebbian learning rules remains unknown.
Interestingly, the presence of binocular competition perturbs normal retinotopic devel-
opment. For example in $\beta2$(TG) mice, in which expression of $\beta2$-containing nAChRs is
restricted to the ganglion cell layer resulting in short-range waves, the retinotopic defects
seen in $\beta2$-nAChR KO mice were rescued only in monocular regions of the SC but not
in the binocular (anteromedial) region (Xu et al., 2011) (Fig. 2.2 D). Similarly, when ChR2
was expressed in RGCs and stimulated to drive RGC activity, retinotopy of ipsilateral
axons in the SC was perturbed when eye-specific segregation was also disrupted (during
synchronous stimulation of both eyes, Figs. 2.2 G–H) but was normal when segregation
occurred normally (during asynchronous stimulation of both eyes, Figs. 2.2 E–F) (Zhang
et al., 2012b). These observations suggest that eye-specific segregation in the SC might
first be necessary in order for axons to refine into retinotopic maps, and that competi-
tion between inputs from different eyes might provide conflicting signals that obstruct
retinotopic map formation. Thus, the learning rules that drive retinotopic refinement
in monocular regions of the SC may be inadequate to drive refinement in the presence
of binocular competition. This is in contrast to what is observed in the dLGN, where
segregation and refinement appear to be somewhat independent processes.

Insights into mechanisms of circuit refinement from theoretical models

Computational models of retinal waves have provided a means to probe how sponta-
neous activity patterns are generated and how they contribute to network refinement.
Since many circuit elements underlying the generation and propagation of cholinergic
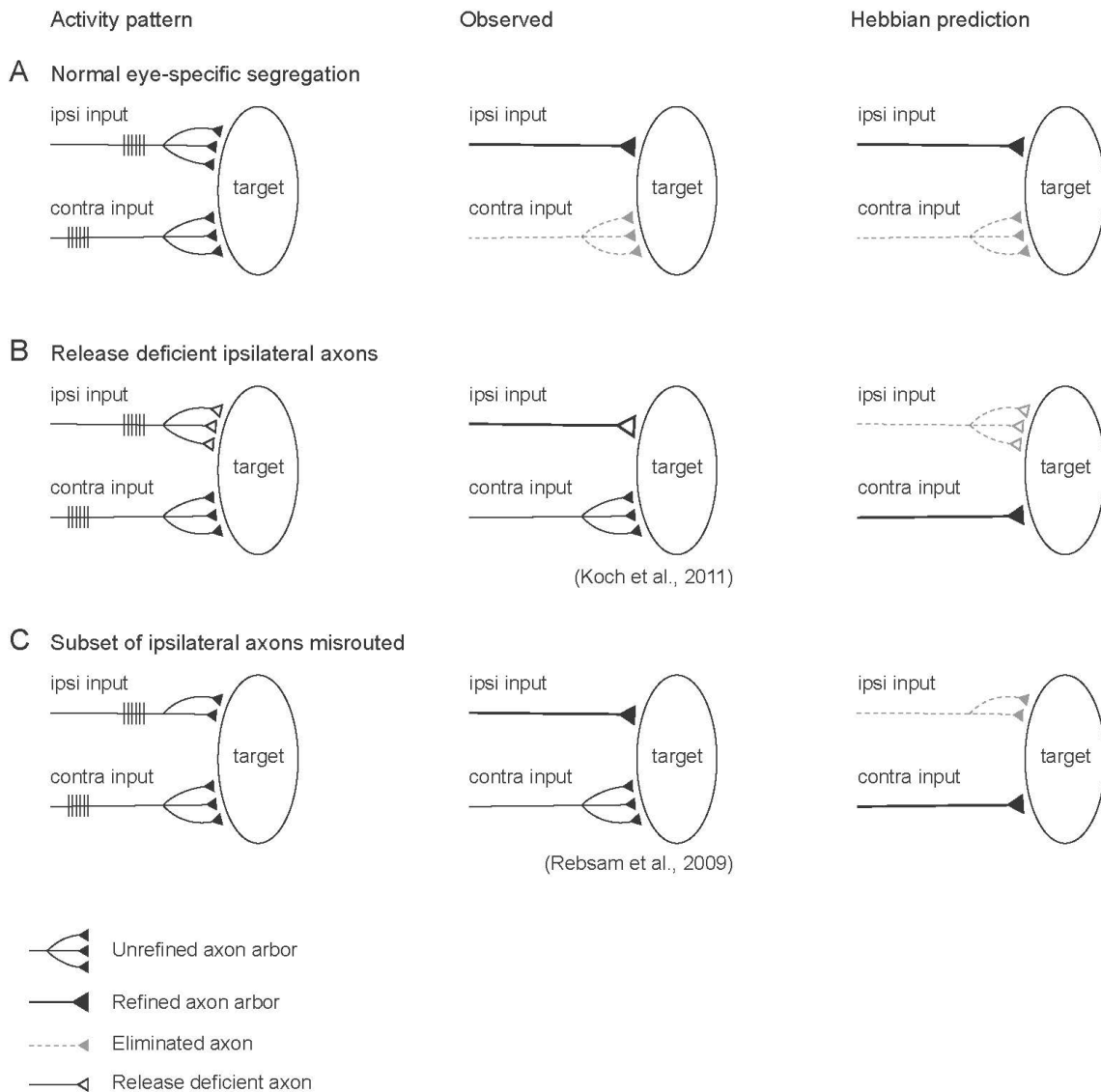
Figure 2.4: **Activity-dependent competition during eye-specific segregation in the dLGN under normal and disrupted glutamate release and targeting** Schematic representations of activity-dependent competition during eye-specific segregation in the dLGN for normal development (A), glutamate release-deficient ipsilateral projecting axons (B) and for a subset of ipsilateral axons that were genetically misrouted to project contralaterally (C), as described in the text. Left panels show afferent activity patterns; middle panels show experimental observation; right panels show prediction according to a Hebbian model of competition.

retinal waves are known—for example, they are initiated by spontaneously-depolarizing starburst amacrine cells (SACs), and their spatial boundaries are set by the slow after-hyperpolarization (sAHP) of SACs, which occurs after a wave passes (Ford et al., 2012)—modeling parameters of cholinergic waves have been based on experimental observations. This has led to the generation of models in which simulated waves closely match the spatial and temporal properties of experimentally observed waves (Ford et al., 2012; Gjorgjieva and Eglen, 2011; Godfrey and Swindale, 2007; Hennig et al., 2009; Markowitz et al., 2012).

Simulated waves generated from these models have served as input for computational studies of network refinement (Butts et al., 2007; Godfrey et al., 2009; Grimbert and Cang, 2012; Tsigankov and Koulakov, 2006; Yates et al., 2004). In general, these refinement models are made of up two parts. The first part includes molecular guidance cues and chemoaffinity ephrin/Eph gradients, which dominate the early stage of development by guiding axon growth to the correct axis, thus setting up global retinotopic structure, in agreement with experimental observation (Feldheim and O'Leary, 2010; Simpson and Goodhill, 2011; Triplett and Feldheim, 2012). The second part is based on activity-dependent processes that underlie subsequent refinement of connections, and has mainly been implemented as a form of Hebbian-based plasticity, which drives refinement via burst-timing dependent synaptic strengthening and weakening between simulated RGC axons and recipient dendritic arbors that are coincidently active (Butts et al., 2007; Godfrey et al., 2009; Grimbert and Cang, 2012; Tsigankov and Koulakov, 2006). One of the major findings produced by this approach is that burst-based learning rules that integrate activity over the 1-sec time scale more accurately represent experimental data in comparison to spike-based learning rules that integrate activity over the 10-ms time scale (Butts and Kanold, 2010; Butts et al., 2007; Godfrey et al., 2009). This finding was recently confirmed with experimental data described above (Zhang et al., 2012b).

Recent insights have come from models that included an additional activity-dependent component that represents axonal competition on much longer time scales than synaptic plasticity (Fig. 2.5). For example, one model implemented a rule in which activity-dependent axonal release of trophic factors promotes self-growth while inhibiting growth of neighboring axons (Godfrey et al., 2009). In a second example, the model implemented a rule in which activity-dependent competition for limited, pre-existing resources in the target areas functioned to constrain the terminal field of RGC axons (Grimbert and Cang, 2012; Tsigankov and Koulakov, 2006). Hence, the action potentials generated from spontaneous network activity may be driving multiple activity-dependent processes functioning on different time scales. Furthermore, since these mechanisms depend on presynaptic activity but not postsynaptic activity, they might be considered a form of non-Hebbian, activity-dependent refinement.

By allowing for systematic variation of the time scales over which learning rules operate and of the spatial structure of correlated firing, models have led to a deeper understanding of what features of retinal waves might be important for driving refinement. One interesting example compares the modeling and experimental results for the effects of β2-nAChR KO firing patterns on retinotopic refinement in the SC. Though β2-nAChR KO exhibit waves, their correlation structure is distinct from WT. Specifically, WT waves show correlation patterns in which the firing properties of neighboring cells are highly correlated, while those of more distant cells are uncorrelated (Wong et al., 1993). β2-nAChR KO waves also show a decreasing correlation index as a function of increasing intercellular distance, but neighboring cells are less correlated than for WT waves, while distant cells are more correlated (Stafford et al., 2009; Sun et al., 2008). Nonetheless, retinotopic refinement is strongly disrupted in β2-nAChR KO mice despite the underlying wave feature of a decrease in correlation index.

A potential explanation for this was provided in a recent model by Godfrey (Godfrey et al., 2009). In this study, refinement was found to be robust to extreme manipulations of some spatiotemporal properties of waves, such as wave velocity, frequency and size, suggesting a limited contribution of these parameters to network refinement. This aspect of the model was experimentally confirmed by the finding that wave size did not influence retinotopy for SC regions that receive monocular input (Xu et al., 2011). When the correlation patterns of simulated waves were modified to match those observed in β2-nAChR KO mice, retinotopic refinement was impaired—axon terminals and RGC receptive field radii were 2 to 2.5-fold greater than those for simulated WT waves. However, this impairment was less severe than that observed experimentally in β2-nAChR KO mice. Hence, they concluded that the correlation properties of waves only partially contribute to retinotopy. These observations support the idea that the relative level of activity between competing cells is more significant than a cell's absolute level of activity in driving refinement, and suggest that many mechanisms likely work in tandem to optimize refinement.

In summary, models of cholinergic waves and network refinement have provided a means for exploring how molecular and activity-dependent mechanisms interact. In addition, they allow researchers to make predictions and apply constraints on the underlying biological variables, as well as provide a consistency check with experiment. The accumulation of more quantitative experimental data and their application to models will offer the potential to tease apart the key processes and interactions that underlie network refinement during development.
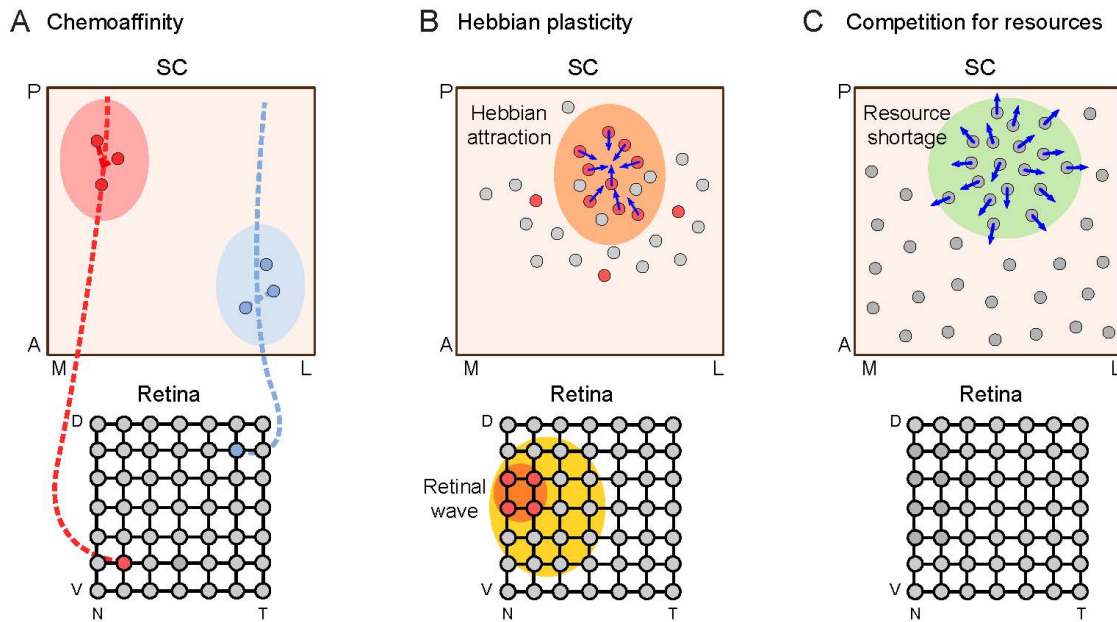
Adapted from Grimbert and Cang, 2012

Figure 2.5: **Components used in theoretical models for retinotipic refinement** Schematic representation of components used in theoretical models for retinotopic refinement: chemoaffinity gradients (A), Hebbian plasticity (B) and competition for resources (C). First, chemoaffinity gradients in the form of ephrin/Eph gradients guide RGC axons to their approximate retinotopic location and to form selective arborization. Second, a Hebbian plasticity component strengthens the synapses of cells that are driven to fire together by retinal waves. Third, competition for limited resources in the target areas function to constrain the termination zone of RGC axons. V: ventral, D: dorsal, T: temporal, N: nasal, A: anterior, P: posterior, M: medial, L: lateral. (Adapted from Grimbert and Cang, 2012).

Conclusions

Approximately two decades after the discovery of correlated spontaneous activity in developing neural circuits, there is considerable evidence that the endogenous patterns of activity drive the refinement and formation of specific features of adult circuits and sensory maps. Many insights have been gained into the learning rules that underlie how afferent patterns of activity dictate refinement of downstream targets. These learning rules likely include a combination of Hebbian and non-Hebbian activity-dependent processes, the molecular underpinnings of which remain to be elucidated. In addition, the learning rules that underlie the segregation of competing axons and the stabilization and refinement of single axon arbors do not appear to be universal across brain regions

or across cell-types, illustrating that multiple factors work in tandem to achieve normal circuit formation. With the continued development of sophisticated genetic manipulations and optogenetic approaches to alter activity in constrained spatial and temporal patterns, combined with a deeper understanding of the plasticity mechanisms that decode the patterns, researchers will continue to unravel the mechanisms underlying how correlated spontaneous activity drives the maturation of nascent circuits.

References for Table 2.1

1. Shatz CJ, Stryker MP (1988) Prenatal tetrodotoxin infusion blocks segregation of retinogeniculate afferents. *Science* 242:87–89.

2. Cook PM, Prusky G, Ramoa AS (1999) The role of spontaneous retinal activity before eye opening in the maturation of form and function in the retinogeniculate pathway of the ferret. *Vis Neurosci* 16:491–501.

3. Penn AA, Riquelme PA, Feller MB, Shatz CJ (1998) Competition in retinogeniculate patterning driven by spontaneous activity. *Science* 279:2108–2112.

4. Rossi FM et al. (2001) Requirement of the nicotinic acetylcholine receptor beta 2 subunit for the anatomical and functional development of the visual system. *Proc Natl Acad Sci USA* 98:6453–6458.

5. Huberman AD et al. (2003) Eye-specific retinogeniculate segregation independent of normal neuronal activity. *Science* 300:994–998.

6. Huberman AD, Stellwagen D, Chapman B (2002) Decoupling eye-specific segregation from lamination in the lateral geniculate nucleus. *J Neurosci* 22:9419–9429.

7. Cang J et al. (2005) Development of precise maps in visual cortex requires patterned spontaneous activity in the retina. *Neuron* 48:797–809.

8. Sun C, Speer CM, Wang G-Y, Chapman B, Chalupa LM (2008) Epibatidine application in vitro blocks retinal waves without silencing all retinal ganglion cell action potentials in developing retina of the mouse and ferret. *J Neurophysiol* 100:3253–3263.

9. Stellwagen D, Shatz CJ (2002) An instructive role for retinal waves in the development of retinogeniculate connectivity. *Neuron* 33:357–367.

10. Speer CM, Sun C, Chapman B (2011) Activity-dependent disruption of intersublaminar spaces and ABAKAN expression does not impact functional on and off organization in the ferret retinogeniculate system. *Neural Development* 6:7.

11. McLaughlin T, Torborg CL, Feller MB, O'Leary DDM (2003) Retinotopic map refinement requires spontaneous retinal waves during a brief critical period of development. *Neuron* 40:1147–1160.

12. Muir-Robinson G, Hwang BJ, Feller MB (2002) Retinogeniculate axons undergo eye-specific segregation in the absence of eye-specific layers. *J Neurosci* 22:5259–5264.

13. Xu H-P et al. (2011) An instructive role for patterned spontaneous retinal activity in mouse visual map development. *Neuron* 70:1115–1127.

14. Torborg CL, Feller MB (2005) Spontaneous patterned retinal activity and the refinement of retinal projections. *Prog Neurobiol* 76:213–235.

15. Blankenship AG et al. (2011) The role of neuronal connexins 36 and 45 in shaping

spontaneous firing patterns in the developing retina. *J Neurosci* 31:9998–10008.

16. Demas J et al. (2006) Failure to maintain eye-specific segregation in nob, a mutant with abnormally patterned retinal activity. *Neuron* 50:247–259.

17. Renna JM, Weng S, Berson DM (2011) Light acts through melanopsin to alter retinal waves and segregation of retinogeniculate afferents. *Nat Neurosci* 14:827–829.

18. Dhande OS et al. (2012) Role of adenylate cyclase 1 in retinofugal map development. *J Comp Neurol* 520:1562–1583.

19. Plas DT, Visel A, Gonzalez E, She WC, Crair MC (2004) Adenylate Cyclase 1 dependent refinement of retinotopic maps in the mouse. *Vision Res* 44:3357–64.

20. Upton AL et al. (1999) Excess of serotonin (5-HT) alters the segregation of ispilateral and contralateral retinal projections in monoamine oxidase A knock-out mice: possible role of 5-HT uptake in retinal ganglion cells during development. *J Neurosci* 19:7007–24.

21. Upton AL et al. (2002) Lack of 5-HT(1B) receptor and of serotonin transporter have different effects on the segregation of retinal axons in the lateral geniculate nucleus compared to the superior colliculus. *Neuroscience* 111:597–610.

22. Pham TA, Rubenstein JL, Silva AJ, Storm DR, Stryker MP (2001) The cre/creb pathway is transiently expressed in thalamic circuit development and contributes to refinement of retinogeniculate axons. *Neuron* 31:409–20.

23. Menna E, Cenni MC, Naska S, Maffei L (2003) The anterogradely transported BDNF promotes retinal axon remodeling during eye specific segregation within the LGN. *Mol Cell Neurosci* 24:972–83.

24. Naska S, Cenni MC, Menna E, Maffei L (2004) ERK signaling is required for eye-specific retino-geniculate segregation. *Development* 131:3559–3570.

25. Huberman AD, Dehay C, Berland M, Chalupa LM, Kennedy H (2005) Early and rapid targeting of eye-specific axonal projections to the dorsal lateral geniculate nucleus in the fetal macaque. *J Neurosci* 25:4014–4023.

26. Pfeiffenberger C et al. (2005) Ephrin-As and neural activity are required for eye-specific patterning during retinogeniculate mapping. *Nat Neurosci* 8:1022–1027.

27. Guido W (2008) Refinement of the retinogeniculate pathway. *J Physiol (Lond)* 586:4357–4362.

28. Datwani A et al. (2009) Classical MHCI Molecules Regulate Retinogeniculate Refinement and Limit Ocular Dominance Plasticity. *Neuron* 64:463–470.

29. Syken J, Grandpre T, Kanold PO, Shatz CJ (2006) PirB restricts ocular-dominance plasticity in visual cortex. 313:1795–1800.

30. Huh GS et al. (2000) Functional requirement for class I MHC in CNS development and plasticity. 290:2155–9.

31.   Bjartmar L et al. (2006) Neuronal pentraxins mediate synaptic refinement in the developing visual system. *J Neurosci* 26:6269–6281.

32.   Koch SM, Ullian EM (2010) Neuronal pentraxins mediate silent synapse conversion in the developing visual system. *J Neurosci* 30:5404–5414.

33.   Xu H-P et al. (2010) The immune protein CD3zeta is required for normal development of neural circuits in the retina. *Neuron* 65:503–515.

34.   Stevens B et al. (2007) The classical complement cascade mediates CNS synapse elimination. *Cell* 131:1164–1178.

35.   Schafer DP et al. (2012) Microglia sculpt postnatal neural circuits in an activity and complement-dependent manner. *Neuron* 74:691–705.

36.   Young TR et al. (2013) Ten-m2 Is Required for the Generation of Binocular Visual Circuits. *J Neurosci* 33:12490–12509.

37.   Leamey CA et al. (2007) Ten_m3 regulates eye-specific patterning in the mammalian visual pathway and is required for binocular vision. *PLoS Biol* 5:e241.

38.   Leamey CA, Ho-Pao CL, Sur M (2003) Role of calcineurin in activity-dependent pattern formation in the dorsal lateral geniculate nucleus of the ferret. *J Neurobiol* 56:153–162.

39.   Noutel J, Hong YK, Leu B, Kang E, Chen C (2011) Experience-Dependent Retinogeniculate Synapse Remodeling Is Abnormal in MeCP2-Deficient Mice. *Neuron* 70:35–42.

40.   Blank M et al. (2011) The Down syndrome critical region regulates retinogeniculate refinement. *J Neurosci* 31:5764–5776.

41.   Culican SM, Bloom AJ, Weiner JA, DiAntonio A (2009) Phr1 regulates retinogeniculate targeting independent of activity and ephrin-A signalling. *Mol Cell Neurosci* 41:304–312.

Chapter III

Retinal Wave Properties in Transgenic Mouse Models

This Chapter consists of my contribution to two separate collaborations, one with Martina Blank from the Garner Lab at Stanford University and the other with Hanmi Lee from the Shatz Lab at Stanford University. The research focus of the Garner Lab is on the molecular and cellular mechanisms of synapse formation, stability and plasticity, and their contribution the neurodevelopmental disorders Down syndrome and autism. The research focus of the Shatz Lab is on the molecular and cellular mechanisms underlying synaptic strengthening and weakening in the developing visual system. In both cases, my contribution was to test whether retinal wave patterns were disrupted in transgenic mouse lines that showed altered eye specific segregation in the dorsal lateral geniculate nucleus (dLGN). For the Garner Lab, the transgenic mouse was a Down syndrome mouse model that shows enhanced eye specific segregation in the dLGN (Ts1Rhr mouse); for the Shatz Lab, the transgenic mouse was a mouse lacking the Major Histocompatibility Class I (MHCI) molecules H2-Kb and H2-Db, which shows a failure of eye specific segregation in the dLGN (KbDb KO mouse). The results from these studies were published in Blank et al., *Journal of Neuroscience* (2011) and Lee et al, *Nature* (2014), respectively.

Relevant publications:

Blank, M., Fuerst, P.G., Stevens, B., Nouri, N., **Kirkby, L. A.**, Warrier, D., Barres, B.A., Feller, M.B., Huberman, A.D., Burgess, R.W., Garner, C. C., (2011). The Down syndrome critical region regulates retinogeniculate refinement. *J Neurosci* **31**, 5764–5776.

Lee, H., Brott, B. K., **Kirkby, L. A.**, Adelson, J. D., Cheng, S., Feller, M. B., Datwani, A., Shatz, C. J., (2014). Synapse elimination and learning rules co-regulated by MHC Class I H2-Db. *Nature* **509**, 195–200.

Abstract

During development, retinal ganglion cell (RGC) projections to their primary targets in the brain undergo significant refinement and sculpting, resulting in the formation of sensory maps. Map formation is driven by a combination of molecular guidance cues and activity-dependent processes, relying on spontaneous activity generated within the retina. Eye-specific segregation in the dorsal lateral geniculate nucleus (dLGN)—a map reflecting inputs from left and right eyes—is enhanced in a Down syndrome mouse model (Ts1Rhr mouse) and reduced in a mouse lacking the Major Histocompatibility Class I (MHCI) molecules H2-Kb and H2-Db (KbDb KO mouse). Here, we test whether spontaneous patterns of retinal activity, termed retinal waves, are altered in Ts1Rhr and KbDb KO mice. We measured spontaneous activity of many cells simultaneously using multi-electrode array recordings of retinas isolated from wild type (WT), Ts1Rhr and KbDb KO mice. We found that Ts1Rhr and KbDb KO retinal wave patterns were indistinguishable from WT over the full period of development. These observations suggest that defects in the segregation patterns observed in Ts1Rhr and KbDb KO mice are not due to indirect disruption of retinal wave properties, but rather due to molecular influence of downstream targets.

Introduction

Retinal ganglion cell projections to the dorsal lateral geniculate nucleus (dLGN) of the thalamus produce a map that reflects input from left and right eyes, referred to as eye-specific segregation. Initially, contralateral axons project over the entire area while ipsilateral axons target a smaller patch that overlaps with the larger contralateral domain. Over the course of development, contralateral axons are expelled from the ipsilateral patch and ipsilateral terminals refine and stabilize within the patch. This refinement occurs before eye opening in mice, over the period of development corresponding to spontaneous retinal waves.

Endogenous patterns of retinal waves have been shown to be instructive in the formation of eye-specific maps (reviewed in Kirkby et al., 2013). In addition, studies have revealed diverse molecular candidates that influence segregation patterns (refer to Table 2.1). An important control is to test whether these candidates disrupt patterns of retinal waves that regulate segregation. In this study, we assess retinal wave properties of two transgenic mouse models that show altered eye-specific segregation in the dLGN: a Down syndrome mouse model with segmental trisomy for the Down syndrome critical region (DSCR) of the genome (Ts1Rhr), and mice lacking the major histocompatibility complex (MHC) class I molecules H2-Db and H2-Kb (KbDb KO). Below, we give an

overview of the phenotype for each mouse line.

Studies of Down syndrome mouse models have revealed alterations in neuronal circuit development that occurs before the onset of sensory experience (reviewed in Gotti et al., 2011). Eye-specific segregation in the developing visual system provides an elegant system to explore whether trisomy influences early circuit refinement. In particular, visual system development is relevant to individuals with Down syndrome, who often show ocular abnormalities (Little et al., 2009; Cregg et al., 2003). Eye-specific segregation is assayed anatomically using vitreal injection of cholera toxin fused to a fluorescent dye, which labels most RGCs and their axon projections. By labeling one eye red and the other eye green, the extent of segregation is measured by the fraction of the LGN that contains red-only or green-only fluorescence (segregated regions), compared to the fraction that contains an overlap of both red and green fluorescence (unsegregated region). In Ts1Rhr mice, eye-specific segregation is enhanced, where the percent of ipsilateral-contralateral overlap in the dLGN is significantly reduced compared to wild type controls (Blank et al., 2011).

Molecules that have been more commonly implicated in eye-specific segregation are immune molecules, in particular class I major histocompatibility complexes (Huh et al., 2000), neuronal pentraxins (Bjartmar et al., 2006; Koch and Ullian, 2010), and components of the classical complement cascade (Stevens et al., 2007). In mice lacking the MHC class I genes H2-Db and H2-Kb (KbDb KO), eye-specific segregation is impaired, where the percent of ipsilateral-contralateral overlap in the dLGN is significantly greater than wild type controls (Lee et al., 2014). These segregation defects are rescued when neuronal H2-Db is expressed in KbDb KO mice, indicating that H2-Db alone causes the defects. In addition, long term depression (LTD), which weakens and eventually eliminates synapses, but not long term potentiation (LTP), which strengthens and stabilizes synapses, is impaired at retino-geniculate synapses.

Here, we tested whether spontaneous retinal activity patterns were altered in Ts1Rhr and KbDb KO mice using multi-electrode array recordings of spontaneous activity in isolated retinas. We found that retinal waves were unaltered relative to WT controls for both Ts1Rhr and KbDb KO mice. These observations indicate that segregation pattern defects observed in Ts1Rhr and KbDb KO mice are due to molecular influence of downstream targets and not due to a disruption of retinal wave properties.

Materials and Methods

Animals: Recordings were performed on mice aged postnatal day P4–P11 from C57BL/6 WT (Harlan Laboratories, Indianapolis), Ts1Rhr (obtained from Stanford University, Gar-

ner Lab, via Roger Reeves, Johns Hopkins), and KbDb KO mice (obtained from Stanford University, Shatz Lab, via Hidde Ploegh, Whitehead Institute). Animal procedures were approved by the University of California, Berkeley Institutional Animal Care and Use Committees and conformed to the National Institutes of Health Guide for the Care and Use of Laboratory Animals, the Public Health Service Policy, and the Society for Neuroscience Policy on the Use of Animals in Neuroscience Research. Animals were anesthetized with isofluorane, decapitated, eyes were enucleated and retinas were removed from eyecups in artificial cerebral spinal fluid (ACSF) containing the following (in mM): 119.0 NaCl, 26.2 $NaHCO_3$, 11 glucose, 2.5 KCl, 1.0 K_2HPO_4, 2.5 $CaCl_2$, and 1.3 $MgCl_2$.

Multielectrode array: Retinas were isolated from C57BL/6 wild type, Ts1Rhr and KbDb KO mice between postnatal ages P4–P11, which corresponds to the period of retinal waves but before eye opening. Isolated pieces of retina were place retinal ganglion cell side down onto a 60-electrode multi-electrode array (MEA) arranged in an 8×8 grid excluding the four corners with $10\,\mu$m diameter electrodes at $100\,\mu$m spacing (Multi Channel Systems). The retina was held in place with a weighted piece of dialysis membrane and superfused continuously with ACSF, oxygenated with 95% O2 and 5% CO2 and maintained at 32°C, pH 7.4. Each preparation was allowed to equilibrate for 20 minutes before starting data acquisition. Spontaneous firing patterns were then recorded for 60 minutes. Voltage traces on each electrode were sampled at 20 kHz and filtered between 120 and 2000 Hz. Events that crossed a spike threshold were sorted offline to identify single units using Plexon Offline Sorter software. Single units were identified by combining principle components analysis together with a valley seeking algorithm and were inspected manually. The mean firing rate of all units over the duration of the recording was calculated and units with a mean firing rate less than 10% of the overall mean firing rate were excluded from further analysis. Spike-sorted data were analyzed in MATLAB (Mathworks).

To identify bursts, we used a modified Poisson Surprise algorithm, outlined below. First, the mean interspike interval (ISI) was determined for each unit. Spike trains of three or more spikes with ISIs less than half the mean ISI for a given unit were then identified. The probability of occurrence of each spike train was then calculated from

$$P_c = \frac{e^{rt} \cdot (rt)^c}{c!}$$

where r is the mean firing rate of the unit, t is duration of the spike train and C is the number of spikes in the train. A spike train was accepted as a burst if the probability of occurrence was $P_c < 10^{-4}$. Upon identification of bursts, the burst duration, t, burst firing rate, C/t, and interburst interval (time between last spike in one burst to first spike in the next) were computed and averaged for each unit and for each retina. Mean values

for each retina were grouped according to age (P5–P8 and P10–P12) and genotype (WT, Ts1Rhr and KbDb KO). Differences between means of different genotypes within each age group were evaluated for statistical significance using a *t*-test.

To determine the spatial properties of waves, a pair-wise correlation index, *CI*, was computed as a function of distance between two cells for all spikes in the recording, using a method described previously (Wong et al., 1993; Torborg et al., 2004b). The correlation index gives a measure of the likelihood relative to chance that a pair of neurons fire together within a given time window, $\Delta t = 100$ ms, where

$$CI = \frac{N_{AB}(\Delta t) \cdot T}{N_A(t) \cdot N_B(t) \cdot (2\Delta t)}$$

$N_A B(\Delta t)$ corresponds to the number of spike pairs for which unit *B* fires within a time window $\Delta t = 100$ ms from unit *A*; $N_A(t)$ corresponds to the total number of spikes fired by unit *A* during the total recording time, *T* (and similarly for $N_B(t)$). The distance between cells was approximated as the distance between the electrodes on which the activity of the cells was recorded. The cell pairs were grouped according to their intercellular distance, and medians were computed over all cell pairs in a given distance group for each individual retina. The median correlation indices were then averaged across retinas, for each age and genotype, and plotted as a function intercellular distance.

Results

Ts1Rhr mice have normal retinal wave properties

During the first two postnatal weeks of development, correlated spontaneous retinal activity, which propagates across the retina in the form of waves, contributes to driving dLGN segregation (reviewed in Huberman et al., 2008). Retinal waves have distinct spatial and temporal properties that are critical for normal segregation. Therefore, it is possible that the enhanced segregation observed in Ts1Rhr mice is attributable to an increase in RGC firing during waves. To determine whether Ts1Rhr mice have altered spontaneous firing patterns, we performed multielectrode array recordings on retinas isolated from Ts1Rhr mice and WT littermate controls. We focused on two different age ranges, P5–P7 (which is in the middle of the period when eye specific segregation occurs in mice) and P11–P13 (after eye-specific segregation is completed), and found that Ts1Rhr mice have similar spontaneous firing patterns from littermate controls for both age ranges (Fig. 3.1).

Spikes produced by individual RGCs were identified as described in Materials and Methods (P5–P7, control, n = 207 cells from 7 retinas; Ts1Rhr, n = 231 cells from 7 retinas; P11–P13, control, n = 332 cells from 4 retinas; Ts1Rhr, n = 290 cells from 4 retinas; all retinas were from different mice). The global firing patterns of individual RGCs were similar between WT and Ts1Rhr mice (Fig. 3.1 A). To assay spatial wave characteristics, we computed a pairwise correlation index as a function of distance between two RGCs (Meister et al., 1991; Wong et al., 1993; Torborg et al., 2004b). We found no significant differences between Ts1Rhr mice and littermate controls. In all retinas, over both age ranges, the correlation index was highest for nearest neighbors and fell off smoothly with increasing intercellular distance (Fig. 3.1 B). To assay the temporal firing characteristics, we computed the following properties: mean firing rate of isolated RGCs, percentage of time a cell was bursting, interburst interval, burst duration, and firing rate during a burst. These properties were similar in Ts1Rhr mice relative to littermate controls for both age ranges (Fig. 3.1 C). Together, these recordings demonstrate that enhanced dLGN segregation in Ts1Rhr mice is not attributable to a variation in the spontaneous RGC firing patterns.

Table 3.1: p-values for temporal properties of spontaneous firing patterns for WT and Ts1Rhr mice.

	Firing rate	Percent of time bursting	Interburst interval	Burst duration	Burst firing rate
Ages P5–P7	0.33	0.94	0.44	0.36	0.27
Ages P11–P13	0.03	< 0.01	< 0.01	0.11	<0.01

KbDb KO mice have normal retinal wave properties

To assess whether KbDb KO mice have altered patterns of spontaneous activity during development, we performed multi-electrode array (MEA) experiments on retinas isolated from WT and KbDb KO mice. We recorded activity from both cholinergic waves (P5–P8) and glutamatergic waves (P10–P12) and found that KbDb KO mice have similar spontaneous firing patterns to WT over both age ranges (Fig. 3.2). To compare temporal firing properties, we computed mean firing rate, burst duration, firing rate during a burst and mean interburst interval for each single unit. These properties were similar in KbDb KO mice compared to WT (Fig. 3.2 A). To compare spatial correlations of firing patterns, we computed a pairwise correlation index as a function of distance be-
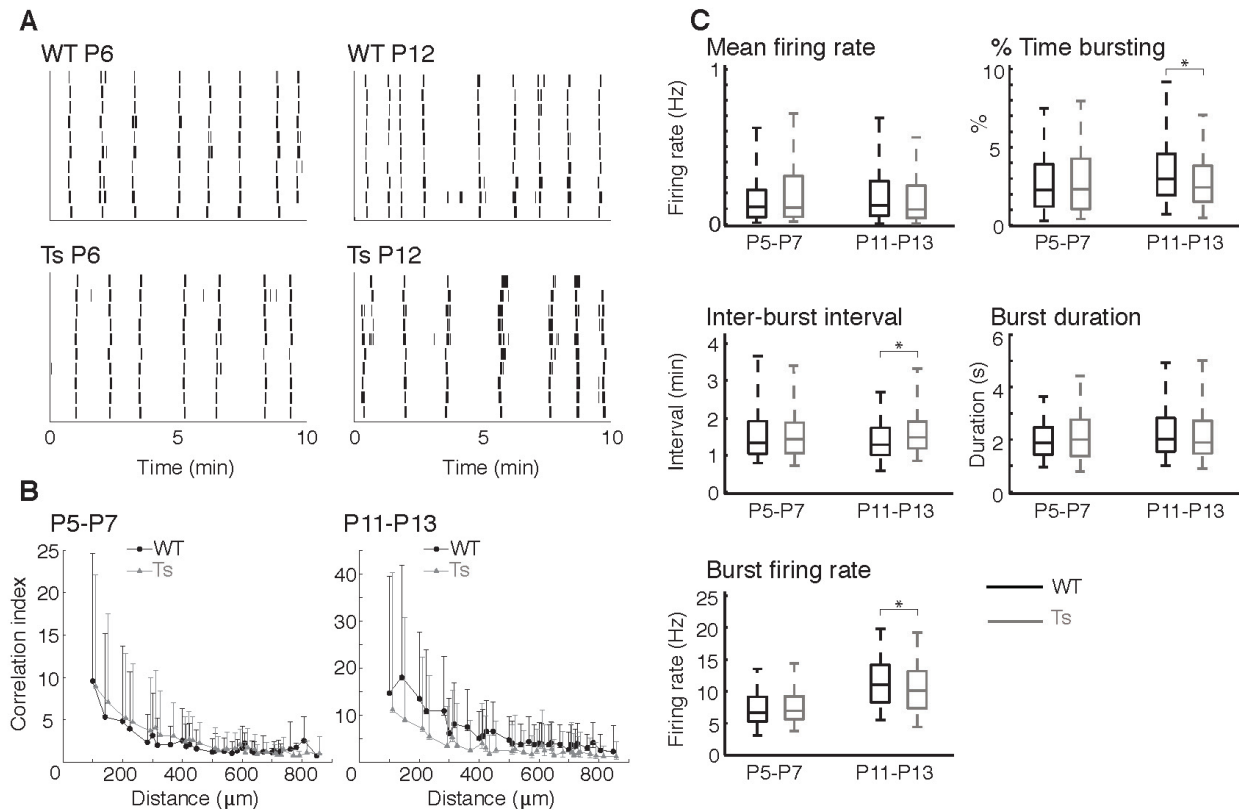
Figure 3.1: **Ts1Rhr mice have normal spontaneous retinal activity during development.**
(A) Raster plots of 10 single-unit spike trains over a 10 min interval, recorded from retinas isolated from a P6 WT (top left) and Ts1Rhr (Ts, bottom left) littermate and a P12 WT (top right) and Ts (bottom right) littermate. (The 10 single units selected corresponded to those with the highest mean firing rate in each sample.) (B) Pairwise correlation index as a function of intercellular distance for WT (black circles) and Ts (gray triangles) littermates at P5–P7 (left, averaged across 7 retinas per genotype) and P11–P13 (right, averaged across 4 retinas per genotype). The data points correspond to median values and the upper error bars are the 75th percentile. [The bottom error bars (25th percentile) stretched to a correlation index of <1 in all cases and have been omitted for clarity.] (C) Summary of the temporal properties of spontaneous firing patterns for retinas isolated from WT (black) and Ts (gray) littermates at P5–P7 and P11-P13. Data are averaged over mean values for each cell of a given age and genotype (P5–P7, 7 retinas per genotype; P11–P13, 4 retinas per genotype). The boxes correspond to medians and quartiles and the whiskers to 5 and 95%. Asterisks imply a significant difference in medians at the 1% significance level as determined by a Wilcoxon's rank sum test; *p* values for all measurements are listed in Table 3.1.

tween all RGCs cell pairs (Wong et al., 1993; Torborg et al., 2004b). Correlation indices in both WT and KbDb KO mice showed a deceasing correlation index as a function of distance, which is characteristic of retinal waves, and no differences were observed between them (Fig. 3.2 B). Waves during P5–P8 were blocked by the nicotinic acetylcholine receptor antagonist di-hydro-β-erythroidine (DHβE, 8 μM), and those during P10–P12 by the glutamatergic antagonists DNQX (20 μM) and D-AP5 (50 μM), confirming that waves in KbDb KO mice undergo the same stages of retinal waves as WT.
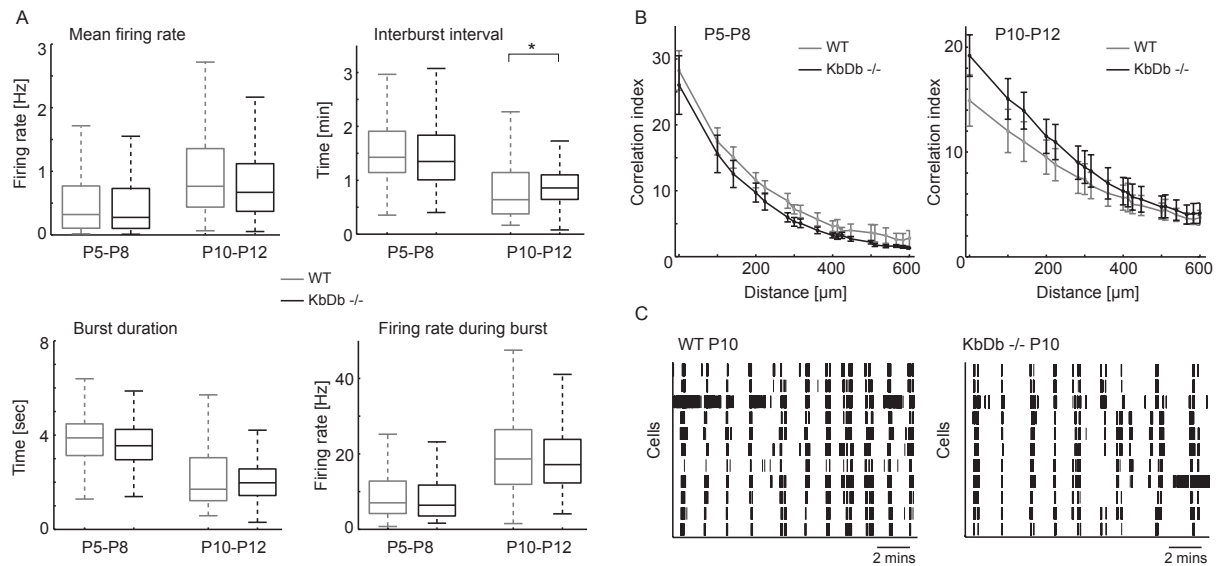
Figure 3.2: **KbDb mice have normal spontaneous retinal activity during development.** (A) Summary of temporal firing patterns for retinas isolated from WT (grey) and KbDb KO (black) mice at P5–P8 (cholinergic waves) and P10–P12 (glutamatergic waves). Data are averaged over mean values for each cell for each age range and genotype. Boxes correspond to median values and whiskers to 5 and 95%. (B) Correlation indices as a function of inter-electrode distance for all cell pairs for WT (grey) and KbDb KO (black) at P5–P8 (left) and P10–P12 (right). Data points correspond to mean values of medians from individual datasets and error bars represent s.e.m. (C) Raster plot of single-unit spike trains from 10 representative cells over a 15 minute interval for P10 WT (left) and KbDb KO (right) mice. Means, standard errors and *p*-values for all measurements are listed in Table 3.2.

Discussion

Our observations show that retinal wave patterns are normal in Ts1Rhr and KbDb KO mice, despite altered eye-specific segregation in the dLGN. Below, we discuss molecular factors that might account for the observed segregation phenotypes.

Table 3.2: Means and std errors of spiking parameters for WT and KbDb KO mice. Significance tested using *t*-test (*p*-value).

	Firing rate [Hz]	Burst duration [s]	Burst firing rate [Hz]	Interburst interval [min]
Ages P5–P8:				
WT	0.47 ± 0.13	4.16 ± 0.17	8.59 ± 1.87	1.85 ± 0.23
KbDb KO	0.51 ± 0.15	3.77 ± 0.12	8.42 ± 1.65	1.57 ± 0.22
p-**value (t-test)**	0.84	0.09	0.95	0.39
Ages P10–P12:				
WT	0.99 ± 0.14	2.60 ± 0.63	19.69 ± 2.11	0.98 ± 0.31
KbDb KO	0.83 ± 0.09	2.07 ± 0.22	18.57 ± 2.16	0.88 ± 0.09
p-**value (t-test)**	0.34	0.42	0.72	0.74

Ts1Rhr mice are trisomic in the DSCR of chromosome 16. A candidate molecule within the DSCR that may account for segregation defects is the cell adhesion molecule Dscam. Dscam has been implicated in dendritic, axonal and somatic tiling and segregation and has been postulated to act through a repulsive mechanism (Hughes et al., 2007; Soba et al., 2007; Millard et al., 2007; Keeley et al., 2012; Fuerst et al., 2008). Blank et al. found that Dscam influenced eye-specific segregation in a dose-dependent manner, where mice with only one copy of Dscam showed reduced segregation compared to WT while mice with three copies showed enhanced segregation. However, Ts1Rhr mice with just two copies of Dscam did not recover WT segregation patterns, suggesting that other molecules in the DSCR likely function together with Dscam to enhance circuit refinement in the dLGN. The mechanisms by which Dscam and other molecules in the DSCR influence segregation remain to be delineated. One possibility is that hypersegregated axons may result from altered fasciculation of RGC axons originating from a given eye. This hypothesis is consistent with the observation that Dscam regulates dendrite fasciculation in the retina, where mice lacking Dscam show extensive fasciculation (Fuerst et al., 2008; Fuerst et al., 2009). Thus, an additional copy of Dscam in Ts1Rhr mice may influence retinal axon fasciculation in a similar manner, resulting in enhanced segregation patterns.

Immune molecules have been implicated in eye-specific segregation, where mice lacking specific immune molecules show impaired segregation (reviewed in Boulanger, 2009;

refer to Table 2.1). Lee et al. showed that in KbDb KO mice, retino-geniculate axons undergo normal LTP but fail to undergo LTD. Reduced LTD in turn reduces axon elimination, which results in decreased segregation. Furthermore, they show that KbDb KO mice have an increase in Ca^{2+}-permeable AMPA receptors. These receptors are known to shift synaptic learning rules away from LTD and towards LTP (Jia et al., 1996; Toyoda et al., 2007). Neuronal expression of H2-Db restored Ca^{2+}-permeable AMPA receptors and rescued LTD, implicating it directly in the regulation of AMPA receptors required for LTD. The mechanism by which H2-Db acts or whether other targets are involved remains an open question. The observation that retinal waves are intact in KbDb KO mice indicates that H2-Db acts downstream of spontaneous retinal activity, and likely is involved in the synaptic learning rules that are implemented for synapse stabilization or elimination.

In summary, although many studies have demonstrated that retinal wave patterns regulate and sculpt segregation patterns in downstream brain targets, additional processes are required to read out retinal activity and translate it into the learning rules required for changes in synaptic connectivity. Transgenic manipulations that result in either enhanced or reduced segregation but leave retinal activity intact are key to identifying factors and molecules that underly the mechanisms of activity-dependent refinement during neuronal development.

Chapter IV

Melanopsin Cells Mediate Plasticity in Retinal Wave Circuits

This Chapter consists of a full reprint of Kirkby and Feller, *Proceedings of the National Academy of Sciences, USA* (2013), in which I was the primary author. The work is included with permission from both authors.

Relevant publications:

Kirkby, L. A. and Feller, M. B., (2013). Intrinsically photosensitive ganglion cells contribute to plasticity in retinal wave circuits. *Proceedings of the National Academy of Sciences, USA* **110**, 12090–12095.

Abstract

Correlated spontaneous activity in the developing nervous system is robust to perturbations in the circuits that generate it, suggesting that mechanisms exist to ensure the maintenance of correlated activity. We examine this phenomenon in the developing retina, where blockade of cholinergic circuits that mediate retinal waves during the first postnatal week leads to the generation of "recovered" waves through a distinct, gap junction mediated circuit. Unlike cholinergic waves, these recovered waves were modulated by dopaminergic and glutamatergic signaling, and required the presence of the gap junction protein connexin 36. Moreover, in contrast to cholinergic waves, recovered waves were stimulated by ambient light via activation of melanopsin-expressing intrinsically photosensitive retinal ganglion cells (ipRGCs). The involvement of ipRGCs in this reconfiguration of wave-generating circuits offers an avenue of retinal circuit plasticity during development that was previously unknown.

Introduction

The computations performed by neural circuits are not determined by hard-wired anatomy but rather can be altered by experience or different neuromodulatory states (Nusbaum et al., 2001; Bargmann, 2012; Turrigiano, 2012). This plasticity is particularly important during development, when neural circuits show remarkable robustness against perturbations that disrupt the patterned, spontaneous activity required for normal development (Blankenship and Feller, 2010). For example, giant depolarizing potentials in the developing hippocampus are maintained against perturbations in GABAergic transmission by changing the strength of glutamatergic transmission (Sipilä et al., 2009). Similarly, spontaneous network activity in the developing spinal cord is maintained against alterations in GABAergic transmission by changes in both the intrinsic excitability of individual neurons and changes in synaptic strength of glutamatergic synapses (Wenner, 2011). The developing retina also shows robustness against perturbations in circuits that generate spontaneous retinal waves (Blankenship and Feller, 2010). For example, disruption of normal cholinergic transmission during the first postnatal week leads to the generation of waves via a distinct gap junction coupled network (Stacy et al., 2005; Sun et al., 2008; Stafford et al., 2009). These observations indicate that degenerate circuit mechanisms exist in the developing retina to maintain spontaneous activity.

Here we explore the hypothesis that intrinsically photosensitive retinal ganglion cells (ipRGCs) contribute to this wave circuit plasticity. ipRGCs are a recently discovered class of photoreceptors that express the photopigment melanopsin (Provencio et al., 1998) and are light sensitive in mice from birth, unlike rod and cone photoreceptors, which become photosensitive after two postnatal weeks of development (Sernagor, 2005). Although

ipRGCs are typically involved in non-image-forming functions, such as entrainment of circadian rhythms (Berson, 2003), they have been shown to support intra-retinal signaling via gap junction coupling and by signaling to dopaminergic amacrine cells (Müller et al., 2010; Zhang et al., 2008; Zhang et al., 2012a). Indeed, light stimulation of ipRGCs can modulate cholinergic retinal circuits during development (Renna et al., 2011).

We use multi-electrode array recordings to compare the spatial and temporal properties of firing patterns recorded in the dark versus the light from wild type (WT) mice and knockout mice lacking normal cholinergic waves (β2-nAChR KO), in addition to lacking the gap junction protein connexin 36 (β2-cx36 dKO) or the photopigment melanopsin (β2-opn4 dKO). Our data support the hypothesis that early light responses from ipRGCs contribute to the circuit that mediates the recovery of correlated spontaneous firing patterns in the absence of cholinergic waves.

Materials and Methods

Animals: Recordings were performed on mice aged postnatal day P4–7 from C57BL/6 wild type (Harlan), β2KO (A.Beaudet, Baylor University (Xu et al., 1999)), β2-Opn4 dKO (D. Copenhagen, UC San Francisco), Opn4-GFP (P.Kofuji, Minnesota University (Schmidt et al., 2008)), β2KO/Opn4-GFP and β2-cx36 dKO (Torborg et al., 2004b). Animal procedures were approved by the University of California, Berkeley Institutional Animal Care and Use Committees and conformed to the National Institutes of Health Guide for the Care and Use of Laboratory Animals, the Public Health Service Policy, and the Society for Neuroscience Policy on the Use of Animals in Neuroscience Research. Animals were anesthetized with isofluorane, decapitated and the eyes were enucleated in a dark room with dim red ambient light. Retinas were removed from eyecups in 95% O2-5% CO2 bicarbonate buffered Ames' solution (purchased from Sigma-Aldrich) under infrared optics.

Multi-electrode array recordings: Isolated pieces of retina were placed RGC-side down onto a 60-electrode commercial multi-electrode array (MEA) arranged in an 8×8 grid excluding the four corners, with 10μm diameter electrodes at 100 μm inter-electrode spacing (Multi Channel Systems). The retina was held in place using a dialysis membrane weighted with a ring of platinum wire. The recording chamber was superfused with Ames' solution bubbled with 95% O2 and 5% CO2 and maintained between 33–35°C, pH 7.4. Each preparation was allowed to equilibrate for 20 minutes in the dark before starting data acquisition. Spontaneous firing patterns were recorded for 30 minutes in the dark followed by 30 minutes of unfiltered broad-band full-field light, delivered by a tungsten-halogen lamp with irradiance (in photons $s^{-1}cm^{-2}$) of $2.4 \cdot 10^{12}$ at 480 nm and $2.9 \cdot 10^{13}$ at 600 nm. This corresponds to a photon flux comparable to that experienced by

newborn pups through closed eyelids (Renna et al., 2011). A second series of dark-light recording conditions was repeated to ensure that any changes in firing patterns were not due to a change in recording conditions over extended periods of time. Raw data were filtered between 120 and 2000 Hz, and spikes sorted offline to identify single units using Plexon Offline Sorter software. The mean firing rate of all units over the duration of the recording was calculated and units with a mean firing rate less than 10% of the overall mean firing rate were excluded from further analysis. Spike-sorted data were analyzed in MATLAB (Mathworks).

To identify wave events, we used a modified Poisson Surprise algorithm, outlined below (Stafford et al., 2009; Kerschensteiner and Wong, 2008). The recording was divided into 1-second bins and the firing rate of each single unit in each 1-second bin was determined. From this, the probability of chance occurrence of the firing rate in each bin given a unitÕs mean firing rate was determined using the Poisson distribution, where the probability of c spikes occurring in a time bin, $t = 1$ second, for a mean firing rate r is

$$P_c = \frac{e^{rt}(rt)^c}{c!}$$

A cell was considered to be bursting if $P_c < 10^{-4}$ in any given bin. We then identified the time bins in which more than 5% of all cells in the recording were bursting with $P_c < 10^{-4}$, and hence computed a pair-wise correlation index, CI, as a function of distance between two cells for all spikes in these bins, where

$$CI = \frac{N_{AB}(\Delta T) \cdot T}{N_A(t) \cdot N_B(t) \cdot (2\Delta t)}$$

$N_{AB}(\Delta t)$ corresponds to the number of spike pairs for which unit B fires within a time window $\pm\Delta t$ from unit A; $N_A(T)$ corresponds to the total number of spikes fired by unit A during the total recording time, T (and similarly for $N_B(T)$) (Wong et al., 1993). We used a correlation time window of $\Delta t = 100$ ms. Thus, only spikes in bins that displayed a decreasing nearest-neighbor correlation index were accepted as waves and considered for analysis of wave properties. Waves detected using this algorithm agreed with those determined by eye. Upon identification of waves, the wave frequency, burst duration during a wave and firing rate during a wave were computed and averaged for each unit.

The correlation index was calculated for all cell pairs in each retina. The distance between cells was approximated as the distance between the electrodes of cell pairs. Pairs were then grouped according to intercellular distance and the medians computed

over all cell pairs. The median correlation index was then plotted as a function of increasing intercellular distance. To establish connectivity maps, we defined two cells as being connected if their correlation index fell in the top 5% of all correlation index values (Blankenship et al., 2011). We then extracted cells that were connected to at least 15% of other cells (red units in Figs. 4.5 B–C). We mapped these units back onto the electrodes on which they were recorded, and computed the distances to their connected units (blue lines in Figs. 4.5 B–C).
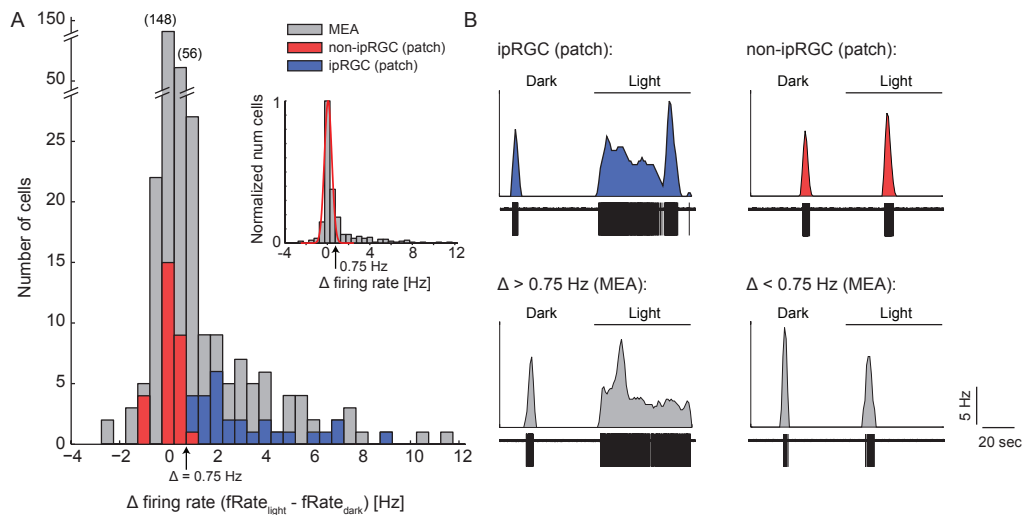
Figure 4.1: **Identifying ipRGCs on multi-electrode array.** (A) Gray bars: Histogram of differences between mean firing rate in the 60-seconds following light onset and mean firing rate in 60-seconds preceding light onset (Æmean firing rate) for 191 WT and 134 β2-nAChR KO units recorded on MEA. Numbers in brackets correspond to number of cells in those bins. Superimposed are the Δmean firing rate of non-ipRGCs (red, $n = 29$) and ipRGCs (blue, $n = 28$) from targeted cell-attached recordings from a transgenic mouse line in which GFP is expressed under the melanopsin promoter (Opn4-EGFP mouse; Schmidt et al., 2008). From these, we select a Δmean firing rate threshold of above 0.75 Hz for ipRGCs (45 additional spikes in a 60 second window). Inset shows normalized MEA distribution with Gaussian fit (red line; Gaussian fit parameters: $\mu = 0.07$ Hz; $\sigma = 0.35$ Hz). (B) Examples of cell-attached (top) and MEA (bottom) recordings and firing rate for ipRGCs (left) and non-ipRGCs (right).

To identify ipRGCs, we computed the difference in a unit's mean firing rate in the 60-seconds following light onset and its mean firing rate in the 60-seconds preceding light onset. Most cells followed a narrow normal distribution centered about 0 Hz difference (Gaussian fit parameters: $\mu = 0.07$ Hz; $\sigma = 0.35$ Hz), which were classified as non-ipRGCs. Units that showed an increase in mean firing rate of at least 0.75 Hz (45 additional spikes in a 60 second window) in the light were classified as ipRGCs. This classification came

from targeted cell-attached recordings from a transgenic mouse line in which GFP is expressed under the melanopsin promoter (Opn4-EGFP mouse; Schmidt et al., 2008). Cell-attached recordings showed that GFP+ RGCs exhibited an increase in mean firing rate following light onset of at least 0.75 Hz, while the difference in mean firing rates for non-GFP+ cells fell into a cluster centered around 0 Hz (refer to Figure S2). Each MEA unit was inspected manually to verify that ipRGCs classified in this manner showed a light response. These units were mapped back on to the electrodes on which they were recorded (turquoise units in Figs. 4.5 B–C).

Pharmacology: Di-hydro-β-erythroidine (DHβE, 8 μM), D-(-)-2- Amino-5- phosphonopentanoic acid (D-AP5, 50 μM), 6,7-Dinitroquinoxaline-2,3-dione (DNQX, 20 μM), SCH23390 hydrochloride (10 μM) and raclopride (8 μM) were added to Ames' media as stock solutions prepared in either distilled water (DHβE, D-AP5, DNQX and SCH23390) or DMSO (raclopride). Antagonists were purchased from Tocris.

Electrophysiology: Isolated retinas were mounted RGC side up on filter paper over a small viewing hole. Retinas were superfused with Ames' solution bubbled with 95% O2 and 5% CO2 and maintained between 33–35°C, pH. 7.4. Retinas were visualized with differential interference contrast optics on an Olympus BX51WI microscope under a LUMPlanFL 60$\times$ water-immersion objective. ipRGCs were identified by GFP signal under epifluorescent illumination at 488 nm. A hole was pierced in the inner limiting membrane of the retina using a glass recording pipette to access the RGC layer. RGCs were targeted under control of a micromanipulator (MP-225, Sutter Instruments). Recording pipettes were pulled with a tip resistance of 4–5 MΩ (Sutter instruments) and filled with filtered NaCl (150 mM). Data were acquired using pCLAMP 10.2 recording software and a Multiclamp 700B amplifier (Molecular Devices), sampled at 6 kHz and filtered between 120 and 2000 Hz.

Results

Recovered waves in mice lacking cholinergic waves are modulated by light.

To investigate firing patterns across retinal ganglion cells (RGCs) in both the dark and light, we performed multi-electrode array (MEA) recordings on retinas acutely isolated from WT mice and in mice lacking the β2 subunit of nAChRs (β2-nAChR KO) at postnatal days 4 to 7 (P4–P7), when cholinergic waves normally occur (Wong et al., 1993; Feller et al., 1997). At these ages, β2-nAChR KO mice exhibit gap junction waves in place of cholinergic ones (Sun et al., 2008; Stafford et al., 2009). In addition, rod and cone photoreceptors are not yet photosensitive and do not contribute to ganglion cell light-responses (Sernagor et al., 2001). WT recordings confirmed previous observations (Stacy

et al., 2005; Stafford et al., 2009; Demas et al., 2003; McLaughlin et al., 2003), where RGCs fired periodic bursts of action potentials that swept across the retina as a wave (Fig. 4.2 A). Immediately following light onset, a subset of cells fired sustained bursts of action potentials, consistent with previously-described light-responses of ipRGCs in early postnatal development (Tu et al., 2005; Neumann et al., 2008).

Recordings of β2-nAChR KO mice also exhibited retinal waves with distinct propagation properties from WT mice. In particular, waves in β2-nAChR KO mice were less frequent and many RGCs fired action potentials that were not associated with retinal waves and therefore were not significantly correlated with one another, in agreement with previous studies (Sun et al., 2008; Stafford et al., 2009; McLaughlin et al., 2003; Torborg et al., 2004b) (Fig. 4.2 B). Surprisingly, we also observed that light stimulation led to an almost two-fold increase in the frequency of waves in β2-nAChR KO retinas, in contrast to WT retinas, for which light stimulation had no effect on wave frequency (Fig. 4.2 C, ***$p < 0.001$). This light-induced increase was observed over a range of starting frequencies, suggesting that the light-induced effect is independent of initial wave frequency. Light stimulation also increased the burst duration during a wave in both WT and β2-nAChR KO retinas (Fig. 4.2 D), as previously reported for WT retinas (Renna et al., 2011).

Because ipRGCs are the only functional photoreceptors at these ages, and because the light-evoked increase in burst duration of cholinergic WT waves is eliminated in melanopsin knockout mice (Opn4 KO) (Renna et al., 2011), we presumed that the observed light-evoked effects on waves in β2-nAChR KO retinas were mediated by ipRGCs. To test this directly, we performed MEA recordings on a β2-melanopsin double KO mouse (β2-Opn4 dKO, kindly provided by David Copenhagen, UCSF). These mice exhibited retinal waves but did not show an increase in wave frequency or burst duration during a wave in the light (Figs. 4.2 C–D). These observations confirm that the photic effects on waves in β2-nAChR KO mice were mediated by ipRGCs.

Waves in β2-nAChR KO mice require connexin 36.

Previous studies have shown that the recovered waves in β2-nAChR KO mice are blocked by gap junction antagonists but not fast neurotransmitter antagonists (Sun et al., 2008). We assessed whether the presence of the neuronal gap junction protein connexin 36 (cx36) was necessary for waves in β2-nAChR KO mice by performing MEA recordings on a β2-cx36 double knockout mouse (β2-cx36 dKO) (Torborg et al., 2004b). Cx36 is the most abundant retinal connexin and couples most ganglion cells to other ganglion or amacrine cells (Bloomfield and Völgyi, 2009). Although cx36KO mice have an increase in asynchronous firing in between retinal waves, they exhibit cholinergic retinal
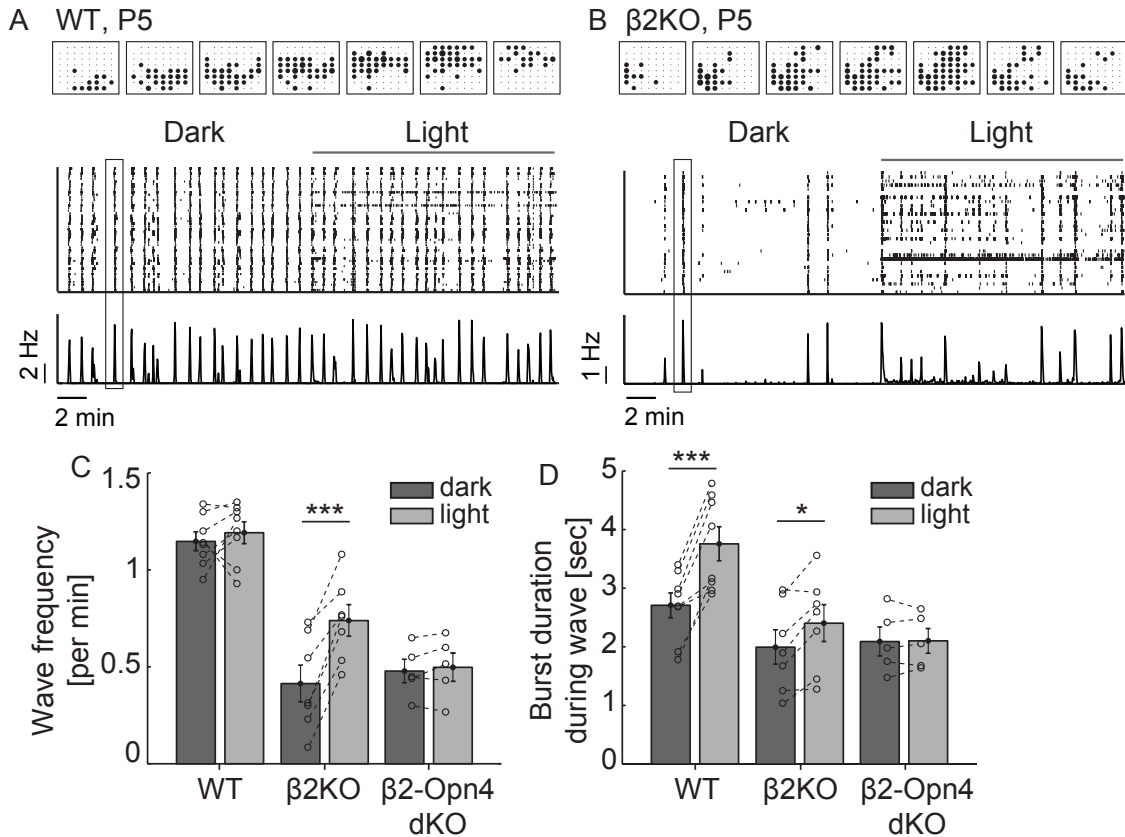
Figure 4.2: **Recovered waves in mice lacking cholinergic waves are modulated by light.**
(A, B) Multi-electrode array recordings from a WT P5 (A) and β2-nAChR KO P5 (B) retina. Top:
Activity pattern corresponding to boxed region in middle panel. Each dot represents an electrode
site and the radius of the dot is proportional to the single unit firing rate recorded at that site.
Frames correspond to 2 seconds; Middle: Raster plot of spike trains of all single units; Bottom:
average firing rate of all units. (C) Summary data of wave frequency in dark and light for
WT, β2-nAChR KO and β2-Opn4 dKO mice. Open circles correspond to individual retinas and
recordings from the same retinas are connected by dotted lines. (D) Summary data of burst
duration during a wave in dark and light for WT, β2-nAChR KO and β2-Opn4 dKO mice. Error
bars in C–D correspond to SEM. *$p < 0.05$; ***$p < 0.001$, paired t-test.

waves with propagation patterns that are indistinguishable from WT during the first postnatal week (Torborg et al., 2004b; Blankenship et al., 2011). We found that β2-cx36 dKO mice did not exhibit recovered retinal waves in either the dark or light (Fig. 4.3 A). Rather, many RGCs fired asynchronous action potentials. We characterized the correlation properties of spiking neurons by computing correlation indices as a function of inter-cellular distance for all cell pairs. This gives a measure of the likelihood relative to chance that two cells fire together within a given time window, where retinal waves are characterized by a correlation index that is high for nearest-neighbors and that falls off with increasing inter-cellular distance (Wong et al., 1993). In contrast, correlation index curves of β2-cx36 dKO mice were flat, confirming the absence of retinal waves (Fig. 4.3 B). In some retinas, we observed synchronous bursting among subsets of cells in the light, however this activity did not propagate in a wave-like manner (Fig. 4.4 A, top panel). These observations confirm that recovered waves in β2-nAChR KO mice are gap junction mediated and show that cx36 is required for their propagation.
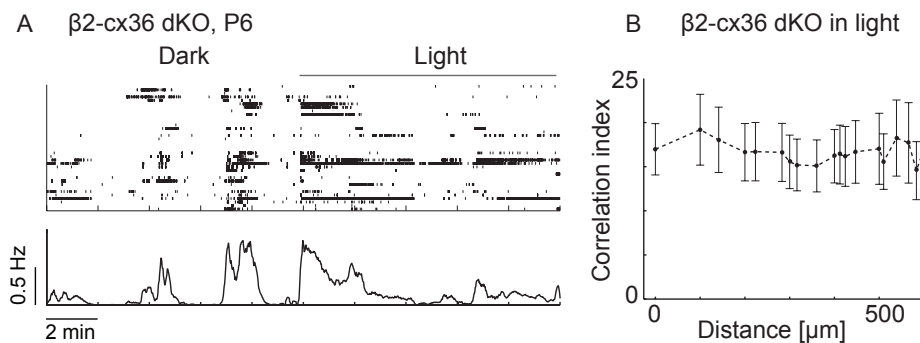
Figure 4.3: **β2-nAChR KO waves require connexin 36.** (A) Multi-electrode array recording of spontaneous activity in β2-cx36 dKO mouse (as in Fig. 4.2 A). (B) Correlation index versus inter-electrode distance for pairs of spike trains in the light for β2-cx36 dKO mice. Data points correspond to averages of median values from individual retinas and error bars correspond to SEM.

ipRGCs do not function as "hub" neurons for recovered waves.

One way in which ipRGCs may increase β2-nAChR KO wave frequency in the light is by functioning as "hub neurons", or highly connected nodes, that link together many cells and thereby impart synchrony within the network. To test this possibility, we first identified neurons whose firing was highly correlated with a large number of other cells and then determined whether these highly connected cells corresponded to ipRGCs.

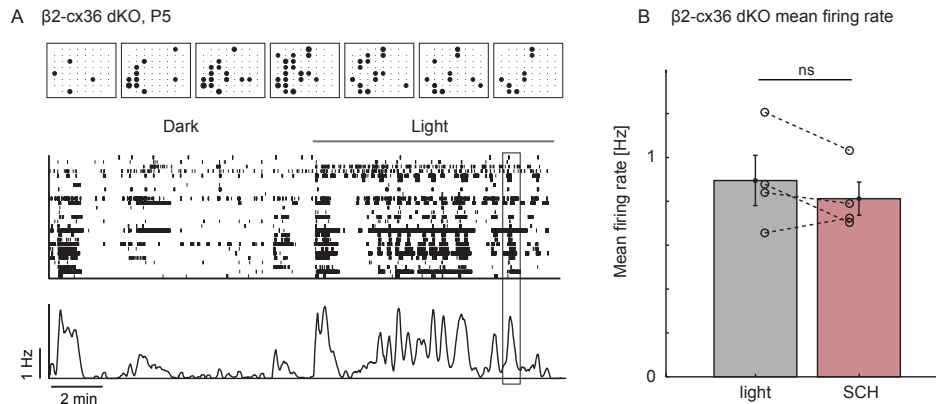Figure 4.4: **Recovered waves are not present in β2-cx36 dKO mice.** (A) Multi-electrode array recording of spontaneous activity in β2-cx36 dKO mouse (as in Figure 1A). (B) Mean firing rate in light and in presence of dopamine receptor antagonist SCH for β2-cx36 dKO mice. D1R antagonist: SCH23390 (SCH), 10μM.

We first computed correlation indices as a function of inter-cellular distance for all cell pairs. WT correlation indices were high for nearest-neighbors and fell off with increasing inter-cellular distance, characteristic of retinal waves (Fig. 4.5 A). β2-nAChR KO correlation index curves were flatter than those for WT (Figure 3A), consistent with larger waves and a faster propagation speed, as described in previous studies (Sun et al., 2008; Stafford et al., 2009). Correlation index curves showed no difference in the dark and light for both WT and β2-nAChR KO mice. We next used these correlation indices to construct connectivity maps, which show connections between neurons with the highest correlation indices (Blankenship et al., 2011; Feldt et al., 2011). In particular, this strategy has been used in the developing hippocampus to identify highly connected hub neurons, which repeatedly initiate activity (Bonifazi et al., 2009). We defined two cells as being connected if their correlation index fell in the top 5% of all correlation index values and extracted cells that were connected to at least 15% of other cells (Figs. 4.5 B–C; "highly connected cells" correspond to red units and their connections are shown by blue lines.)

For WT retinas, highly connected cells fell in a cluster of adjacent units with a median connection length of 145μm (Figs. 4.5 B and D). Highly connected cells in β2-nAChR KO mice were more dispersed than in WT, with a median connection length of 260μm (Figs. 4.5 C and D). Median connection lengths in the dark were similar to those in the light for both WT and β2-nAChR KO mice (Fig. 4.5 D), indicating that light does not alter the underlying spatial architecture of waves.

We determined the locations of ipRGCs on the MEA by identifying units that showed

at least 45 additional spikes in the 60 second window following light onset compared to the 60 seconds preceding light onset (0.75 Hz increase, see Fig. 4.1). This threshold was determined using targeted cell-attached recordings of ipRGCs in Opn4-EGFP mice, in which GFP is expressed under the melanopsin promoter (Schmidt et al., 2008). We next determined whether identified ipRGCs (turquoise units in Figs. 4.5 B–C) function as hub neurons for retinal waves by computing the percentage of ipRGCs that were highly connected and comparing this to the percentage we would expect by chance. In the dark, the percentage of ipRGCs that were highly connected did not differ from chance for both WT and β2-nAChR KO mice (Fig. 4.5 E). Surprisingly, in the light the percentage of ipRGCs that were highly connected was significantly less than chance (Fig. 4.5 E, **p < 0.01). These observations show that ipRGCs do not function as hub neurons, since activation of ipRGCs in the light does not directly activate many other RGCs. Rather, they suggest that the action of light on wave frequencies in β2-nAChR KO mice is an indirect effect of ipRGCs on the network. Below we explore whether this modulation occurs via dopaminergic signaling.

β2-nAChR KO waves are modulated by dopaminergic and glutamatergic signaling.

ipRGCs are thought to influence retinal networks via glutamatergic stimulation of dopamine release from dopaminergic amacrine cells (DACs) (Zhang et al., 2008; Zhang et al., 2012a), but see (Cameron et al., 2009). Dopamine is produced in mice as early as P4 by DACs (Yoshida et al., 2011) and is a major player in regulation of gap junction coupling via cAMP-dependent post-translational phosphorylation(Bloomfield and Völgyi, 2009; Witkovsky, 2004). In general, activation of D1-like receptors decreases gap junction coupling while activation of D2-like receptors increases coupling, although the magnitude of the effects are highly cell-type specific (Mills et al., 2007; Kothmann et al., 2009; Hu et al., 2010). Thus, one way that ipRGCs could exert an indirect effect on network synchrony is via a dopaminergic pathway.

We first tested whether dopamine signaling regulates wave frequencies in WT and β2-nAChR KO mice by performing MEA recordings in dopamine receptor antagonists. We found that neither a D1 receptor antagonist (SCH23390, 10 μM) nor a D2 receptor antagonist (raclopride, 8 μM) had an effect on wave frequency in WT retinas (Fig. 4.6 A). However raclopride strongly reduced wave frequency in β2-nAChR KO mice in the light, whereas SCH23390 increased their frequency (Fig. 4.6 B). Neither antagonist significantly influenced mean baseline firing rates relative to the mean firing rate in the light (Fig. 4.6 C), suggesting that the observed effects are likely due to modulation of gap junction coupling required for waves and not modulation of a cell's overall firing properties. Furthermore, application of SCH23390 to β2-cx36 dKO mice did not induce the generation of waves, nor did it change mean baseline firing rates relative to the mean
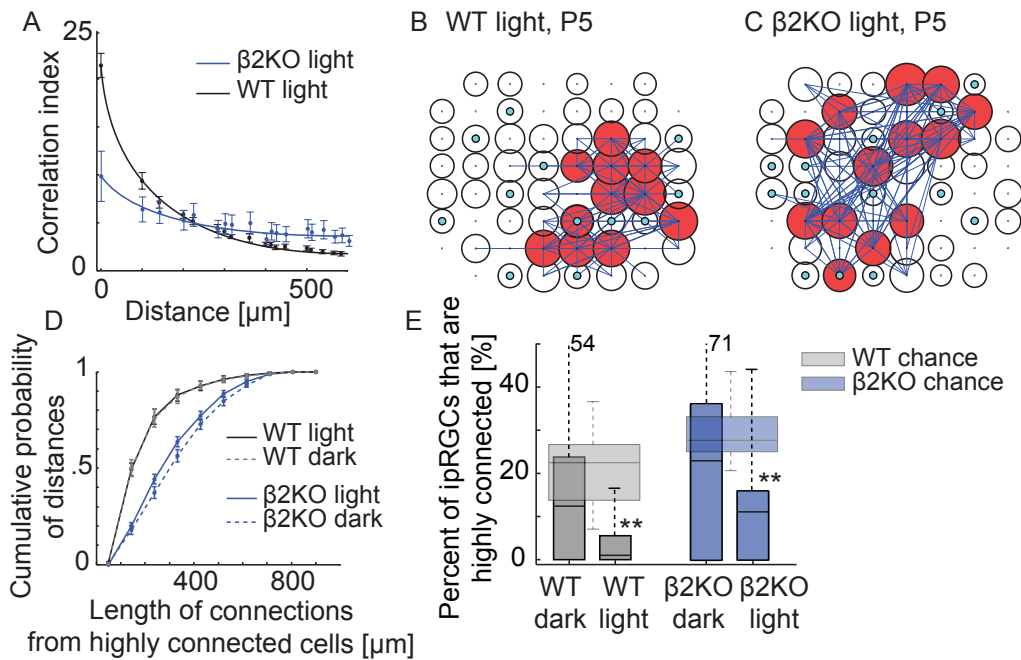
Figure 4.5: **ipRGCs do not function as hub neurons for retinal waves.** (A) Correlation index versus inter-electrode distance for pairs of spike trains for WT (black) and β2-nAChR KO (blue) mice, in the light. Data points correspond to averages of median values from individual retinas and error bars correspond to SEM. (B, C) Connectivity maps of WT P5 (B) and β2-nAChR KO P5 (C) in the light. Circles correspond to location of single units with diameter scaled by the magnitude of the normalized correlation index. Red circles correspond to units that were connected to at least 15% of other units and blue lines show their connections. Turquoise circles correspond to units identified as ipRGCs. (D) Cumulative probability distributions of the distances of connections from highly connected cells for WT (black) and β2-nAChR KO (blue) retinas in the dark and light. (E) Percent of ipRGCs that are highly connected "hub" neurons for WT (grey) and β2KO (blue) activity, in dark and light. Box plots range from lower to upper quartiles (25% and 75%) with median values indicated by central black line; whiskers (dotted lines) range from 5% to 95%. Faded box plots correspond to percentage of ipRGCs that are highly connected that we would expect from chance. **$p < 0.01$, Wilcoxon rank sum test.

firing rate in the light (Fig. 4.4 B), indicating that cx36 is a possible target of D1 receptor activation. These observations show that dopamine signaling strongly modulates the frequency of recovered waves, where waves are stimulated by D2 receptor activation but suppressed by D1 receptor activation.

Recent experiments indicate that ipRGCs form excitatory glutamatergic synapses onto DACs (Zhang et al., 2008; Zhang et al., 2012a). Thus, if the observed light-evoked increase in wave frequency in β2-nAChR KO mice were mediated by ipRGC-feedback onto DACs, we would expect that blocking glutamate receptors would block the effect. To test this hypothesis, we performed MEA recordings of β2-nAChR KO mice in glutamate receptor antagonists in the light (D-AP5, 50 μM and DNQX, 20 μM). In 4 out of 5 retinas tested, wave frequencies returned to dark levels in the presence of glutamate receptor antagonists with no effect on baseline firing rates (Figs. 4.6 D–E), suggesting that the antagonists influence wave properties but not a cellÕs overall firing properties. To test whether these glutamatergic effects were dependent on light-evoked firing of ipRGCs, we repeated the measurements in β2-Opn4 dKO mice. We found that glutamate receptor antagonists had no effect on wave frequencies in these mice (Fig. 4.5 F), indicating that the glutamatergic reduction of wave frequency in β2-nAChR KO mice in the light was melanopsin-dependent. Together, these observations are consistent with the model that ipRGCs influence retinal networks via glutamatergic signaling, and likely via a dopaminergic pathway.

Light-sensitive, non-cholinergic wave circuit is present but latent in WT mice.

The differential modulation by light and dopamine receptor antagonists between cholinergic and recovered gap junction waves indicates that they are mediated by distinct circuits. Does a non-cholinergic wave circuit exist as a "latent" circuit in WT retinas or does it require an extended perturbation provided by the β2-nAChR KO mouse? To address this question, we tested whether acute block of cholinergic waves in WT mice unmasked a light- and dopamine-sensitive wave-generating circuit. We monitored light-evoked activity after a 20-minute nAChR blockade using di-hydroβ-erythroidine (DHβE, 8μM). Approximately 2 minutes after light onset, we observed rhythmic bursting with a periodicity of a few seconds (Fig. 4.7 A), similar to that observed in another study after prolonged (10 hr) nAChR blockade (Stacy et al., 2005), but we did not detect propagating waves.

We next tested whether recovery of waves was being suppressed by D1 receptor signaling by applying the D1 receptor antagonist SCH23390 for 20 minutes in the dark to DHβE-treated retinas, and monitoring activity in the dark and light. Light stimulation led to the generation of propagating, correlated wave-like events, with similar
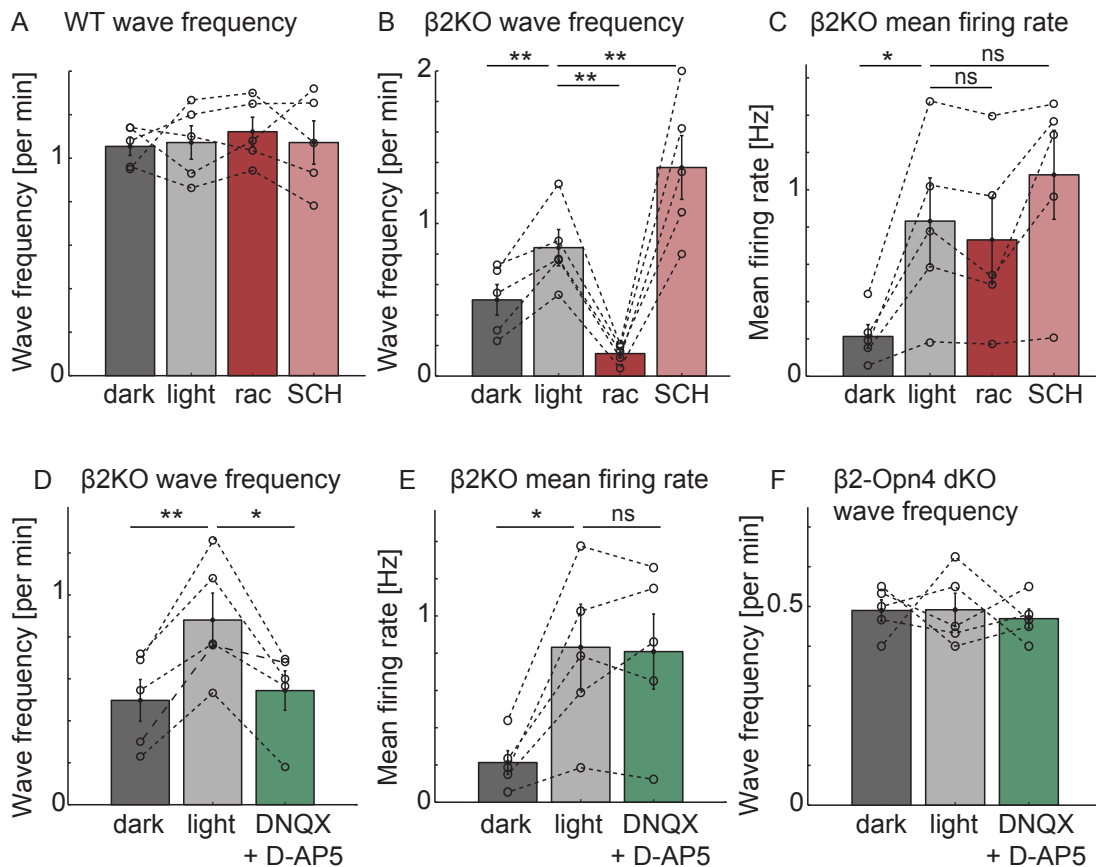
Figure 4.6: **β2-nAChR KO waves are modulated by dopaminergic and glutamatergic signaling.** (A, B) Wave frequency in dark, light and in presence of dopamine receptor antagonists in light for WT (A) and β2-nAChR KO (B) mice. (C) Mean firing rate in dark, light and in presence of dopamine receptor antagonists in light for β2-nAChR KO mouse. (D) Wave frequency in dark, light and in presence of glutamate receptor antagonists in light for β2-nAChR KO mice. (E) Mean firing rate in dark, light and in presence of glutamate receptor antagonists in light for β2-nAChR KO mice. (D) Wave frequency in dark, light and in presence of glutamate receptor antagonists in light for β2-Opn4 dKO mice. For all plots, open circles correspond to individual retinas and recordings from the same retinas are connected by dotted lines. Error bars correspond to SEM. D1R antagonist: SCH23390 (SCH), 10μM; D2R antagonist: raclopride (rac), 8μM. AMPAR and NMDAR antagonists: DNQX and D-AP5, 20 and 50μM). *$p < 0.05$; **$p < 0.01$, paired t-test.

spatial-temporal properties to waves in β2-nAChR KO mice (Figs. 4.6 B–K). Specifically, connectivity maps of recovered waves matched those observed in β2-nAChR KO mice, where highly connected cells had a dispersed, gap junction signature rather than a clustered, cholinergic one (Figs. 4.6 I–J). In addition, the coincidence of highly connected cells with ipRGCs was lower than chance in the light, as observed in β2-nAChR KO mice (Fig. 4.6 K, **$p < 0.01$). Finally, although some recovered waves were present in the dark in some retinas, the frequency of waves increased significantly in the light (Fig. 4.6 C, ***$p < 0.001$). Together, these observations show that an auxiliary wave-generating circuit is latent in WT mice, where it is normally suppressed by a combination of nAChR activation together with D1R signaling. Light stimulation of ipRGCs facilitates the activation of this auxiliary circuit, indicating that ipRGCs contribute to the recovery of correlated spontaneous firing patterns in the absence of cholinergic waves.

Discussion

In this study we demonstrate for the first time that intrinsically photosensitive retinal ganglion cells (ipRGCs) are used in degenerate circuit mechanisms to maintain correlated spontaneous activity in the developing retina. These observations show that retinal wiring diagrams are dynamic and malleable during development and suggest a novel function for ipRGCs in mediating retinal wave plasticity that underlies the maintenance of correlated activity.

We found that in the absence of cholinergic waves during retinal development, a distinct light-modulated wave circuit was activated (Figs. 4.2 and 4.7). Cx36 was necessary for waves in β2-nAChR KO mice (Fig. 4.3) and, since neither light nor dopamine antagonists induced waves in β2-cx36 dKO mice, we postulate that gap junctions are the likely target of the observed light- and dopamine- modulation of non-cholinergic waves. Similar modulation of gap junctions has been observed in many retinal circuits, implicating gap junctions as sites of plasticity in both developing and adult retinal circuits. For example, light and dopamine modulation of coupling has been extensively described for horizontal cells (Bloomfield et al., 1995), AII amacrine cells (Kothmann et al., 2009; Mills and Massey, 1995) and alpha-ganglion cells (Mills et al., 2007; Hu et al., 2010).

Based on the observation that ipRGCs likely signal to the retina via dopaminergic signaling (Zhang et al., 2008; Zhang et al., 2012a) but see (Cameron et al., 2009), we propose the following model. During cholinergic waves, the dominant circuit is starburst amacrine cell release of acetylcholine onto ganglion cells and other amacrine cells (Fig. 4.8 A). Upon cholinergic block, ipRGCs increase their contribution to network dynamics and the dominant circuit becomes a gap junction coupled network regulated by ipRGCs acting through modulation of dopamine release (Fig. 4.8 B). In this model,
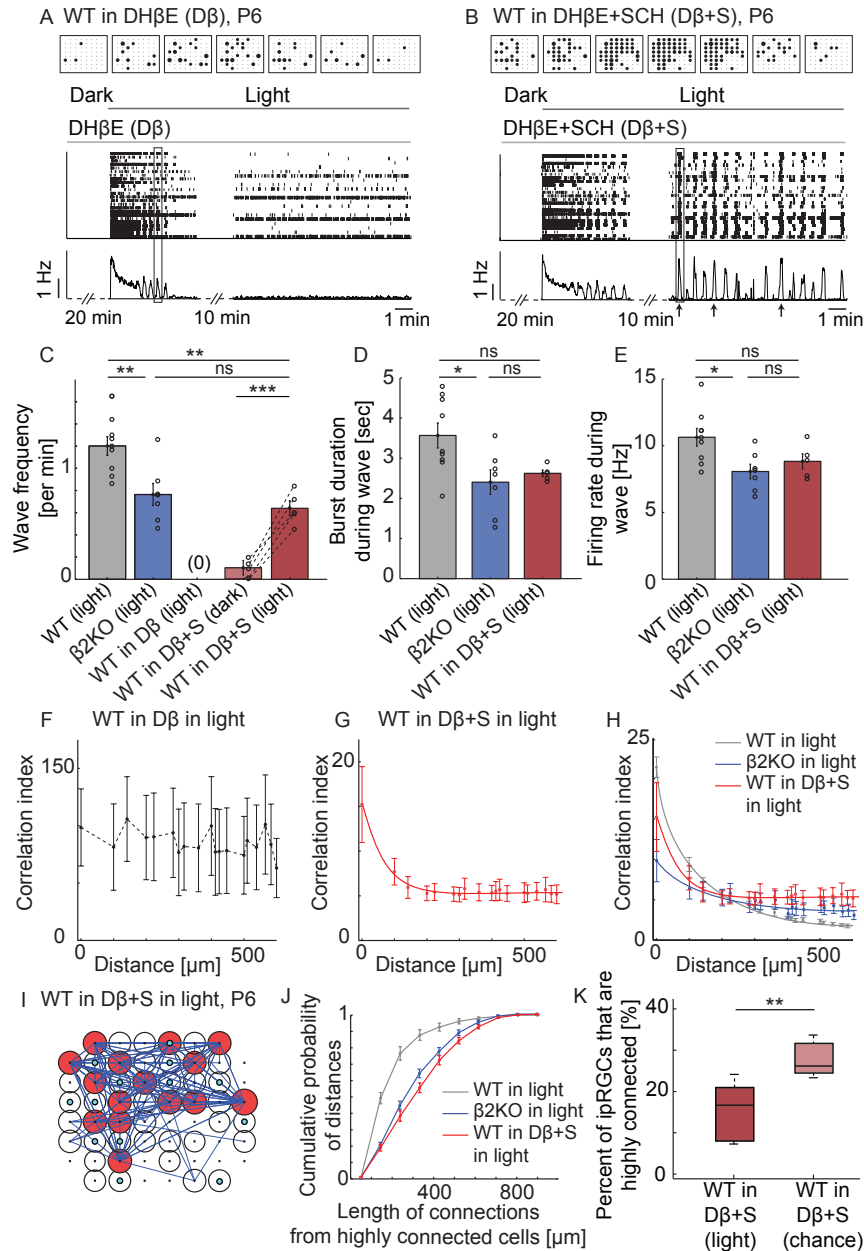
Figure 4.7: **Light-sensitive, non-cholinergic wave circuit is present but latent in WT mice.** (A, B) Multi-electrode array recordings from a WT P6 retina after 20 minutes of DHβE (Dβ) application in dark (A) and after 20 minutes of DHβE+SCH (Dβ+S) application in dark (B), (as in Fig. 4.2 A). (C, D, E) Frequencies (C), burst duration (D) and firing rates (E) of waves in WT (grey), β2KO (blue) and WT in DHβE+SCH (red). Open circles correspond to individual retinas. (F, G) Correlation indices versus inter-electrode distance for WT in DHβE alone (F) and DHβE+SCH (G) in the light. (H) Data from Figs. 4.5 A and 4.7 G for WT (grey), β2KO (blue) and WT in DHβE+SCH (red). (I) Connectivity map for WT in DHβE+SCH in the light (as in Fig. 4.5 B). (K) Cumulative probability distributions of the lengths of connections from highly connected cells (WT and β2KO curves correspond to those from Figure 3D). C-E: $*p < 0.05$, $**p < 0.01$, one-way ANOVA; C: $***p < 0.001$, paired t-test; K: $**p < 0.01$ Wilcoxon rank sum test. nAChR antagonist: DHβE (Dβ), 8μM; D1R antagonist: SCH23390 (SCH or S), 10μM.

we depict the ipRGC-DAC synapse as a reciprocal connection since ipRGCs themselves express dopamine receptors (Van Hook et al., 2012). How a gap junction coupled network is activated in the absence of cholinergic waves remains to be delineated. However one possibility is that RGCs experience a change in gap junction coupling in response to reduced cholinergic input. This has previously been shown to occur in rat adrenal medulla, where acute pharmacological block of nAChRs leads to an increase in dye coupling of adrenal chromaffin cells together with an increase in junctional currents (Martin et al., 2003).

Further, we found that reduced D1 receptor signaling was required to recover wave-like events in the absence of cholinergic waves in WT retinas (Fig. 4.7), suggesting that dopamine signaling may normally suppress the auxiliary wave circuit during cholinergic waves. In addition, we found that recovered waves in β2-nAChR KO mice were suppressed by activation of D1 receptors but stimulated by activation of D2 receptors (Fig. 4.6 B). Since D2 receptors are approximately ten-fold more sensitive to dopamine than D1 receptors (Witkovsky, 2004), a balance of the opposing effects of D1 and D2 receptor activation can likely be achieved in vivo with a low concentration of dopamine. Interestingly, although blockade of D2 receptors blocked waves, it did not decrease the mean firing rate of individual RGCs (Fig. 4.6 C). Hence, we postulate that light stimulation of ipRGCs does not increase wave frequency by a general increase in network excitability, but rather via further increases in gap junction coupling, thus lowering the threshold for wave events. Together, these observations suggest that the absence of cholinergic waves might result in changes in dopamine signaling, which facilitate activation of recovered waves and sculpt their dynamics.

Our data suggests that the circuits that mediate both cholinergic and recovered gap junction waves exist in WT retina as opposed to emerging after the prolonged activity blockade that accompanies genetic deletions. Specifically, a short-term cholinergic block resulted in periodic activity and correlated wave-like activity emerged when D1 receptor signaling was low (Fig. 4.7). Hence, the wiring diagram of the developing retina may include several "overconnected circuits", in which some circuits are closed and others activated depending on the internal state of the system (Bargmann, 2012), such as classically described in the stomatogastric ganglia (Nusbaum et al., 2001) and recently described in C.elegans (Macosko et al., 2009). The data presented here indicates that the developing retina may use a similar overconnection strategy as a means of maintaining spontaneous firing patterns. Such a strategy has the advantage of allowing the network to rapidly change its properties without having to construct new circuits. It is interesting to postulate whether this is a general mechanism used by other developing networks.
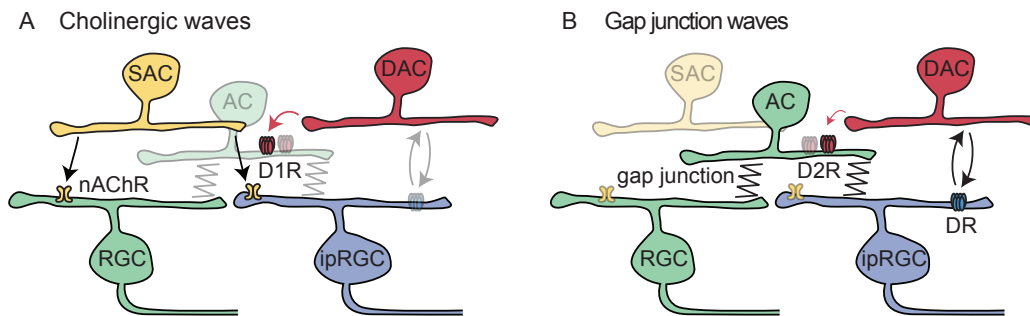
Figure 4.8: **Model of overlapping wave circuits.** (A) During cholinergic waves, the dominant circuit is nAChR activation by acetylcholine, which is spontaneously released from starburst amacrine cells. Activation of D1 receptors inhibits the gap junction circuit (B) Following cholinergic block, ipRGCs may modulate dopamine release from dopaminergic amacrine cells, which, via activation of D2 receptors, modulates the strength of gap junction coupling between ganglion cells (not pictured) or amongst a network of amacrine and ganglion cells. SAC: Starburst amacrine cell; AC: Amacrine cell; DAC: Dopaminergic amacrine cell; RGC: Retinal ganglion cell; ipRGC: intrinsically photosensitive retinal ganglion cell.

Chapter V

Electrical Coupling of Melanopsin Cells During Development

This Chapter consists of my contribution to a study done in collaboration with David Arroyo, a graduate student in the Feller Lab, in preparation for Kirkby*, Arroyo* et al., (2014) in which we share primary authorship. Experiments performed and analyzed by David Arroyo have not been included in this draft. Razvan Druma and Jordan Xu contributed to experiments and analysis included here, performed under my supervision.

Relevant publications:

Kirkby, L. A.*, Arroyo, D.*, Druma, R., Xu, J., and Feller, M. B., (2014). Electrically-coupled network of melanopsin cells regulated by retinal waves. *In preparation*.

Abstract

Developing neural circuits generate correlated spontaneous activity, which is required for the normal development of adult circuits. Remarkably, correlated activity patterns persist following disruption of the underlying circuits that mediate them, suggesting that recovery mechanisms exist to ensure patterned activity is maintained. In the developing retina, activation of intrinsically photosensitive retinal ganglion cells (ipRGCs) facilitates recovery of correlated activity, resulting in the emergence of a light-sensitive network. In contrast, correlated activity in the wild type network, mediated by cholinergic transmission, is largely light-insensitive. Here, we explore how a light-sensitive network emerges in the absence of cholinergic signaling. Multi-electrode array recordings revealed that pharmacological blockade of cholinergic signaling resulted in an increase in the duration of light-evoked activity and in the number of light-responsive cells. In addition, light-responsive cells oscillated together in a rhythmic activity pattern, where cross correlograms of spike trains revealed direct coupling between oscillating cells. These effects were abolished by the gap junction antagonist meclofenamic acid (MFA), suggesting they are mediated by an increase in electrical coupling of ipRGCs in the absence of cholinergic input. These findings indicate that ipRGC connectivity is modulated by synaptic input, and may reveal a mechanism by which ipRGC contribution to network activity is regulated.

Introduction

Across the developing nervous system, immature networks generate spontaneous activity that is correlated amongst neighboring groups of cells (reviewed in Blankenship and Feller, 2010). This correlated activity drives activity-dependent mechanisms of axonal and synaptic refinement, which is required for the correct establishment of adult neural circuits (reviewed in Kirkby et al., 2013). Interestingly, immature networks are highly robust to perturbations in the circuits that generate correlated activity, indicating that plasticity mechanisms exist to ensure it is maintained.

This form of network plasticity is prevalent in the developing retina. Correlated activity is usually mediated by cholinergic signaling and propagates across the retina as a wave (Feller et al., 1996). However, retinal waves persist even in the absence of cholinergic signaling, where correlated activity is mediated instead by electrical coupling via gap junctions (Stacy et al., 2005; Sun et al., 2008; Stafford et al., 2009; Kirkby and Feller, 2013). Previously, we discovered that retinal waves in the absence of cholinergic signaling were recovered via a light-sensitive circuit, composed in part of intrinsically photosensitive retinal ganglion cells (ipRGCs) (Kirkby and Feller, 2013). ipRGCs express the photopigment melanopsin and are classically involved in non-image-forming parts

of vision, such as entrainment of circadian rhythms (Rollag et al., 2003; Berson, 2003; Hattar et al., 2003). Unlike rod and cone photoreceptors they are photosensitive early in development (Sekaran et al., 2005). However, they exert only a modest effect on cholinergic wave properties, rendering the cholinergic wave circuit largely insensitive to ambient light (Renna et al., 2011; Kirkby and Feller, 2013).

What causes the switch from a light-insensitive to a light-sensitive circuit in the absence of cholinergic waves is unknown; are the light-response properties of the immature retina regulated by cholinergic signaling? To address this question, we used multi-electrode array (MEA) recordings to assess how cholinergic signaling influences the temporal and spatial properties of light-responsive cells. We found that blockade of cholinergic signaling led to an increase in the firing duration and number of active cells following light stimulation. Further, these cells oscillated together in a gap junction coupled network—a phenomenon not present under cholinergic waves. These results indicate that electrical coupling via gap junctions permits melanopsin-driven signals in ipRGCs to propagate to other neurons, and that this coupling is acutely modulated by synaptic input during development.

Materials and Methods

Animals: Recordings were performed on mice aged postnatal day P4–7 from C57BL/6 wild type (Harlan) and Opn4-GFP (P.Kofuji, Minnesota University (Schmidt et al., 2008)). Animal procedures were approved by the University of California, Berkeley Institutional Animal Care and Use Committees and conformed to the National Institutes of Health Guide for the Care and Use of Laboratory Animals, the Public Health Service Policy, and the Society for Neuroscience Policy on the Use of Animals in Neuroscience Research. Animals were anesthetized with isofluorane, decapitated and the eyes were enucleated in a dark room with dim red ambient light. Retinas were removed from eyecups in 95% O_2-5% CO_2 bicarbonate buffered Ames' solution (purchased from Sigma-Aldrich).

Multi-electrode array: Isolated pieces of retina were placed RGC-side down onto a 60-electrode commercial multi-electrode array (MEA) arranged in an 8×8 grid excluding the four corners, with 10μm diameter electrodes at 100μm inter-electrode spacing (Multi Channel Systems). The retina was held in place using a dialysis membrane weighted with a ring of platinum wire. The recording chamber was superfused with Ames' solution bubbled with 95% O_2 and 5% CO_2 and maintained between 33–35°C, pH 7.4. Each preparation was allowed to equilibrate for 20 minutes in the dark before starting data acquisition. Spontaneous firing patterns were recorded for 30 minutes in the dark followed by 30 minutes of unfiltered broad-band full-field light, delivered by a tungsten-

halogen lamp with irradiance (in photons $s^{-1}cm^{-2}$) of $2.4 \cdot 10^{12}$ at $480\,nm$ and $2.9 \cdot 10^{13}$ at $600\,nm$. This corresponds to a photon flux comparable to that experienced by newborn pups through closed eyelids (Renna et al., 2011). Raw data were filtered between 120 and $2000\,Hz$, and spikes sorted offline to identify single units using Plexon Offline Sorter software. The mean firing rate of all units over the duration of the recording was calculated and units with a mean firing rate less than 10% of the overall mean firing rate were excluded from further analysis. Spike-sorted data were analyzed in MATLAB (Mathworks).

To identify ipRGCs, we first computed the instantaneous firing rate of each cell using a 2 second sliding window and determined the firing rate within that window, sliding in 0.5 second increments. Light-responsive cells were easily identifiable by eye, showing an increase in firing rate at light onset (refer to Figs. 5.1 B). To isolate all spikes within the light response, we defined a threshold mean firing rate of $0.5\,Hz$; if a cell's mean firing rate fell below $0.5\,Hz$ over a $10\,s$ interval following light onset, then we defined the end of the light response as the time at which the firing rate fell below threshold (right-most red markers in Figs. 5.1 B). Using this definition, the firing rate of cells that did not show a light response never exceeded this threshold, allowing for straightforward separation of cells with and without a light response. Next, we calculated the light response duration (time between red markers in Figs. 5.1 B), mean firing rate over this period, peak firing rate inside this period (blue marker in Figs. 5.1 B), and latency to peak firing rate (time between light onset and time of peak firing rate) for all light-responsive units. We inspected each cell manually to ensure that light response parameters identified automatically agreed with what we would expect by eye.

Pharmacology: Di-hydro-β-erythroidine (DHβE, $8\,\mu$M), D-(-)-2- Amino-5- phosphonopentanoic acid (D-AP5, $50\,\mu$M), 6,7-Dinitroquinoxaline-2,3-dione (DNQX, $20\,\mu$M), SR-95531 (GABAzine, $5\,\mu$M), Strychnine ($4\,\mu$M), Meclofenamic acid (MFA, $100\,\mu$M), Dopamine (DA, $100\,\mu$M), SCH23390 hydrochloride ($10\,\mu$M) and raclopride ($8\,\mu$M) were added to Ames' media as stock solutions prepared in either distilled water (DHβE, D-AP5, DNQX, GABAzine, strychnine, MFA, DA and SCH23390) or DMSO (raclopride). Antagonists were purchased from Tocris.

Electrophysiology: Isolated retinas were mounted RGC side up on filter paper over a small viewing hole. Retinas were superfused with Ames' solution bubbled with 95% O2 and 5% CO2 and maintained between 33–35°C, pH. 7.4. Retinas were visualized with differential interference contrast optics on an Olympus BX51WI microscope under a LUMPlanFL 60× water-immersion objective. ipRGCs were identified by GFP signal under epifluorescent illumination at $488\,nm$. A hole was torn in the inner limiting mem-

brane of the retina using a glass recording pipette to access the RGC layer. RGCs were targeted under control of a micromanipulator (MP-225, Sutter Instruments). Recording pipettes were pulled with a tip resistance of 4–5 MΩ (Sutter instruments) and filled with filtered potassium gluconate internal solution for whole-cell recordings (in mM 98.3 K-gluconate, 40 HEPES, 1.7 KCl, 0.6 EGTA, 5 MgCl2, 2 Na2ATP, and 0.3 Na-GTP; pH adjusted to 7.25 with KOH) or NaCl for cell-attached recordings (150 mM). Data were acquired using pCLAMP 10.2 recording software and a Multiclamp 700B amplifier (Molecular Devices), sampled at 6 kHz and filtered between 120 and 2000 Hz.

Membrane resistances were calculated by injecting a hyperpolarizing step from -60 to -80 mV, in whole-cell voltage-clamp mode, and measuring the magnitude of the hyperpolarizing current. Irradiance-response curves were performed in cell-attached mode. Firing rates were measured in response to a 5 s pulse of full-field, white light illumination of increasing light intensity. Light intensity was adjusted using optical density (OD) filters. All firing rates were normalized to the maximal response at OD = 0 (no filter present).

Cell culture: D2 cell-based neurotransmitter fluorescent engineered reporters (CNiFERs) were kindly provided by D. Kleinfeld and P. Slesinger (UCSD). CNiFERs were maintained in a humidified incubator at 37°C with 5% (v/v) CO_2 in growth media containing Dulbecco's Minimum Essential Medium (DMEM, containing 4.5 g/L glucose, L-glutamine and Na pyruvate; Invitrogen) supplemented with 10% heat-inactivated FBS (Invitrogen). Cells were trypsinized (0.05%), triturated, and seeded into new flasks at density ratio 1:5 upon confluence (approximately every 2–3 days).

Fluorescence resonance energy transfer (FRET) imaging: Before experiments, CNiFERs were removed from culture flasks using brief (30 second) application of trypsin (0.05%) and concentrated in growth media. CNiFERs were deposited on top of the inner limiting membrane (ILM) using a micropipette to transfer solution on top of filter-mounted retinal piece, mounted ganglion cell side up, and allowed to settle onto the surface. Clusters of 2–3 cells were imaged at focal plane, $\sim$5–10 μm above the ILM. In imaging with simultaneous patch clamp recordings of RGCs, a hole in the ILM was torn $\sim$50–200 μm from the imaged CNiFERs. Fluorescence resonance energy transfer (FRET) images were acquired at 2 Hz using a 60× objective and an excitation wavelength of 435 nm. Individual FRET channel detection was accomplished by using a Dual-View image splitter (Optical Insights) with appropriate yellow and cyan channel filters. Background fluorescence was subtracted from both channels. FRET ratios were computed as background-corrected YFP/CFP fluorescence averaged over a region of interest around a single CNiFER.

Results

Blockade of cholinergic signaling increases light-evoked firing patterns

To measure light-evoked activity of many cells simultaneously, we performed multi-electrode array (MEA) recordings of acutely isolated, dark-adapted wild type (WT) retinas at postnatal days 4–6 (P4–P6). At these ages, rod and cone photoreceptors are not yet photosensitive and do not contribute to ganglion cell light responses (Sernagor et al., 2001). Light stimulation evoked spiking on 41%±7% of active channels (Fig. 5.1 A, Table 5.1). On average, single-unit responses showed a high-firing rate transient peak followed by a lower-firing rate tail, similar to spike-trains observed in other studies (Tu et al., 2005) (Fig. 5.1 B, upper panel). We quantified light response properties by their duration, mean firing rate, peak firing rate, and latency to peak firing rate from light onset (refer to methods and Fig. 5.1 B).

In contrast to other studies (Tu et al., 2005; Perez-Leighton et al., 2011), our multi-unit responses did not exhibit multiple, distinct classes of ipRGCs based on their physiological output; this discrepancy could be due to different ages of recordings, with our recordings being from mice 2–3 days younger (P8 for Tu et al., 2005 and P6–P8 for Perez-Leighton et al., 2011), or different light stimuli (480 nm light vs. our use of white light). Nonetheless, single-unit responses showed high diversity across parameters. In particular, light response durations were varied across cells, where most cells fired continuously for approximately 1–2 minutes following light onset, while a subset of cells (~10%) showed sustained firing over the duration of light exposure (Fig. 5.1 C, black lines).

Light-responsive cells fired bursts of action potentials during retinal waves, in agreement to other studies (Renna et al., 2011; Kirkby and Feller, 2013). We confirmed that ipRGCs receive cholinergic input during waves by targeting melanopsin positive cells for whole-cell recordings using a mouse line that expresses GFP under the melanopsin promoter (Opn4-EGFP mouse; Schmidt et al., 2008) (Fig. 5.2 A). GFP positive cells showed periodic bursts of action potentials in current-clamp mode holding at 0 pA and corresponding large inward currents in voltage-clamp mode holding at -60 mV, which were blocked by the nicotinic acetylcholine receptor (nAChR) antagonist di-hydro-β-erythroidine (DHβE, 8 μM) (Fig. 5.2 B). The current-voltage relationship of synaptic events revealed activation of an inward rectifying ion channel with a reversal potential of 0 mV, characteristic of nAChR activation (Fig. 5.2 C).

To determine the effect of cholinergic signaling on ipRGC light-response properties, we blocked retinal waves using DHβE and measured light-evoked activity after
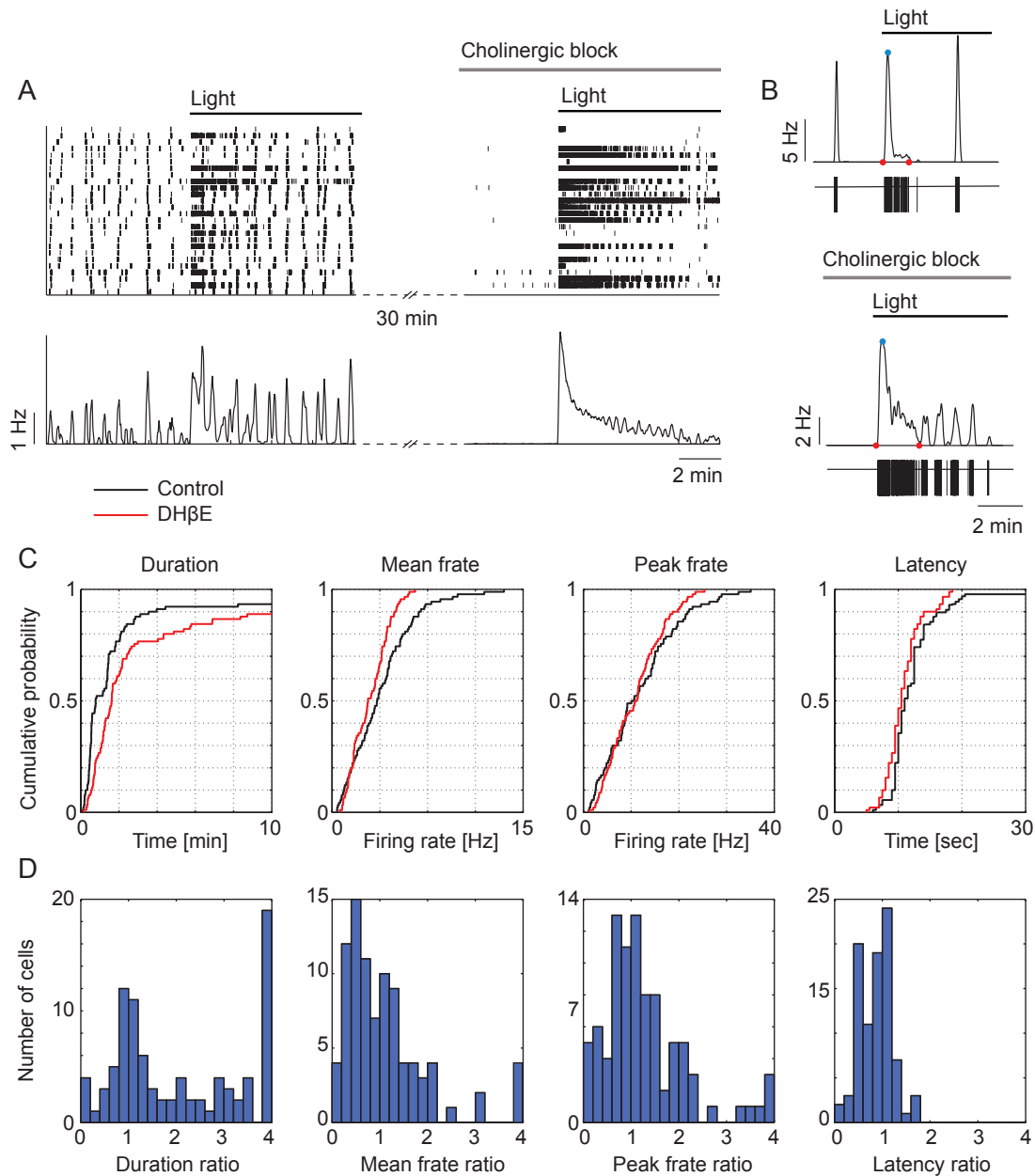
Figure 5.1: **Blockade of cholinergic input alters light-evoked RGC firing properties.**
(A) Multi-electrode array recording of light-evoked activity from a WT P6 retina before and after cholinergic block using DHβE. Top: Raster plot of single unit spike trains for subset of cells; Bottom: average firing rate of all units. (B) Example of single unit spike trains and instantaneous firing rates before (top) and after (bottom) cholinergic block. Red points mark beginning and end of light-evoked activity; blue point marks peak firing rate. (C) Cumulative probability distributions of light response parameters before (control, black) and after (DHβE, red) cholinergic block. (D) Ratio of light response parameters for units that showed light-evoked activity both before and after cholinergic block (Ratio = DHβE/control).

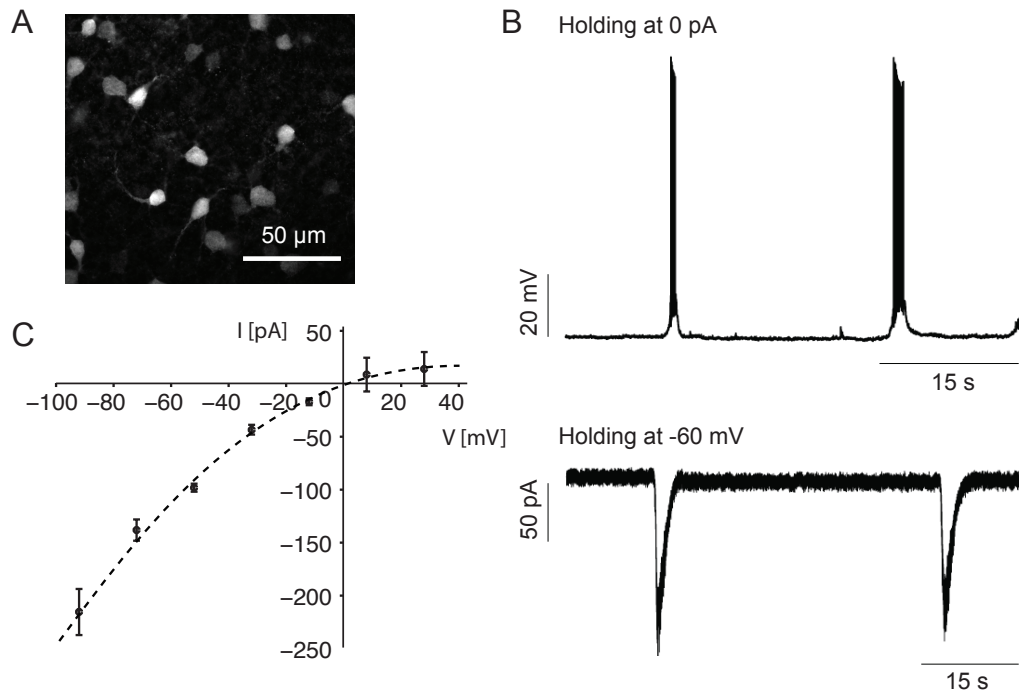Figure 5.2: **ipRGCs receive cholinergic input during waves.** (A) ipRGC cells labeled by GFP expression under melanopsin promoter in Opn4-EGFP mouse, P5 retina. (B) Example current-clamp (top) and voltage clamp (bottom) recordings of ipRGCs during retinal waves. (C) Current-voltage relationship of synaptic input onto ipRGCs during retinal waves.

30-minute blockade in the dark. Light stimulation evoked spiking on 56%±10% of active channels (Fig. 5.1 A, Table 5.1). A direct comparison of firing units in the presence and absence of cholinergic waves revealed that 53% of all light responsive units showed light-evoked activity in both the presence and absence of waves. In contrast, 36% "gained" a light response in the absence of waves, while the remaining 11% "lost" their response (Table 5.1). Repetitive trials of light exposure in control conditions showed that on average, 64% of light-responsive units maintained their response, 22% gained a response and 14% lost their response, indicating inherent variability in isolating light-responsive units from MEA recordings. Analysis of light-evoked firing properties showed that cells that were either lost or gained had lower peak firing rates on average, suggesting they may exhibit a weaker response and hence not be detected for all light exposure trials (Figs. 5.3). Nonetheless, since a higher percentage of cells were gained than lost in DHβE compared to repeated trials in control, our observations suggest that there might a net gain in light-responsive cells in the absence of cholinergic signaling.

Analysis of the single units that showed light responses in both control and DHβE

Table 5.1: Percent of light responsive units detected on multi-electrode array as (1) percent of total active units, and (2) percent of light responsive (LR) units that maintain, gain or lose their light response from control to pharmacological treatment. ($n = 4$ retinas for control and MFA; $n = 5$ retinas for DHβE and full block.)

Treatment (Control →)	LR units [% total units]	Maintained [% LR units]	Gained [% LR units]	Lost [% LR units]
Control	41±7	64±15	22±13	14±6
DHβE	56±10	53±18	36±7	11±8
Full block	51±19	51±24	37±15	12±9
MFA	24±7	42±11	9±7	49±18
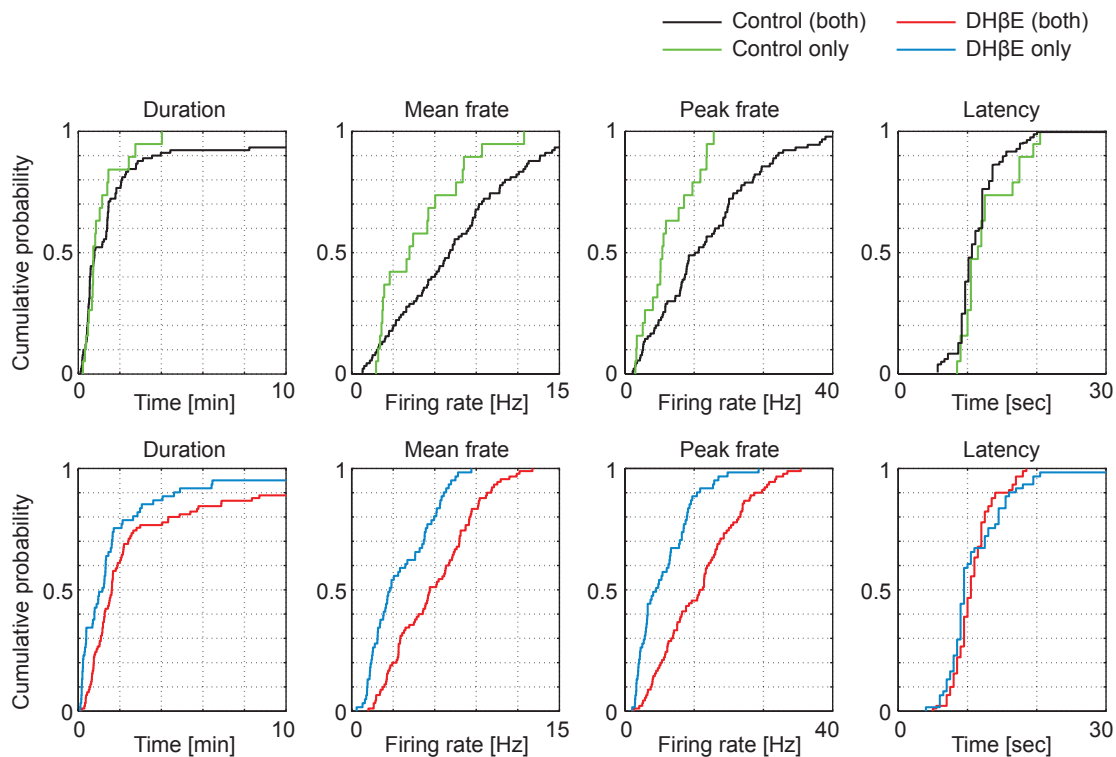
Figure 5.3: **Low firing rate ipRGCs are gained or lost.** Cumulative probability distributions of light response parameters before (control, top panels) and after (DHβE, bottom panels) cholinergic block. Response parameters are separated for cells that showed light-evoked activity in both control and DHβE (black and red lines), compared to cells that showed light-evoked activity in control only (green lines) or DHβE only (blue lines).

revealed that on average, the light response duration was prolonged in the absence of cholinergic signaling (Figs. 5.1 B–D). In contrast, peak firing rate or latency did not change (Figs. 5.1 C–D). In addition, a subset of cells showed synchronous, rhythmic bursting that, in some cases, persisted throughout the duration of light-exposure, similar to another study (Kirkby and Feller, 2013) (Figs. 5.1 A–B and Fig. 5.4). This correlated firing of light-sensitive cells was not observed in the presence of cholinergic waves. Rhythmic activity showed a periodicity of approximately 20 seconds, and individual cells were highly phase locked to other cells (Fig. 5.4 B). Together, these observations show that ipRGC firing properties are modulated by cholinergic input, and that a light-sensitive, oscillatory network emerges in the absence of cholinergic signaling. Below, we explore whether chemical or electrical signaling underlies the oscillatory network and whether intrinsic ipRGC light response properties are altered in the absence of cholinergic input.
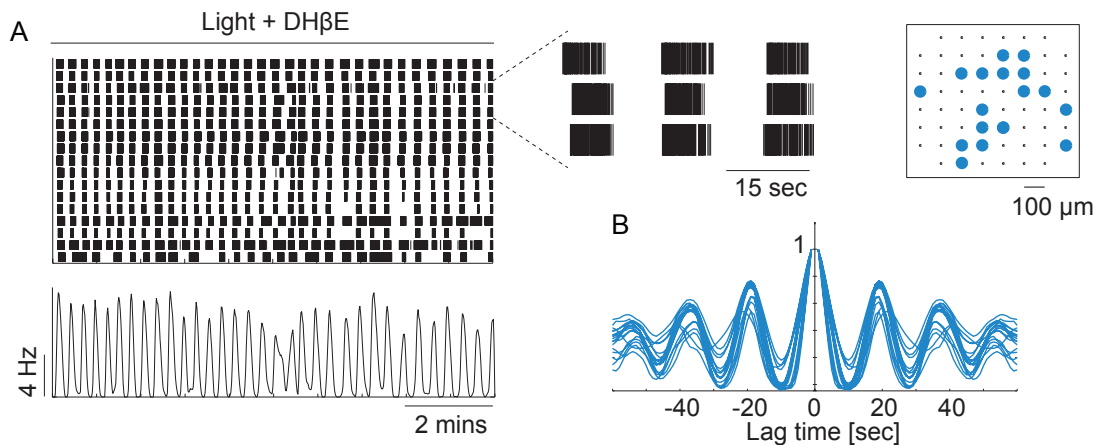
Figure 5.4: **Light responsive cells undergo oscillatory firing.** (A) Multi-electrode array recording of light-evoked activity from a WT P5 retina after cholinergic block using DHβE. Left: (Top) Raster plot of single unit spike trains for subset of cells. Inset shows expanded spike trains for three representative units; (Bottom) average firing rate of all units. Right: MEA location of cells represented in raster plot. (B) Autocorrelation functions of spike trains undergoing oscillatory firing in DHβE. Each line represents the autocorrelation function of different unit shown in raster plot A.

Altered light-evoked firing patterns mediated by electrical coupling via gap junctions

First, we established whether blockade of all fast synaptic chemical signaling eliminated the prolonged firing and oscillatory bursting observed in cholinergic block. We recorded light-evoked activity after 30-minute blockade of glutamatergic (D-AP5, 50 μM; DNQX, 20 μM), GABAergic (GABAzine, 5 μM), glycinergic (strychnine, 4 μM) and cholinergic

(DHβE, 8 μM) signaling. We observed similar light response properties compared to blockade of just cholinergic signaling alone (Fig. 5.5). Specifically, we saw a net prolonged light response and a subset of cells underwent oscillatory firing. In addition, we observed a net increase in the total number of light responsive cells under full block, similar to what we observed in DHβE alone (Table 5.1). These observations suggest that changes in light-evoked firing patterns observed in the absence of cholinergic signaling are not mediated by another form of fast chemical transmission.

Next we performed a complete pharmacological isolation of ipRGCs by additionally blocking electrical signaling using the non-selective gap junction antagonist meclofenamic acid (MFA, 100 μM). Light stimulation evoked spiking on 27$\pm$7% of active channels. None of the light-responsive cells showed a prolonged light response duration, and all units were silent after 1–2 minutes of activity (Fig. 5.6). Furthermore, no cells underwent rhythmic, oscillatory firing, suggesting that gap junctions likely underly the reverberant circuit observed in cholinergic block.

A direct comparison with firing units in the presence of cholinergic waves revealed that 42% of all light responsive units showed light-evoked activity in both control and MFA-treated retina, while 9% gained a light response and the remaining 49% lost their light response (Table 5.1). Therefore, we observe a net loss of light responsive cells in MFA, in contrast to the net increase observed in cholinergic block alone or full synaptic block. These observations suggest that electrical signaling may contribute to ipRGC light response properties even under control conditions, and that signaling may be enhanced in the absence of cholinergic waves.

Analysis of single unit responses showed that cells in combined full block plus MFA had lower mean and peak firing rates during their light response (Fig. 5.6 B, C). Although MFA is an effective gap junction antagonist and is favored for retinal preparations when compared to other antagonists (Pan et al., 2007; Veruki and Hartveit, 2009), it has been reported to open M-type potassium channels which may lead to membrane hyperpolarization and reduced firing rate (Peretz et al., 2005). However, MFA did not influence the firing rate of ipRGCs in adult rat retina (Weng et al., 2009), indicating that ipRGCs may not express the potassium channel composition that is subject to modulation by MFA. Nonetheless, further control experiments are necessary to establish the effects of MFA on physiological properties of ipRGCs.

From these data, we conclude that gap junction signaling mediates the increase in light-evoked activity and oscillatory firing that emerges following cholinergic block, thus propagating ipRGC light responses to a network of cells in the absence of cholinergic waves. Additionally, since MFA reduced the number, duration and firing rate of
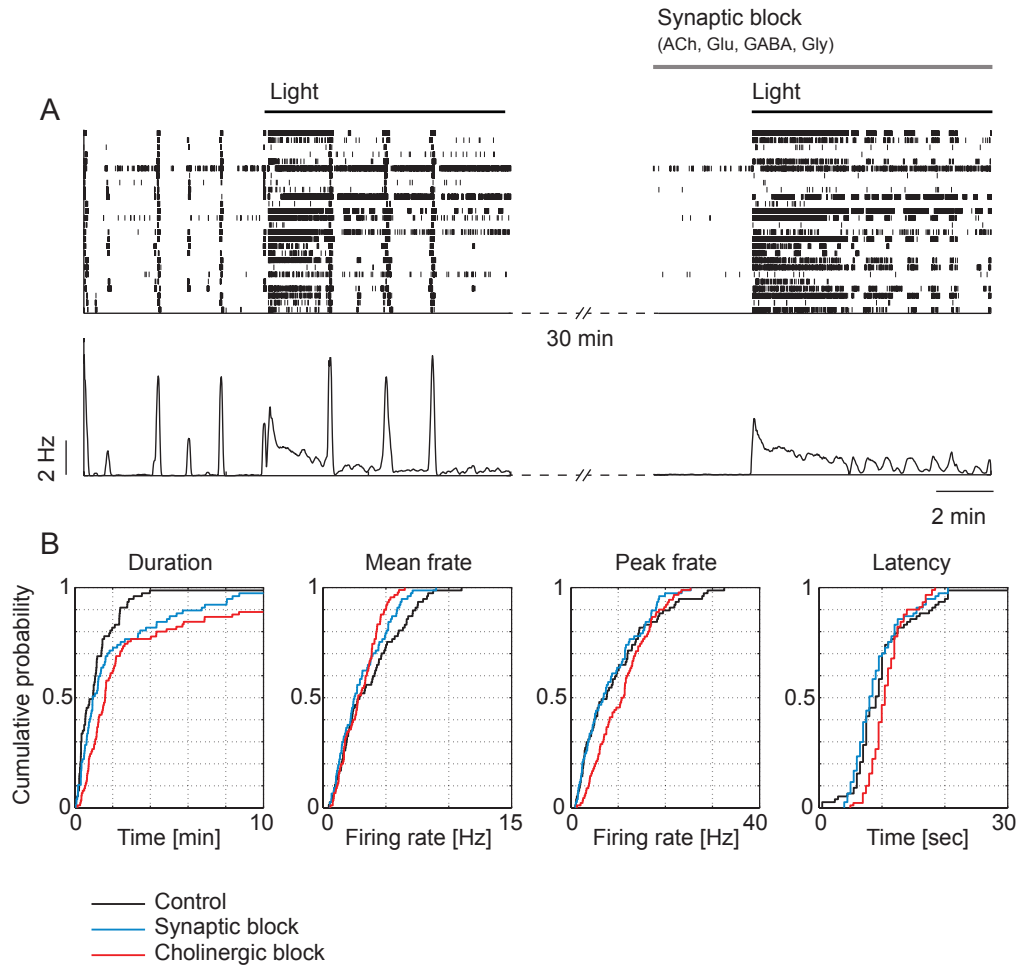
Figure 5.5: **ipRGC network not mediated by fast synaptic signaling.** (A) Multi-electrode array recording of light-evoked activity from a WT P6 retina before and after full synaptic block using D-AP5, DNQX, GABAzine, strychnine and DHβE. Top: Raster plot of single unit spike trains for subset of cells; Bottom: average firing rate of all units. (B) Cumulative probability distributions of light response parameters before (black, control) and after full synaptic block (blue). Overlaid for comparison are light response parameters after cholinergic block alone as shown in Fig. 5.1 C (red).
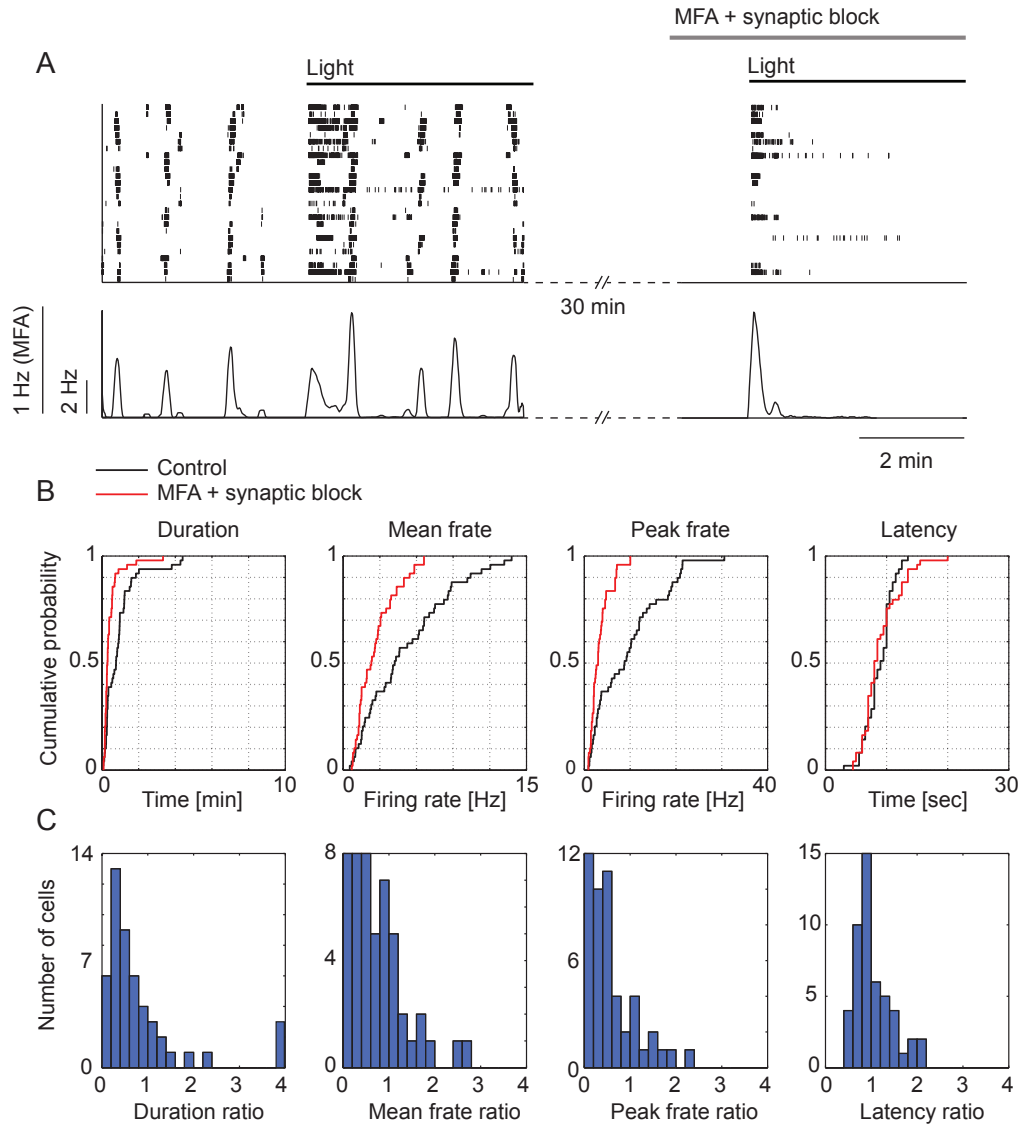
Figure 5.6: **ipRGC network mediated by electrical coupling.** (A) Multi-electrode array recording of light-evoked activity from a WT P6 retina before and after full synaptic and gap junction block using D-AP5, DNQX, GABAzine, strychnine, DHβE and MFA. Top: Raster plot of single unit spike trains for subset of cells; Bottom: average firing rate of all units. (B) Cumulative probability distributions of light response parameters before (black, control) and after blockade (red). (C) Ratio of light response parameters for units that showed light-evoked activity both before and after blockade (Ratio = (MFA+synaptic block)/control).

light-responsive cells relative to control conditions, they may also contribute to boosting ipRGC light responses even in the presence of cholinergic waves.

Light-sensitive cells show direct coupling to one another

To infer more about the connectivity properties of the light-evoked oscillatory network, we measured cross-correlograms (CCGs) of spiking units. Direct RGC-RGC coupling is characterized by a double-peak signature with peaks around ± 3 ms and a characteristic dip at 0 ms (Hu and Bloomfield, 2003; Bloomfield and Völgyi, 2009). We examined CCGs across cell pairs from each retina. In a given retina, we observed subsets of 2–3 units that showed the signature CCG of direct RGC-RGC coupling (Fig. 5.7), similar to another study (Tu et al., 2005). On average, coupled units were spaced on electrodes 100–200 μm apart—a distance that is within the dendritic diameter of ipRGCs, which is on average 200 μm from P5–P7 (Schmidt et al., 2008). This double peak CCG signature was eliminated by MFA and in addition was absent from CCGs of light-evoked activity in cholinergic waves (Fig. 5.7 B), suggesting that direct RGC-RGC coupling might usually be suppressed by cholinergic input. Interestingly, we observed some instances of units that showed direct coupling with another unit in the absence of cholinergic waves but no light-evoked activity in the presence of waves (see Fig. 5.7, cell *b*, for example). Whether these units correspond to melanopsin positive cells or whether they gain their light response via coupling to ipRGCs remains to be established.

Intrinsic light-response properties are unaltered by cholinergic signaling

We next tested whether the intrinsic excitability and light response properties of ipRGCs were dependent on cholinergic input. We used Opn4-EGFP mice to identify ipRGCs for targeted recordings. Membrane input resistance (R_m) is one measure of cellular excitability; cells with higher R_m typically require small synaptic current (ΔI) to depolarize them by a given amount (ΔV), in accordance with Ohm's law, $\Delta V = \Delta I \cdot R_m$. We determined the membrane resistance of melanopsin positive cells by measuring the amount of current required to hyperpolarize the cell from a holding potential of -60 mV to -80 mV and used Ohm's law to calculate R_m. We found that in the presence of cholinergic waves, ipRGCs had a membrane resistance of 280 ± 30 MΩ (Fig. 5.8 A). In the absence of cholinergic input, membrane resistances were 450 ± 60 MΩ, which was significantly higher than in control ($^*p < 0.05$).

We tested whether this difference manifested itself as an increased sensitivity of ipRGCs to light by measuring their irradiance-response curves. We performed cell-attached recordings of ipRGCs and measured their light-evoked firing rate by exposing them to a 5-second full-field light flash of increasing intensities, controlled us-
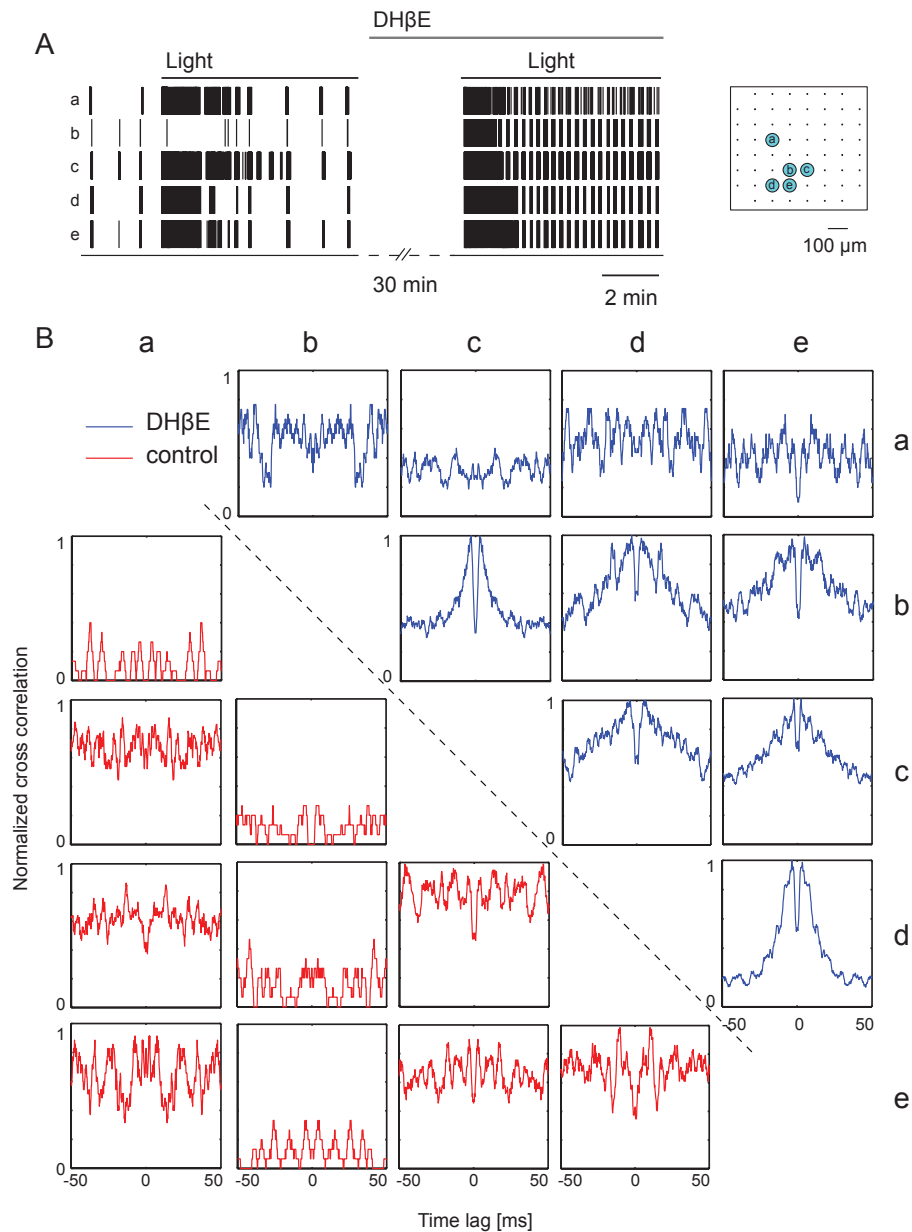
Figure 5.7: **RGCs show direct coupling in absence of waves.** (A) Left: Raster plot of 5 cells undergoing oscillatory firing in presence of DHβE; Right: Location of 5 cells on MEA. (B) Cross-correlograms (CCG) for all cell pairs shown in A, in the presence (control, red) and absence (DHβE, blue) of cholinergic waves. Cells *b–c* and *d–e* show direct coupling in the absence of waves, indicated by double peak signature in CCG; Cell *a* is an example of a cell whose spiking is not correlated with cells *b–e*, despite undergoing oscillatory firing, indicated by a relatively flat CCG. Other combinations of *b–e* show a mixture of indirect and direct coupling, indicated by a broad but peaked CCG combined with a dip at 0 ms.

ing optical density (OD) filters. ipRGCs showed a half-maximal response (IR50) of $\sim$ $1.08 \cdot 10^{13}$ photons s^{-1} cm^{-2} to white light stimulation, similar to another study (Schmidt et al., 2008). Blocking cholinergic input did not shift irradiance-response curves to lower light-intensities and showed a similar IR50 to control (Fig. 5.8 B). These results indicate that the light-sensitivity of ipRGCs is not increased by the absence of cholinergic waves, despite showing an increase in membrane resistance.
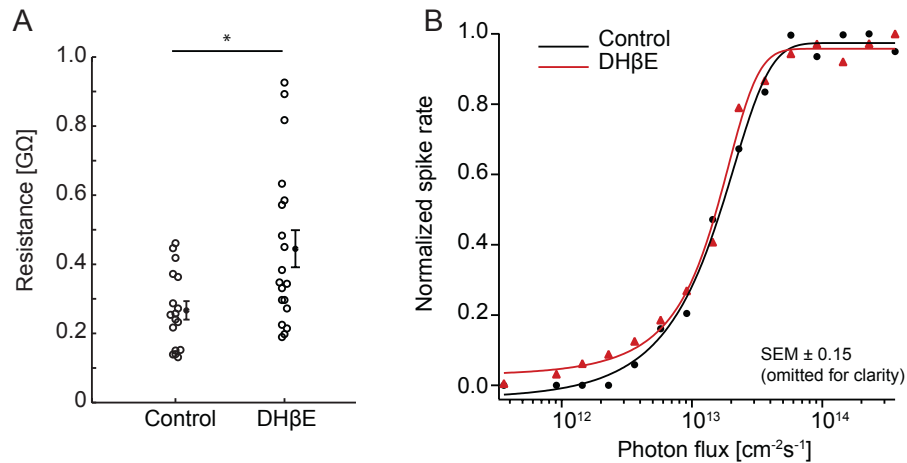
Figure 5.8: **Intrinsic light response properties of ipRGCs are unaltered.** (A) Membrane resistance of ipRGCs identified using the Opn4-EGFP mouse (refer to Fig. 5.2 A. (B) Irradiance-response curves of ipRGCs identified using the Opn4-EGFP mouse in the presence (control, black) and absence (DHβE, red) of cholinergic input.

Dopamine is produced and metabolized early in development

How does a gap junction coupled network of ipRGCs emerge in the absence of cholinergic signaling? One possibility is an indirect modulation of gap junction coupling by decreased dopamine signaling following cholinergic blockade. Several observations support this hypothesis. First, M1-type ipRGC dendrites tightly co-stratify with dopaminergic amacrine cell dendrites (DAC) (Vugler et al., 2007). There are at least five subtypes of ipRGCS (Schmidt et al., 2011), with the M1 subtype being prevalent during development (Tu et al., 2005). Second, ipRGCs express the D1 dopamine receptor, which, when activated, decreases ipRGC photocurrent in adult rat retina (Van Hook et al., 2012). Third, dopamine is a potent modulator of gap junction coupling (see Bloomfield and Völgyi, 2009 for review). Fourth, blockade of dopamine signaling stimulates the emergence of recovered gap junction waves in the absence of cholinergic waves (Kirkby and Feller, 2013).

To test this hypothesis, we first tested whether dopamine is produced and metabolized early in development. DACs can be identified by staining for tyrosine hydroxylase (TH) (Wulle and Schnitzer, 1989; Yoshida et al., 2011). Using an anti-TH antibody, we detected TH positive cells as young as P4, confirming DACs are present over the time window of our experiments (Fig. 5.9 A–B). We next tested whether dopamine was produced and metabolized at these ages by performing high-performance liquid chromatography (HPLC) with electrochemical detection (Mills et al., 2007) (HPLC dopamine extraction performed by Vanderbilt neurochemistry core). Dopamine (DA) and its primary metabolite dihydroxyphenylacetic acid (DOPAC) were present in all retinas tested, confirming dopamine is indeed produced and metabolized early in development (Fig. 5.9 C). The ratio of [DOPAC]/[DA] provides a measure of dopamine turnover rate; in adult retina, it is a low ratio of 1:1, consistent with distance diffusion of dopamine to exert effects in the outer retina before reuptake (Witkovsky, 2004; Cameron et al., 2009). In the developing retina, we measured a ratio of approximately 10:1, indicative of a relatively high turnover rate when compared to adult retina.
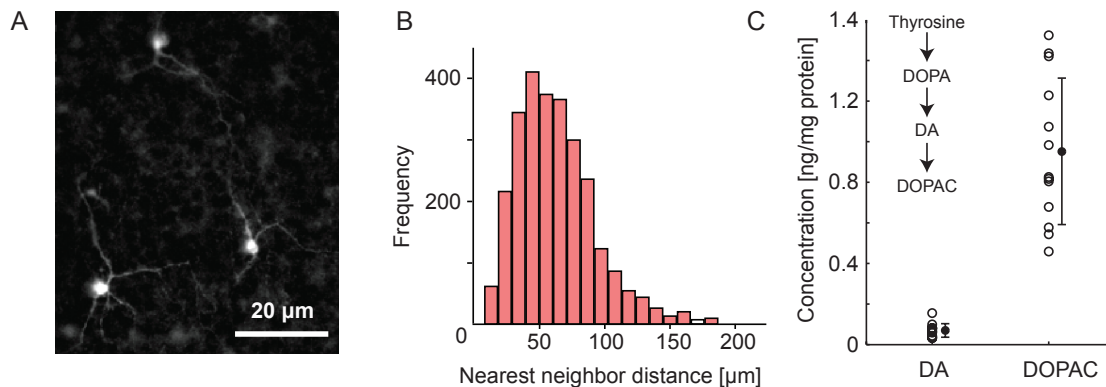
Figure 5.9: **Dopamine is produced and metabolized early in development.** (A) DACs labeled by anti-TH immunostaining in P4 whole mount retina. (B) Nearest neighbor distances of TH-positive cells (C) Concentrations of DA and DOPAC in P4–P6 retinas detected using HPLC. Each data point corresponds to a different retina, both retinas were extracted from each mouse.

Dopamine is released during cholinergic waves

Next, we tested whether dopamine is released during retinal waves using a cell-based neurotransmitter fluorescent engineered reporter (CNiFER), kindly provided by David Kleinfeld and Paul Slesinger (UCSD). These are HEK-293 cells that express the D2 receptor, which has been engineered to couple to the PLC pathway rather than the endogenous cAMP pathway. In addition, they express the FRET-based Ca^{2+} indicator TN-XXL. Increases in extracellular DA are thus reported as an increase in FRET ratio, resulting from

activation of D2 receptors and subsequent release of Ca^{2+} from inter-cellular stores. D2-CNiFERs can detect extracelluar DA within a range of 1–100 nM (Muller et al., *submitted*).

To test for diffuse release of DA during waves, we deposited CNiFERs on top of the inner-limiting membrane (ILM) of isolated whole-mount retinas using a micropipette and imaged their fluorescence in blue and yellow channels. We performed simultaneous whole-cell voltage-clamp recordings of nearby ganglion cells to monitor when a cholinergic wave passes over the retina in close proximity (Figs. 5.10 A–B). We observed spontaneous and transient increases in FRET ratio of imaged CNiFERs, indicative of dopamine detection (Fig. 5.10 C, black traces). Simultaneous voltage-clamp recordings revealed that FRET transients were often accompanied by large EPSCs associated with cholinergic waves (Fig. 5.10 C, red traces). Often times, we observed EPSCs that did not show an associated FRET transient (Fig. 5.10 C, left panel).

We determined whether there was a correlation between FRET ratio amplitude—a measurement of DA concentration—and the likelihood of observing isolated or consecutive dopamine events associated with consecutive waves. In general, isolated events showed a larger FRET ratio compared to consecutive events (Fig. 5.10 D). To determine how FRET ratio varied with [DA], we constructed a dose-response curve of CNiFERs on the ILM. We used a pressure injector to puff dopamine of known concentration above CNiFER cells and measured their FRET ratio. Our dose-response curve showed sensitivity to [DA] in the range of approximately 3–100 nM (Fig. 5.10 E). The amplitude of spontaneous FRET ratios ranged from 0.1–0.3, which corresponded to [DA] of approximately 6–40 nM. Isolated events showed an average FRET ratio of 0.24 ($\sim$25–30 nM) compared to 0.08 ($\sim$8–9 nM) for consecutive events (Figs. 5.10 D–E). These observations are consistent with a refractory period associated with the sensor, where high [DA] (large FRET ratio) reduces the probability of detecting consecutive events.

To determine a temporal correlation between waves and dopamine events, we measured the time between each FRET transient and the nearest wave. We found that on average, FRET transients followed a wave by 20–30 seconds (Fig. 5.10 F). In addition, there were some FRET transients that preceded waves by up to 1 minute. The time course of FRET signals were much slower than wave-associated EPSCs, where the full width at half maximum of signals was up to 30 seconds long. This is likely a consequence of the slow signaling cascaded that underlies increases in FRET ratio. In contrast, the width of EPSCs were approximately 3–5 seconds long.

We quantified whether the observed peak at 20–30 seconds could have occurred by chance by assuming that waves and dopamine transients occurred independently and simulating data as follows. We measured the mean and standard deviation of wave

and FRET rates from our dataset. Next, we simulated recordings using these rates, assuming that the two events were independent of one another, and calculated the time between each FRET transient and nearest wave. From this simulation, we would expect only $16\pm5\%$ of all FRET transients in our dataset to follow a wave by 10–30 seconds (Fig. 5.10 F). In contrast, our data showed that 57% of observed FRET transients fell within this time lag. These data suggest that, despite slow sensor kinetics and a broad distribution of FRET-to-wave time lags, most dopamine-associated FRET events were correlated with retinal waves within a 10–30 second window. In addition to slow sensor kinetics, this long time lag could result from the diffusion time of DA from release sites at DAC terminals to CNiFERs above the ILM.

Dopamine is released by stimulation of retinal cells

As an additional test of a refractory period, we puffed high-potassium (K^+) solution into the inner-nuclear layer—where DACs are located—to stimulate release of DA by depolarizing DACs and other nearby cells. We observed FRET transients with ratios in the range of 0.1–0.3, which accompanied K^+ puffs with a lag of approximately 10–20 seconds—a similar time lag to that observed during wave events (Fig. 5.11 A). Interestingly, a second puff approximately one minute later elicited only a modest increase in FRET ratio, provided the response to the first puff was small (< 0.1). This is consistent with the hypothesis that a refractory period inherent to the CNiFER sensor limits the ability to detect multiple, consecutive events. After monitoring for signal recovery, K^+-stimulated events were blocked by the D2 receptor antagonist raclopride ($4\,\mu M$), confirming they were due to detection of extracellular DA and not by direct stimulation of CNiFERs by K^+ (Fig. 5.11 B). Finally, in the presence of GABAzine to block GABA-A receptors, FRET responses were larger than in control, reaching ratios up to 0.5–0.6 (Fig. 5.11 C). These observations suggest that DA release may usually be partially inhibited by GABAergic signaling.

Dopamine release is reduced following blockade of waves

Finally, we tested whether dopamine-associated FRET transients were eliminated following blockade of cholinergic waves. We imaged CNiFERs while blocking cholinergic waves with DHβE. We observed small FRET transients, which were not associated with EPSCs recorded in nearby ganglion cells (Fig. 5.12 A). However, we observed an occasional wave-associated EPSC, albeit with lower frequency than in the absence of DHβE, and thus cannot rule out the possibility that FRET events were triggered by residual cholinergic signaling. The amplitude of these events ranged from a FRET ratio of approximately 0.01–0.05 (Fig. 5.12 B). These corresponded to [DA] of approximately 1–3 nM—over an order of magnitude lower than those associated with cholinergic waves.
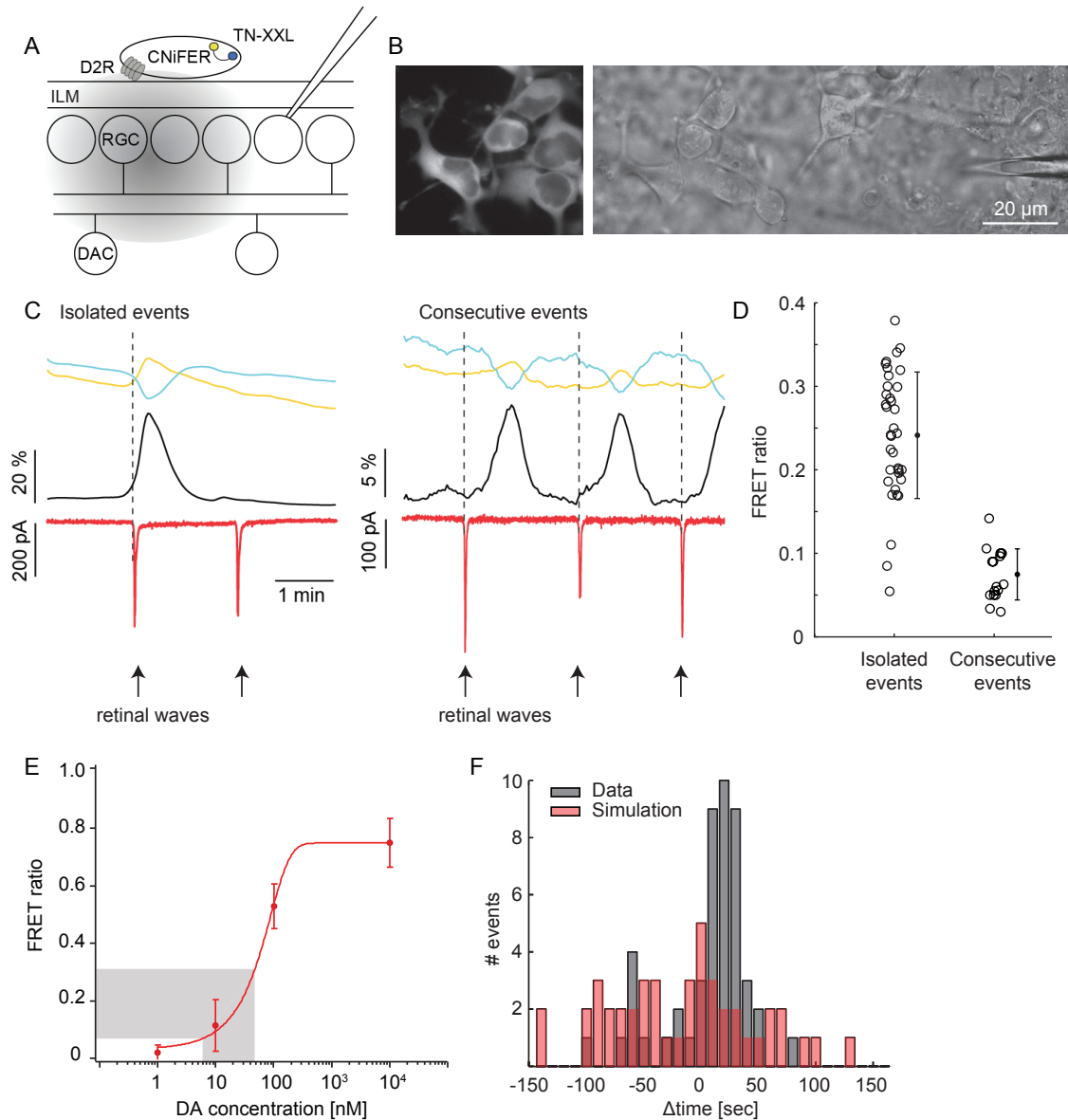
Figure 5.10: **Dopamine is released during cholinergic waves.** (A) Schematic of experimental setup (refer to text). (B) Bright field (left) and fluorescence (right) image of CNiFERs above ILM and patch electrode. (C) Example traces of CNiFER imaging and simultaneous RGC recordings for isolated FRET event (left) and consecutive FRET events (right): FRET-ratio (black) corresponds to the ratio of YFP (yellow) to CFP (blue) channels; whole-cell voltage-clamp recording (red) of nearby RGC. Large EPSCs are associated with retinal waves. (D) Amplitude of FRET ratio for isolated and consecutive events. (E) Dose-response curve of CNiFERs. (F) Time from each FRET event to nearest wave-associated EPSC for observed data (black) compared to simulated data (red). ILM: inner-limiting membrane; CNiFER: cell-based neurotransmitter fluorescent engineered reporter; RGC: retinal ganglion cell; DAC: dopaminergic amacrine cell.
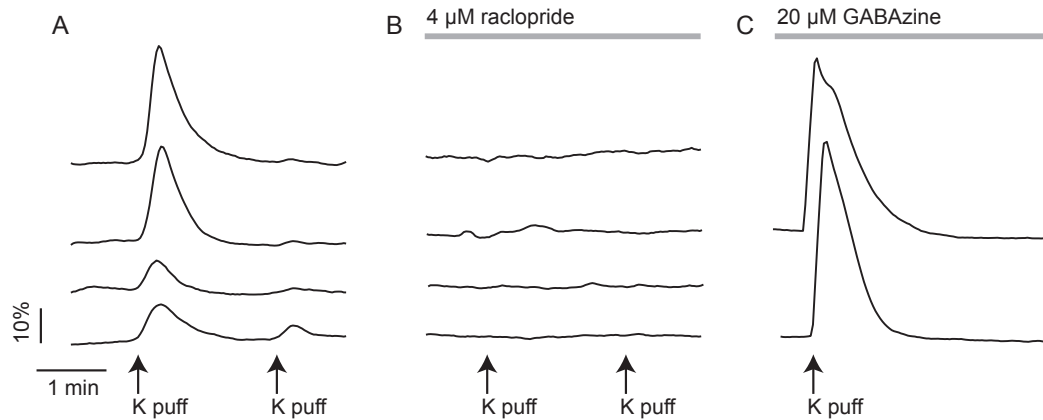
Figure 5.11: **Dopamine is released by stimulation of retinal cells.** Example FRET traces of CNiFER responses to 0.5 s puff of high-potassium solution in control (A), under blockade of D2 dopamine receptors (raclopride, 4 μM; B), and under blockade of GABA-A receptors (GABAzine, 20 μM; C).

Therefore, we conclude that spontaneous cholinergic waves result in diffuse release of dopamine, and that release is reduced but not blocked entirely upon blockade of cholinergic waves.
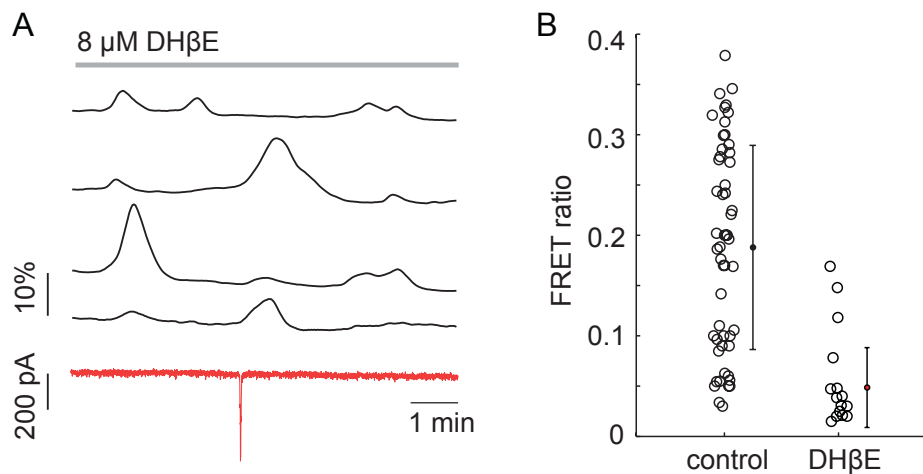
Figure 5.12: **Dopamine release is reduced in absence of cholinergic waves.** (A) Example traces of spontaneous CNiFER FRET transients in presence of DHβE to block retinal waves (black). Simultaneous recording of nearby RGC showed occasional wave-associated EPSCs (red). (B) Amplitude of FRET ratio in DHβE compared to control.

Dopamine blockade alone does not alter ipRGC firing patterns

Based on the above observation that dopamine is released during cholinergic waves and reduced following wave blockade, we postulated that our observed changes in light response properties of ipRGCs could be due to an indirect reduction of dopaminergic signaling onto ipRGCs. We tested whether blockade of dopamine signaling alone, while maintaining cholinergic signaling, produced similar changes to those observed under cholinergic block alone. We used MEA recordings to measure the light-response properties following 30-minute blockade of either D1 or D2 dopamine receptors, using the antagonists SCH-23390 ($10\,\mu$M) and raclopride ($8\,\mu$M), respectively. Surprisingly, neither drug showed a large effect on light-evoked firing, although a subset of cells in one retina showed oscillatory firing following blockade of D1 receptors (Fig. 5.13 A–B). These observations suggest that blockade of dopamine signaling alone is not sufficient to alter light response properties of ipRGCs. However, it does not rule out the possibility that the combined reduction of both dopaminergic and cholinergic signaling is required.

To test this possibility, we bath applied dopamine while blocking cholinergic waves. We found that the enhanced light response and oscillatory firing observed under blockade of cholinergic waves alone was occluded when combined with DA application (Fig. 5.13 B, right panel). These results point to a mechanism by which a combined reduction of both cholinergic and dopaminergic signaling is required to enhance electrical coupling of ipRGCs, similar to what is observed for the recovery of correlated gap junction waves in the absence of cholinergic signaling (Kirkby and Feller, 2013). Below, we discuss possible functions and mechanisms that might underly the dynamic regulation of ipRGC electrical coupling by cholinergic input during retinal development.

Discussion

In this study we demonstrate that the light-evoked firing properties of ipRGCs are modulated by cholinergic input received during retinal waves. In the absence of cholinergic waves, ipRGCs formed an electrically-coupled gap junction network, which resulted in a prolonged light response duration and oscillatory, synchronous firing with other cells (Figs. 5.1 and 5.4). In addition, we detected an increase in the number of light-responsive units in the absence of cholinergic waves, suggesting that gap junctions might propagate light-responses among ganglion cells. Blockade of gap junctions in addition to cholinergic waves not only blocked the changes in light-evoked activity patterns but also led to a reduction in the number of light-responsive units relative to control conditions (Fig. 5.6 and Table 5.1). These findings might implicate gap junctions in propagating ipRGC light responses in the intact retinal circuit, albeit to a lesser extent than in the absence of cholinergic waves.
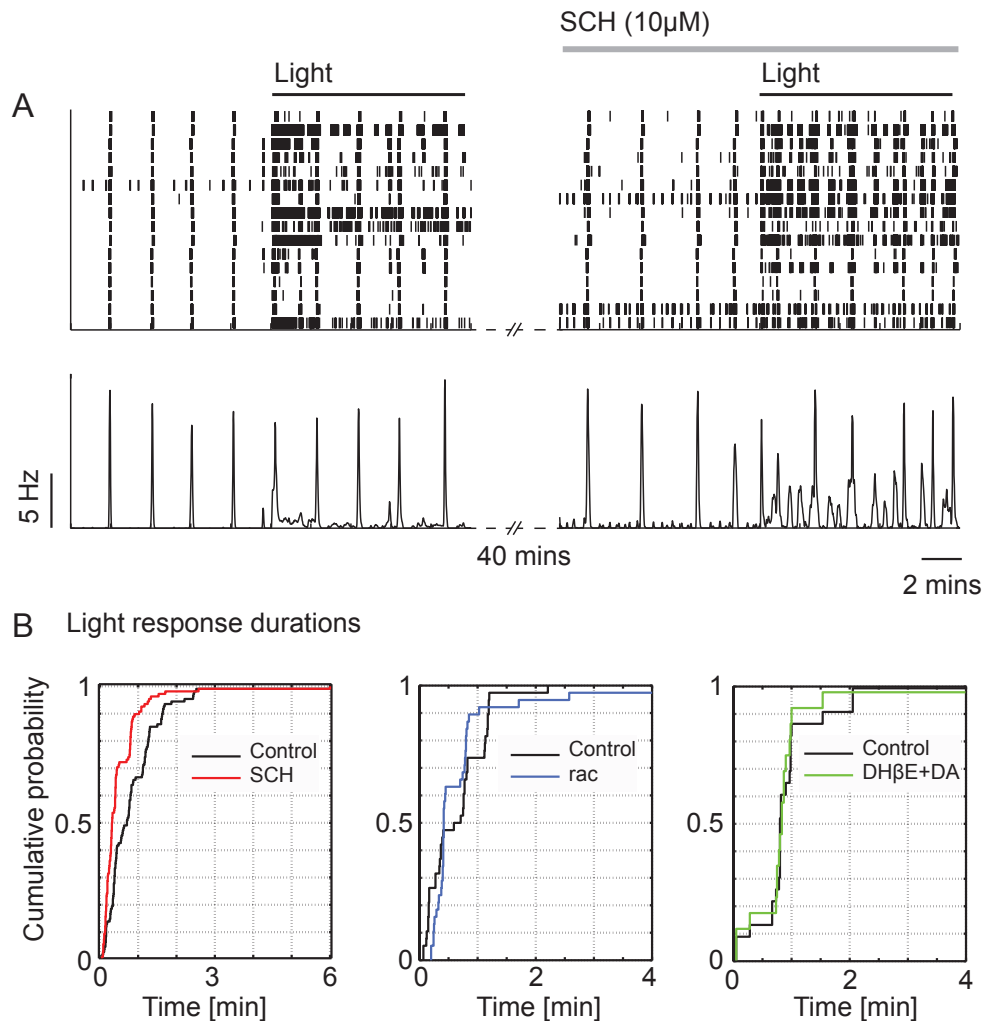
Figure 5.13: **Blockade of dopamine signaling alone does not alter light response.** (A) Multi-electrode array recording of light-evoked activity from a WT P5 retina before and after blockade of dopamine D1 receptors using SCH-23390. Top: Raster plot of single unit spike trains for subset of cells; Bottom: average firing rate of all units. (B) Cumulative probability distributions of light response duration before (black, control) and after blockade of D1 receptors (red, SCH), D2 receptors (blue, rac), and combined blockade of cholinergic waves plus supplied dopamine (green, DHβE+DA).

The identity of cells coupled to ipRGCs remains to be delineated. Our observations indicate direct coupling between ganglion cells, either to other ipRGCs or to another class of RGCs (Fig. 5.7). However, there is no precedence of this type of direct RGC–RGC coupling of ipRGCs, either during development or in the adult. Several studies have reported evidence of gap junction coupling of ipRGCs during development, as indicated by a reduction in the number of light-responsive cells using a calcium imaging assay (Sekaran et al., 2003; Sekaran et al., 2005 but see Bramley et al., 2011), or by a change in the physiological membrane properties of ipRGCs (Schmidt et al., 2008) upon application of gap junction antagonists, but the identity of coupled cells remains unknown. In the adult, ipRGCs show neurobiotin tracer coupling to wild field GABAergic amacrine cells (Müller et al., 2010), however, their firing properties are not found to be dependent on gap junction signaling (Weng et al., 2009). In order to further elucidate gap junction ipRGC circuits, we propose to combine neurobiotin tracer coupling of ipRGCs with calcium imaging to detect light responsive cells and immunohistochemistry against melanopsin. This will allow us to assess whether anatomically coupled cells are also functionally coupled, and whether they correspond to ipRGCs. Using this setup, we can probe whether RGCs that gain a light response in the absence of cholinergic waves are melanopsin positive and whether they directly couple to other ipRGCs.

There is growing evidence of the coexistence and functional interaction of chemical and electrical synapses across the nervous system (reviewed in Pereda, 2014). These interactions are particularly prevalent in the inferior olive, where recent studies have shown that electrical coupling can be strengthen (Turecek et al., 2014) or weakened (Mathy et al., 2014) by glutamatergic signaling through NMDA receptors, and additionally be weakened by inhibitory GABAergic signaling (Lefler et al., 2014). Here, we show that electrical coupling of ipRGCs emerges following reduced cholinergic transmission (Figs. 5.6 and 5.7). Similar increase in electrical coupling following reduced cholinergic input has been observed in adrenal chromaffin cells (Martin et al., 2003). Our observations suggest that a combined reduction in cholinergic and dopaminergic signaling is required for the change in electrical coupling (Fig. 5.13), although the detailed mechanisms remains to be elucidated. Other studies have implicated a change in calcium influx and phosphorylation by neuromodulators in mechanisms underlying the regulation of gap junction expression and conductivity, respectively (reviewed in Pereda, 2014). Thus, we postulate that the reduced cholinergic input could result in reduced calcium influx, which could increase gap junction expression, while reduced dopaminergic signaling could result in increased gap junction conductivity. Consistent with this hypothesis is that dopamine release is stimulated by cholinergic waves, and that release is reduced upon blockade of waves (Figs. 5.10 and 5.12). Furthermore, this hypothesis is supported by our observations that dopamine blockade alone does not alter light-evoked firing pat-

terns, but that the change is occluded by application of dopamine (Fig. 5.13).

The functional implications of cholinergic modulation of gap junction coupling of ipRGCs are diverse. First, ipRGCs mediate plasticity in retinal wave circuits, whereby they stimulate recovery of correlated activity via gap junctions in the absence of cholinergic waves (Kirkby and Feller, 2013). Thus, an increase in their electrical coupling upon blockade of cholinergic input not only triggers synchronous firing among subsets of cells (Fig. 5.4) but also increases the contribution of ipRGCs to network activity, thereby transitioning from a light-insensitive cholinergic wave circuit to a light-sensitive gap junction wave circuit. Second, ipRGCs themselves are involved in a variety of developmental functions, including light-avoidance behavior in pups (Johnson et al., 2010), the development of eye vasculature (Rao et al., 2013), and perhaps also in the refinement of RGC projections to the dorsal lateral geniculate nucleus (Renna et al., 2011). We postulate that the mechanism underlying our observations could provide a means for cholinergic signaling to regulate ipRGC firing in a homeostatic manner, whereby ipRGCs undergo an increase in coupling and light-evoked activity upon reduced excitatory drive (cholinergic waves), thus allowing them to maintain a homeostatic set point for driving light-dependent developmental functions.

In summary, our results demonstrate that gap junction coupling of ipRGCs are dynamically regulated in development by cholinergic input during retinal waves. Our findings provide mechanistic insight into how ipRGCs influence and are influenced by visual circuits. It is interesting to postulate whether functional interaction between chemical and electrical communication might also be required for normal function of ipRGCs in adult retina.

Bibliography

Ackman, J. B., Burbridge, T. J., and Crair, M. C. (2012). Retinal waves coordinate patterned activity throughout the developing visual system. *Nature* **490**, 219–225.

Bansal, A et al. (2000). Mice lacking specific nicotinic acetylcholine receptor subunits exhibit dramatically altered spontaneous activity patterns and reveal a limited role for retinal waves in forming ON and OFF circuits in the inner retina. *The Journal of neuroscience : the official journal of the Society for Neuroscience* **20**, 7672–7681.

Bargmann, C. I. (2012). Beyond the connectome: how neuromodulators shape neural circuits. *BioEssays : news and reviews in molecular, cellular and developmental biology* **34**, 458–465.

Berson, D. M. (2003). Strange vision: ganglion cells as circadian photoreceptors. *Trends in neurosciences* **26**, 314–320.

Bjartmar, L. et al. (2006). Neuronal pentraxins mediate synaptic refinement in the developing visual system. *The Journal of neuroscience : the official journal of the Society for Neuroscience* **26**, 6269–6281.

Blank, M. et al. (2011). The Down syndrome critical region regulates retinogeniculate refinement. *The Journal of neuroscience : the official journal of the Society for Neuroscience* **31**, 5764–5776.

Blankenship, A. G. and Feller, M. B. (2010). Mechanisms underlying spontaneous patterned activity in developing neural circuits. *Nature reviews Neuroscience* **11**, 18–29.

Blankenship, A. G. et al. (2011). The role of neuronal connexins 36 and 45 in shaping spontaneous firing patterns in the developing retina. *The Journal of neuroscience : the official journal of the Society for Neuroscience* **31**, 9998–10008.

Bloomfield, S. A., Xin, D, and Persky, S. E. (1995). A comparison of receptive field and tracer coupling size of horizontal cells in the rabbit retina. *Visual neuroscience* **12**, 985–999.

Bloomfield, S. A. and Völgyi, B. (2009). The diverse functional roles and regulation of neuronal gap junctions in the retina. *Nature reviews Neuroscience* **10**, 495–506.

Blumberg, M. S., Marques, H. G., and Iida, F. (2013). Twitching in sensorimotor development from sleeping rats to robots. *Current biology : CB* **23**, R532–7.

Bonifazi, P et al. (2009). GABAergic hub neurons orchestrate synchrony in developing hippocampal networks. *Science (New York, NY)* **326**, 1419–1424.

Boulanger, L. M. (2009). Immune proteins in brain development and synaptic plasticity. *Neuron* **64**, 93–109.

Bramley, J. R., Wiles, E. M., Sollars, P. J., and Pickard, G. E. (2011). Carbenoxolone blocks the light-evoked rise in intracellular calcium in isolated melanopsin ganglion cell photoreceptors. *PLoS One* **6**, e22721.

Brustein, E. et al. (2003). Steps during the development of the zebrafish locomotor network. *Journal of physiology, Paris* **97**, 77–86.

Butts, D. A. (2002). Retinal waves: implications for synaptic learning rules during development. *The Neuroscientist : a review journal bringing neurobiology, neurology and psychiatry* **8**, 243–253.

Butts, D. A. and Kanold, P. O. (2010). The applicability of spike time dependent plasticity to development. *Frontiers in synaptic neuroscience* **2**, 30.

Butts, D. A., Kanold, P. O., and Shatz, C. J. (2007). A burst-based "Hebbian" learning rule at retinogeniculate synapses links retinal waves to activity-dependent refinement. *PLoS biology* **5**, e61.

Cameron, M. A. et al. (2009). Light regulation of retinal dopamine that is independent of melanopsin phototransduction. *The European journal of neuroscience* **29**, 761–767.

Chalupa, L. M. (2009). Retinal waves are unlikely to instruct the formation of eye-specific retinogeniculate projections. *Neural Development* **4**, 25.

Chandrasekaran, A. R., Plas, D. T., Gonzalez, E., and Crair, M. C. (2005). Evidence for an instructive role of retinal activity in retinotopic map refinement in the superior colliculus of the mouse. *The Journal of neuroscience : the official journal of the Society for Neuroscience* **25**, 6929–6938.

Chen, C and Regehr, W. G. (2000). Developmental remodeling of the retinogeniculate synapse. *Neuron* **28**, 955–966.

Chub, N and O'Donovan, M. J. (1998). Blockade and recovery of spontaneous rhythmic activity after application of neurotransmitter antagonists to spinal networks of the chick embryo. *Journal of Neuroscience* **18**, 294–306.

Clarke, L. E. and Barres, B. A. (2013). Emerging roles of astrocytes in neural circuit development. *Nature reviews Neuroscience* **14**, 311–321.

Cline, H. (2003). Sperry and Hebb: oil and vinegar? *Trends in neurosciences* **26**, 655–661.

Colonnese, M. T. and Khazipov, R. (2010). "Slow activity transients" in infant rat visual cortex: a spreading synchronous oscillation patterned by retinal waves. *The Journal of neuroscience : the official journal of the Society for Neuroscience* **30**, 4325–4337.

Colonnese, M. T. et al. (2010). A conserved switch in sensory processing prepares developing neocortex for vision. *Neuron* **67**, 480–498.

Cregg, M. et al. (2003). Development of refractive error and strabismus in children with Down syndrome. *Investigative ophthalmology & visual science* **44**, 1023–1030.

Crisp, S., Evers, J. F., Fiala, A., and Bate, M. (2008). The development of motor coordination in Drosophila embryos. . . . *Development* **135**, 3707–3717.

Crisp, S. J., Evers, J. F., and Bate, M. (2011). Endogenous patterns of activity are required for the maturation of a motor network. *The Journal of neuroscience : the official journal of the Society for Neuroscience* **31**, 10445–10450.

Dehorter, N, Vinay, L, Hammond, C, and Ben-Ari, Y (2012). Timing of developmental sequences in different brain structures: physiological and pathological implications. *The European journal of neuroscience* **35**, 1846–1856.

Demas, J. A., Payne, H., and Cline, H. T. (2012). Vision drives correlated activity without patterned spontaneous activity in developing Xenopus retina. *Developmental neurobiology* **72**, 537–546.

Demas, J., Eglen, S. J., and Wong, R. O. L. (2003). Developmental loss of synchronous spontaneous activity in the mouse retina is independent of visual experience. *The Journal of neuroscience : the official journal of the Society for Neuroscience* **23**, 2851–2860.

Dhande, O. S. et al. (2011). Development of single retinofugal axon arbors in normal and *β*2 knock-out mice. *The Journal of neuroscience : the official journal of the Society for Neuroscience* **31**, 3384–3399.

Eglen, S. J., Demas, J., and Wong, R. O. L. (2003). Mapping by waves. Patterned spontaneous activity regulates retinotopic map refinement. *Neuron* **40**, 1053–1055.

Feldheim, D. A. and O'Leary, D. D. M. (2010). Visual map development: bidirectional signaling, bifunctional guidance molecules, and competition. *Cold Spring Harbor perspectives in biology* **2**, a001768.

Feldt, S., Bonifazi, P., and Cossart, R. (2011). Dissecting functional connectivity of neuronal microcircuits: experimental and theoretical insights. *Trends in neurosciences* **34**, 225–236.

Feller, M. B. (1999). Spontaneous correlated activity in developing neural circuits. *Neuron* **22**, 653–656.

Feller, M. B. et al. (1996). Requirement for cholinergic synaptic transmission in the propagation of spontaneous retinal waves. *Science (New York, NY)* **272**, 1182–1187.

Feller, M. B. et al. (1997). Dynamic processes shape spatiotemporal properties of retinal waves. *Neuron* **19**, 293–306.

Feller, M. B. (2009). Retinal waves are likely to instruct the formation of eye-specific retinogeniculate projections. *Neural Development* **4**, 24.

Ford, K. J. and Feller, M. B. (2012). Assembly and disassembly of a retinal cholinergic network. *Visual neuroscience* **29**, 61–71.

Ford, K. J., Félix, A. L., and Feller, M. B. (2012). Cellular mechanisms underlying spatiotemporal features of cholinergic retinal waves. *The Journal of neuroscience : the official journal of the Society for Neuroscience* **32**, 850–863.

Fuerst, P. G., Koizumi, A., Masland, R. H., and Burgess, R. W. (2008). Neurite arborization and mosaic spacing in the mouse retina require DSCAM. *Nature* **451**, 470–474.

Fuerst, P. G. et al. (2009). DSCAM and DSCAML1 function in self-avoidance in multiple cell types in the developing mouse retina. *Neuron* **64**, 484–497.

Furman, M. and Crair, M. C. (2012). Synapse maturation is enhanced in the binocular region of the retinocollicular map prior to eye opening. *Journal of neurophysiology* **107**, 3200–3216.

Furman, M., Xu, H.-P., and Crair, M. C. (2013). Competition driven by retinal waves promotes the morphological and functional synaptic development of neurons in the superior colliculus. *Journal of neurophysiology*.

Galli, L and Maffei, L (1988). Spontaneous impulse activity of rat retinal ganglion cells in prenatal life. *Science (New York, NY)* **242**, 90–91.

Gastinger, M. J., Tian, N., Horvath, T., and Marshak, D. W. (2006). Retinopetal axons in mammals: emphasis on histamine and serotonin. *Current eye research* **31**, 655–667.

Gjorgjieva, J. and Eglen, S. J. (2011). Modeling developmental patterns of spontaneous activity. *Current opinion in neurobiology* **21**, 679–684.

Godfrey, K. B. and Swindale, N. V. (2007). Retinal wave behavior through activity-dependent refractory periods. *PLoS computational biology* **3**, e245.

Godfrey, K. B., Eglen, S. J., and Swindale, N. V. (2009). A multi-component model of the developing retinocollicular pathway incorporating axonal and synaptic growth. *PLoS computational biology* **5**, e1000600.

Gonzalez-Islas, C. and Wenner, P. (2006). Spontaneous network activity in the embryonic spinal cord regulates AMPAergic and GABAergic synaptic strength. *Neuron* **49**, 563–575.

Goodman, C. S. and Shatz, C. J. (1993). Developmental mechanisms that generate precise patterns of neuronal connectivity. *Cell* **72 Suppl**, 77–98.

Gotti, S., Caricati, E., and Panzica, G. (2011). Alterations of brain circuits in Down syndrome murine models. *Journal of chemical neuroanatomy* **42**, 317–326.

Grimbert, F. and Cang, J. (2012). New model of retinocollicular mapping predicts the mechanisms of axonal competition and explains the role of reverse molecular signaling during development. *The Journal of neuroscience : the official journal of the Society for Neuroscience* **32**, 9755–9768.

Grubb, M. S., Rossi, F. M., Changeux, J.-P., and Thompson, I. D. (2003). Abnormal functional organization in the dorsal lateral geniculate nucleus of mice lacking the beta 2 subunit of the nicotinic acetylcholine receptor. *Neuron* **40**, 1161–1172.

Guido, W. (2008). Refinement of the retinogeniculate pathway. *The Journal of physiology* **586**, 4357–4362.

Gurung, B. and Fritzsch, B. (2004). Time course of embryonic midbrain and thalamic auditory connection development in mice as revealed by carbocyanine dye tracing. *The Journal of comparative neurology* **479**, 309–327.

Hamburger, V and Balaban, M (1963). Observations and experiments on spontaneous rhythmical behavior in the chick embryo. *Developmental biology* **6**, 533–545.

Hanganu, I. L., Ben-Ari, Y., and Khazipov, R. (2006). Retinal waves trigger spindle bursts in the neonatal rat visual cortex. *The Journal of neuroscience : the official journal of the Society for Neuroscience* **26**, 6728–6736.

Hanson, M. G. and Landmesser, L. T. (2004). Normal patterns of spontaneous activity are required for correct motor axon guidance and the expression of specific guidance molecules. *Neuron* **43**, 687–701.

Hattar, S et al. (2003). Melanopsin and rod–cone photoreceptive systems account for all major accessory visual functions in mice. *Nature* **424**, 75–81.

Hennig, M. H., Adams, C., Willshaw, D., and Sernagor, E. (2009). Early-stage waves in the retinal network emerge close to a critical state transition between local and global functional connectivity. *The Journal of neuroscience : the official journal of the Society for Neuroscience* **29**, 1077–1086.

Hennig, M. H., Grady, J., Coppenhagen, J. van, and Sernagor, E. (2011). Age-dependent homeostatic plasticity of GABAergic signaling in developing retinal networks. *The Journal of neuroscience : the official journal of the Society for Neuroscience* **31**, 12159–12164.

Hooks, B. M. and Chen, C. (2006). Distinct roles for spontaneous and visual activity in remodeling of the retinogeniculate synapse. *Neuron* **52**, 281–291.

Hu, E. H. and Bloomfield, S. A. (2003). Gap junctional coupling underlies the short-latency spike synchrony of retinal alpha ganglion cells. *The Journal of neuroscience : the official journal of the Society for Neuroscience* **23**, 6768–6777.

Hu, E. H., Pan, F., Völgyi, B., and Bloomfield, S. A. (2010). Light increases the gap junctional coupling of retinal ganglion cells. *The Journal of physiology* **588**, 4145–4163.

Huberman, A. D. (2007). Mechanisms of eye-specific visual circuit development. *Current opinion in neurobiology* **17**, 73–80.

Huberman, A. D. et al. (2003). Eye-specific retinogeniculate segregation independent of normal neuronal activity. *Science (New York, NY)* **300**, 994–998.

Huberman, A. D., Feller, M. B., and Chapman, B. (2008). Mechanisms underlying development of visual maps and receptive fields. *Annual review of neuroscience* **31**, 479–509.

Hughes, M. E. et al. (2007). Homophilic Dscam interactions control complex dendrite morphogenesis. *Neuron* **54**, 417–427.

Huh, G. S. et al. (2000). Functional requirement for class I MHC in CNS development and plasticity. *Science (New York, NY)* **290**, 2155–2159.

Jia, Z et al. (1996). Enhanced LTP in mice deficient in the AMPA receptor GluR2. *Neuron* **17**, 945–956.

Johnson, J. et al. (2010). Melanopsin-dependent light avoidance in neonatal mice. *Proceedings of the National Academy of Sciences of the United States of America* **107**, 17374–17378.

Johnson, S. L. et al. (2011). Position-dependent patterning of spontaneous action potentials in immature cochlear inner hair cells. *Nature neuroscience* **14**, 711–717.

Johnson, S. L. et al. (2012). The resting transducer current drives spontaneous activity in prehearing mammalian cochlear inner hair cells. *The Journal of neuroscience : the official journal of the Society for Neuroscience* **32**, 10479–10483.

Johnson, S. L. et al. (2013). Presynaptic maturation in auditory hair cells requires a critical period of sensory-independent spiking activity. *Proceedings of the National Academy of Sciences of the United States of America* **110**, 8720–8725.

Kandler, K and Friauf, E (1993). Pre- and postnatal development of efferent connections of the cochlear nucleus in the rat. *The Journal of comparative neurology* **328**, 161–184.

Kandler, K., Clause, A., and Noh, J. (2009). Tonotopic reorganization of developing auditory brainstem circuits. *Nature neuroscience* **12**, 711–717.

Kastanenka, K. V. and Landmesser, L. T. (2010). In vivo activation of channelrhodopsin-2 reveals that normal patterns of spontaneous activity are required for motoneuron guidance and maintenance of guidance molecules. *The Journal of neuroscience : the official journal of the Society for Neuroscience* **30**, 10575–10585.

Katz, L. C. and Shatz, C. J. (1996). Synaptic activity and the construction of cortical circuits. *Science (New York, NY)* **274**, 1133–1138.

Keeley, P. W. et al. (2012). Neuronal clustering and fasciculation phenotype in Dscam- and Bax-deficient mouse retinas. *The Journal of comparative neurology* **520**, 1349–1364.

Kerschensteiner, D. and Wong, R. O. L. (2008). A precisely timed asynchronous pattern of ON and OFF retinal ganglion cell activity during propagation of retinal waves. *Neuron* **58**, 851–858.

Kirkby, L. A. and Feller, M. B. (2013). Intrinsically photosensitive ganglion cells contribute to plasticity in retinal wave circuits. *Proceedings of the National Academy of Sciences of the United States of America* **110**, 12090–12095.

Kirkby, L. A., Sack, G. S., Firl, A., and Feller, M. B. (2013). A role for correlated spontaneous activity in the assembly of neural circuits. *Neuron* **80**, 1129–1144.

Koch, S. M. and Ullian, E. M. (2010). Neuronal pentraxins mediate silent synapse conversion in the developing visual system. *The Journal of neuroscience : the official journal of the Society for Neuroscience* **30**, 5404–5414.

Koch, S. M. et al. (2011). Pathway-specific genetic attenuation of glutamate release alters select features of competition-based visual circuit refinement. *Neuron* **71**, 235–242.

Kothmann, W. W., Massey, S. C., and O'Brien, J. (2009). Dopamine-stimulated dephosphorylation of connexin 36 mediates AII amacrine cell uncoupling. *The Journal of neuroscience : the official journal of the Society for Neuroscience* **29**, 14903–14911.

Krahe, T. E. and Guido, W. (2011). Homeostatic plasticity in the visual thalamus by monocular deprivation. *The Journal of neuroscience : the official journal of the Society for Neuroscience* **31**, 6842–6849.

Landmesser, L. T. and O'Donovan, M. J. (1984). Activation patterns of embryonic chick hind limb muscles recorded in ovo and in an isolated spinal cord preparation. *The Journal of physiology* **347**, 189–204.

Lee, H. et al. (2014). Synapse elimination and learning rules co-regulated by MHC class I H2-D(b.) *Nature* **509**, 195–200.

Lefler, Y., Yarom, Y., and Uusisaari, M. Y. (2014). Cerebellar inhibitory input to the inferior olive decreases electrical coupling and blocks subthreshold oscillations. *Neuron* **81**, 1389–1400.

Lippe, W. R. (1994). Rhythmic spontaneous activity in the developing avian auditory system. *Journal of Neuroscience* **14**, 1486–1495.

Little, J.-A., Woodhouse, J. M., Lauritzen, J. S., and Saunders, K. J. (2009). Vernier acuity in Down syndrome. *Investigative ophthalmology & visual science* **50**, 567–572.

Macosko, E. Z. et al. (2009). A hub-and-spoke circuit drives pheromone attraction and social behaviour in C. elegans. *Nature* **458**, 1171–1175.

Markowitz, J., Cao, Y., and Grossberg, S. (2012). From retinal waves to activity-dependent retinogeniculate map development. *PLoS One* **7**, e31553.

Martin, A. O., Mathieu, M.-N., and Guérineau, N. C. (2003). Evidence for long-lasting cholinergic control of gap junctional communication between adrenal chromaffin cells. *The Journal of neuroscience : the official journal of the Society for Neuroscience* **23**, 3669–3678.

Mathy, A., Clark, B. A., and Häusser, M. (2014). Synaptically induced long-term modulation of electrical coupling in the inferior olive. *Neuron* **81**, 1290–1296.

McLaughlin, T., Torborg, C. L., Feller, M. B., and O'Leary, D. D. M. (2003). Retinotopic map refinement requires spontaneous retinal waves during a brief critical period of development. *Neuron* **40**, 1147–1160.

Meister, M, Wong, R. O., Baylor, D. A., and Shatz, C. J. (1991). Synchronous bursts of action potentials in ganglion cells of the developing mammalian retina. *Science (New York, NY)* **252**, 939–943.

Millard, S. S. et al. (2007). Dscam2 mediates axonal tiling in the Drosophila visual system. *Nature* **447**, 720–724.

Mills, S. L. and Massey, S. C. (1995). Differential properties of two gap junctional pathways made by AII amacrine cells. *Nature* **377**, 734–737.

Mills, S. L. et al. (2007). Dopaminergic modulation of tracer coupling in a ganglion-amacrine cell network. *Visual neuroscience* **24**, 593–608.

Momose-Sato, Y. and Sato, K. (2013). Large-scale synchronized activity in the embryonic brainstem and spinal cord. *Frontiers in cellular neuroscience* **7**, 36.

Moody, W. J. and Bosma, M. M. (2005). Ion channel development, spontaneous activity, and activity-dependent development in nerve and muscle cells. *Physiological Reviews* **85**, 883–941.

Müller, L. P. D. S. et al. (2010). Tracer coupling of intrinsically photosensitive retinal ganglion cells to amacrine cells in the mouse retina. *The Journal of comparative neurology* **518**, 4813–4824.

Müller, M and Holländer, H (1988). A small population of retinal ganglion cells projecting to the retina of the other eye. An experimental study in the rat and the rabbit. *Experimental brain research. Experimentelle Hirnforschung. Expérimentation cérébrale* **71**, 611–617.

Neumann, T., Ziegler, C., and Blau, A. (2008). Multielectrode array recordings reveal physiological diversity of intrinsically photosensitive retinal ganglion cells in the chick embryo. *Brain research* **1207**, 120–127.

Nishimaru, H and Kudo, N (2000). Formation of the central pattern generator for locomotion in the rat and mouse. *Brain research bulletin* **53**, 661–669.

Nusbaum, M. P. et al. (2001). The roles of co-transmission in neural network modulation. *Trends in neurosciences* **24**, 146–154.

O'Donovan, M. J. (1999). The origin of spontaneous activity in developing networks of the vertebrate nervous system. *Current opinion in neurobiology* **9**, 94–104.

Pan, F., Mills, S. L., and Massey, S. C. (2007). Screening of gap junction antagonists on dye coupling in the rabbit retina. *Visual neuroscience* **24**, 609–618.

Pereda, A. E. (2014). Electrical synapses and their functional interactions with chemical synapses. *Nature reviews Neuroscience* **15**, 250–263.

Peretz, A. et al. (2005). Meclofenamic acid and diclofenac, novel templates of KCNQ2/Q3 potassium channel openers, depress cortical neuron activity and exhibit anticonvulsant properties. *Molecular pharmacology* **67**, 1053–1066.

Perez-Leighton, C. E. et al. (2011). Intrinsic phototransduction persists in melanopsin-expressing ganglion cells lacking diacylglycerol-sensitive TRPC subunits. *The European journal of neuroscience* **33**, 856–867.

Provencio, I et al. (1998). Melanopsin: An opsin in melanophores, brain, and eye. *Proceedings of the National Academy of Sciences of the United States of America* **95**, 340–345.

Rao, S. et al. (2013). A direct and melanopsin-dependent fetal light response regulates mouse eye development. *Nature* **494**, 243–246.

Rebsam, A., Petros, T. J., and Mason, C. A. (2009). Switching retinogeniculate axon laterality leads to normal targeting but abnormal eye-specific segregation that is activity dependent. *The Journal of neuroscience : the official journal of the Society for Neuroscience* **29**, 14855–14863.

Renna, J. M., Weng, S., and Berson, D. M. (2011). Light acts through melanopsin to alter retinal waves and segregation of retinogeniculate afferents. *Nature neuroscience* **14**, 827–829.

Ripley, K. L. and Provine, R. R. (1972). Neural correlates of embryonic motility in the chick. *Brain research* **45**, 127–134.

Rollag, M. D., Berson, D. M., and Provencio, I. (2003). Melanopsin, ganglion-cell photoreceptors, and mammalian photoentrainment. *Journal of biological rhythms* **18**, 227–234.

Rossi, F. M. et al. (2001). Requirement of the nicotinic acetylcholine receptor beta 2 subunit for the anatomical and functional development of the visual system. *Proceedings of the National Academy of Sciences of the United States of America* **98**, 6453–6458.

Rubel, E. W. and Fritzsch, B. (2002). Auditory system development: primary auditory neurons and their targets. *Annual review of neuroscience* **25**, 51–101.

Ruthazer, E. S. and Cline, H. T. (2004). Insights into activity-dependent map formation from the retinotectal system: a middle-of-the-brain perspective. *Journal of neurobiology* **59**, 134–146.

Saint-Amant, L and Drapeau, P (2001). Synchronization of an embryonic network of identified spinal interneurons solely by electrical coupling. *Neuron* **31**, 1035–1046.

Schafer, D. P. et al. (2012). Microglia sculpt postnatal neural circuits in an activity and complement-dependent manner. *Neuron* **74**, 691–705.

Schmidt, T. M., Taniguchi, K., and Kofuji, P. (2008). Intrinsic and extrinsic light responses in melanopsin-expressing ganglion cells during mouse development. *Journal of neurophysiology* **100**, 371–384.

Schmidt, T. M., Chen, S.-K., and Hattar, S. (2011). Intrinsically photosensitive retinal ganglion cells: many subtypes, diverse functions. *Trends in neurosciences* **34**, 572–580.

Sekaran, S et al. (2005). Melanopsin-dependent photoreception provides earliest light detection in the mammalian retina. *Current biology : CB* **15**, 1099–1107.

Sekaran, S., Foster, R. G., Lucas, R. J., and Hankins, M. W. (2003). Calcium imaging reveals a network of intrinsically light-sensitive inner-retinal neurons. *Current biology : CB* **13**, 1290–1298.

Sernagor, E, Eglen, S. J., and Wong, R. O. (2001). Development of retinal ganglion cell structure and function. *Progress in retinal and eye research* **20**, 139–174.

Sernagor, E. (2005). Retinal development: second sight comes first. *Current biology : CB* **15**, R556–9.

Shah, R. D. and Crair, M. C. (2008). Retinocollicular synapse maturation and plasticity are regulated by correlated retinal waves. *The Journal of neuroscience : the official journal of the Society for Neuroscience* **28**, 292–303.

Siegel, F., Heimel, J. A., Peters, J., and Lohmann, C. (2012). Peripheral and central inputs shape network dynamics in the developing visual cortex in vivo. *Current biology : CB* **22**, 253–258.

Simpson, H. D. and Goodhill, G. J. (2011). A simple model can unify a broad range of phenomena in retinotectal map development. *Biological cybernetics* **104**, 9–29.

Sipilä, S. T. et al. (2009). Compensatory enhancement of intrinsic spiking upon NKCC1 disruption in neonatal hippocampus. *The Journal of neuroscience : the official journal of the Society for Neuroscience* **29**, 6982–6988.

Soba, P. et al. (2007). Drosophila sensory neurons require Dscam for dendritic self-avoidance and proper dendritic field organization. *Neuron* **54**, 403–416.

Sretavan, D. W. and Shatz, C. J. (1986). Prenatal development of cat retinogeniculate axon arbors in the absence of binocular interactions. *Journal of Neuroscience* **6**, 990–1003.

Sretavan, D. W., Shatz, C. J., and Stryker, M. P. (1988). Modification of retinal ganglion cell axon morphology by prenatal infusion of tetrodotoxin. *Nature* **336**, 468–471.

Stacy, R. C. et al. (2005). Disruption and recovery of patterned retinal activity in the absence of acetylcholine. *The Journal of neuroscience : the official journal of the Society for Neuroscience* **25**, 9347–9357.

Stafford, B. K., Sher, A., Litke, A. M., and Feldheim, D. A. (2009). Spatial-temporal patterns of retinal waves underlying activity-dependent refinement of retinofugal projections. *Neuron* **64**, 200–212.

Stellwagen, D and Shatz, C. J. (2002). An instructive role for retinal waves in the development of retinogeniculate connectivity. *Neuron* **33**, 357–367.

Stevens, B. et al. (2007). The classical complement cascade mediates CNS synapse elimination. *Cell* **131**, 1164–1178.

Sun, C. et al. (2008). Retinal waves in mice lacking the beta2 subunit of the nicotinic acetylcholine receptor. *Proceedings of the National Academy of Sciences of the United States of America* **105**, 13638–13643.

Syed, M. M., Lee, S., He, S., and Zhou, Z. J. (2004). Spontaneous waves in the ventricular zone of developing mammalian retina. *Journal of neurophysiology* **91**, 1999–2009.

Torborg, C., Wang, C.-T., Muir-Robinson, G., and Feller, M. B. (2004a). L-type calcium channel agonist induces correlated depolarizations in mice lacking the beta2 subunit nAChRs. *Vision research* **44**, 3347–3355.

Torborg, C. L. and Feller, M. B. (2005). Spontaneous patterned retinal activity and the refinement of retinal projections. *Progress in neurobiology* **76**, 213–235.

Torborg, C. L., Hansen, K. A., and Feller, M. B. (2004b). High frequency, synchronized bursting drives eye-specific segregation of retinogeniculate projections. *Nature neuroscience* **8**, 72–78.

Toyoda, H. et al. (2007). Time-dependent postsynaptic AMPA GluR1 receptor recruitment in the cingulate synaptic potentiation. *Developmental neurobiology* **67**, 498–509.

Triplett, J. W. and Feldheim, D. A. (2012). Eph and ephrin signaling in the formation of topographic maps. *Seminars in cell & developmental biology* **23**, 7–15.

Tritsch, N. X. et al. (2007). The origin of spontaneous activity in the developing auditory system. *Nature* **450**, 50–55.

Tsigankov, D. N. and Koulakov, A. A. (2006). A unifying model for activity-dependent and activity-independent mechanisms predicts complete structure of topographic maps in ephrin-A deficient mice. *Journal of computational neuroscience* **21**, 101–114.

Tu, D. C. et al. (2005). Physiologic diversity and development of intrinsically photosensitive retinal ganglion cells. *Neuron* **48**, 987–999.

Turecek, J. et al. (2014). NMDA Receptor Activation Strengthens Weak Electrical Coupling in Mammalian Brain. *Neuron* **81**, 1375–1388.

Turrigiano, G. (2012). Homeostatic synaptic plasticity: local and global mechanisms for stabilizing neuronal function. *Cold Spring Harbor perspectives in biology* **4**, a005736.

Turrigiano, G. G. and Nelson, S. B. (2004). Homeostatic plasticity in the developing nervous system. *Nature reviews Neuroscience* **5**, 97–107.

Van Hook, M. J., Wong, K. Y., and Berson, D. M. (2012). Dopaminergic modulation of ganglion-cell photoreceptors in rat. *The European journal of neuroscience*, 1–13.

Veruki, M. L. and Hartveit, E. (2009). Meclofenamic acid blocks electrical synapses of retinal AII amacrine and on-cone bipolar cells. *Journal of neurophysiology* **101**, 2339–2347.

Vugler, A. A. et al. (2007). Dopamine neurones form a discrete plexus with melanopsin cells in normal and degenerating retina. *Experimental neurology* **205**, 26–35.

Warp, E. et al. (2012). Emergence of patterned activity in the developing zebrafish spinal cord. *Current biology : CB* **22**, 93–102.

Weliky, M and Katz, L. C. (1999). Correlational structure of spontaneous neuronal activity in the developing lateral geniculate nucleus in vivo. *Science (New York, NY)* **285**, 599–604.

Weng, S., Wong, K. Y., and Berson, D. M. (2009). Circadian modulation of melanopsin-driven light response in rat ganglion-cell photoreceptors. *Journal of biological rhythms* **24**, 391–402.

Wenner, P. (2011). Mechanisms of GABAergic homeostatic plasticity. *Neural plasticity* **2011**, 489470.

— (2012). Motor development: activity matters after all. *Current biology : CB* **22**, R47–8.

Wilhelm, J. C. and Wenner, P. (2008). GABAA transmission is a critical step in the process of triggering homeostatic increases in quantal amplitude. *Proceedings of the National Academy of Sciences of the United States of America* **105**, 11412–11417.

Wilhelm, J. C., Rich, M. M., and Wenner, P. (2009). Compensatory changes in cellular excitability, not synaptic scaling, contribute to homeostatic recovery of embryonic network activity. *Proceedings of the National Academy of Sciences of the United States of America* **106**, 6760–6765.

Witkovsky, P. (2004). Dopamine and retinal function. *Documenta ophthalmologica. Advances in ophthalmology* **108**, 17–40.

Wong, R. O. (1999). Retinal waves and visual system development. *Annual review of neuroscience* **22**, 29–47.

Wong, R. O., Meister, M, and Shatz, C. J. (1993). Transient period of correlated bursting activity during development of the mammalian retina. *Neuron* **11**, 923–938.

Wulle, I and Schnitzer, J (1989). Distribution and morphology of tyrosine hydroxylase-immunoreactive neurons in the developing mouse retina. *Brain research Developmental brain research* **48**, 59–72.

Xu, H.-P. et al. (2011). An instructive role for patterned spontaneous retinal activity in mouse visual map development. *Neuron* **70**, 1115–1127.

Xu, H., Clement, A., Wright, T. M., and Wenner, P. (2007). Developmental reorganization of the output of a GABAergic interneuronal circuit. *Journal of neurophysiology* **97**, 2769–2779.

Xu, W et al. (1999). Multiorgan autonomic dysfunction in mice lacking the beta2 and the beta4 subunits of neuronal nicotinic acetylcholine receptors. *The Journal of neuroscience : the official journal of the Society for Neuroscience* **19**, 9298–9305.

Yates, P. A. et al. (2004). Computational modeling of retinotopic map development to define contributions of EphA-ephrinA gradients, axon-axon interactions, and patterned activity. *Journal of neurobiology* **59**, 95–113.

Yoshida, M. et al. (2011). Overexpression of neurotrophin-3 stimulates a second wave of dopaminergic amacrine cell genesis after birth in the mouse retina. *The Journal of neuroscience : the official journal of the Society for Neuroscience* **31**, 12663–12673.

Young, T. R. et al. (2013). Ten-m2 Is Required for the Generation of Binocular Visual Circuits. *The Journal of neuroscience : the official journal of the Society for Neuroscience* **33**, 12490–12509.

Zhang, D.-Q. et al. (2008). Intraretinal signaling by ganglion cell photoreceptors to dopaminergic amacrine neurons. *Proceedings of the National Academy of Sciences of the United States of America* **105**, 14181–14186.

Zhang, D.-Q. et al. (2012a). Melanopsin mediates retrograde visual signaling in the retina. *PLoS One* **7**, e42647.

Zhang, J., Ackman, J. B., Xu, H.-P., and Crair, M. C. (2012b). Visual map development depends on the temporal pattern of binocular activity in mice. *Nature neuroscience* **15**, 298–307.

Zhang, R.-W., Wei, H.-p., Xia, Y.-m., and Du, J.-L. (2010). Development of light response and GABAergic excitation-to-inhibition switch in zebrafish retinal ganglion cells. *The Journal of physiology* **588**, 2557–2569.

Ziburkus, J., Dilger, E. K., Lo, F.-S., and Guido, W. (2009). LTD and LTP at the developing retinogeniculate synapse. *Journal of neurophysiology* **102**, 3082–3090.